2020

REMODELING IN THE ACTIN CORE OF THE AUDITORY HAIR CELL STEREOCILIA AS A NOVEL COMPONENT OF TEMPORARY NOISE-INDUCED HEARING LOSS

Jonathan Michael Grossheim
University of Kentucky, jmikeg224@uky.edu
Digital Object Identifier: https://doi.org/10.13023/etd.2020.410

STUDENT AGREEMENT:

I represent that my thesis or dissertation and abstract are my original work. Proper attribution has been given to all outside sources. I understand that I am solely responsible for obtaining any needed copyright permissions. I have obtained needed written permission statement(s) from the owner(s) of each third-party copyrighted matter to be included in my work, allowing electronic distribution (if such use is not permitted by the fair use doctrine) which will be submitted to UKnowledge as Additional File.

I hereby grant to The University of Kentucky and its agents the irrevocable, non-exclusive, and royalty-free license to archive and make accessible my work in whole or in part in all forms of media, now or hereafter known. I agree that the document mentioned above may be made available immediately for worldwide access unless an embargo applies.

I retain all other ownership rights to the copyright of my work. I also retain the right to use in future works (such as articles or books) all or part of my work. I understand that I am free to register the copyright to my work.

REVIEW, APPROVAL AND ACCEPTANCE

The document mentioned above has been reviewed and accepted by the student's advisor, on behalf of the advisory committee, and by the Director of Graduate Studies (DGS), on behalf of the program; we verify that this is the final, approved version of the student's thesis including all changes required by the advisory committee. The undersigned agree to abide by the statements above.

Jonathan Michael Grossheim, Student

Dr. Gregory I. Frolenkov, Major Professor

Dr. Kenneth S. Campbell, Director of Graduate Studies

REMODELING IN THE ACTIN CORE OF THE AUDITORY HAIR CELL STEREOCILIA AS A NOVEL COMPONENT OF TEMPORARY NOISE-INDUCED HEARING LOSS

DISSERTATION

A dissertation submitted in partial fulfillment of the requirements for the degree of Doctor of Philosophy in the College of Medicine at the University of Kentucky

By
Jonathan Michael Grossheim
Lexington, Kentucky

Director: Dr. Gregory I. Frolenkov, Professor of Physiology

Lexington, Kentucky
2020

ABSTRACT OF DISSERTATION

REMODELING IN THE ACTIN CORE OF THE AUDITORY HAIR CELL STEREOCILIA AS A NOVEL COMPONENT OF TEMPORARY NOISE-INDUCED HEARING LOSS

The rigid, paracrystalline actin core of auditory hair cell stereocilia is extremely stable and after initial formation must persist for the life of the cell to preserve hearing in mammals. In healthy hair cells, turnover of actin molecules occurs only in a small region near the tips of stereocilia, while the actin filaments of the shaft are stable. For decades damage to the actin core of stereocilia from acoustic trauma has only been attributed to cases of permanent noise-induced hearing loss. Here, we show that repairable actin core damage occurs in temporary noise-induced hearing loss from moderate acoustic trauma.

We have found that moderate noise exposure causing a temporary hearing loss results in damage to the stereocilia actin core in the form of small, submicron breaks in the filamentous actin (F-actin) at the base of the stereocilia, and displacement of the stereocilia from its anchoring rootlet. The same damages were recapitulated *in vitro* after mechanical overstimulation of stereocilia bundles by fluid-jet. Despite the well-established stable nature of the F-actin within stereocilia, 24 hours after the damage we observed complete repair of this damage *in vitro* and only partial repair *in vivo*, indicating slower *in vivo* recovery. The mechanism of this repair appears to involve actin remodeling in the upper portion of the rootlet located within the stereocilia shaft.

Our results suggest that repairable damage to the F-actin at the base of stereocilia is a novel component of temporary noise-induced hearing loss. We believe that restoration of hearing thresholds after moderate noise exposure includes the repair of this damage. Although the exact mechanism of this repair is unknown, this is the first evidence for actin cytoskeleton repair in the stereocilia of auditory hair cells which have to maintain their structure and mechanosensitivity throughout the life of an organism.

KEYWORDS: Temporary noise-induced hearing loss, temporary threshold shifts, stereocilia actin core repair, rootlets.

Jonathan Michael Grossheim

(Name of Student)

09/04/2020

Date

REMODELING IN THE ACTIN CORE OF THE AUDITORY HAIR CELL STEREOCILIA AS A NOVEL COMPONENT OF TEMPORARY NOISE-INDUCED HEARING LOSS

By

Jonathan Michael Grossheim

Dr. Gregory I. Frolenkov
Director of Dissertation

Dr. Kenneth S. Campbell
Director of Graduate Studies

09/04/2020
Date

DEDICATION

To my father,

who always encouraged me to question.

ACKNOWLEDGMENTS

This dissertation is the denouement of a 25-year-long odyssey in higher education. The path has been non-traditional, arduous, and protracted. Nevertheless, despite a myriad of hardships over the years, the direction has remained steadfastly and inexorably forward. Although there were times when the abdication of my pursuit seemed inevitable, the journey has come to its successful end and, true to its purpose, has culminated in a faculty position educating future healthcare providers and aspiring scientists.

Nearly 400 years ago, as part of his *Devotions upon Emergent Occasions*, John Donne wrote, "No man is an island, entire of itself…" Notwithstanding the likelihood that Donne's use of "man" was not intended as a sobriquet for "human," and despite the vituperations such a philosophy receives today from those espousing bootstrap levitation as pragmatic, I embrace the sentiment from a humanist perspective. While not ignoring the relevance of such a credo to the crises of our time, I instead utilize it here in multipartite fashion to concede not only that this accomplishment is not mine alone, but also that my failure to fully attribute more than 4 decades of innumerable contributions from others is inescapable.

I wish to thank my advisor and committee chair, Dr. Gregory Frolenkov, for his guidance and stalwart support over the years; these many, many years. From the very first day of my time in his lab I was forthright with my aspirations... I do not think he believed me. I have seen him inspire students in the lab to pursue careers in research and I think he believed he might be able to do the same with me. The exact moment at which he was fully disabused of this notion may never be known, but I do know that it improved our

dynamic. Unfortunately, even with that realization we still do not speak the same language, and this led to many a strident misunderstanding as a result. Although we have not always seen eye to eye during the process, this dissertation would not have been possible without him. I have a great deal of respect for Gregory's talents and I am delighted to leave the research to his capable hands.

I want to thank the other members of my PhD committee: Dr. Francisco 'Paco' Andrade, Dr. Rebecca Dutch, Dr. Karyn Esser, and Dr. Timothy McClintock. Their advice, insight, and encouragement throughout the prolonged and unconventional path to my PhD is much appreciated. Along with Gregory, they have been my Sherpas as I sought the summit in an environment for which I am ill-suited. An extra thank you to Dr. Karyn Esser for remaining on the committee after relocating to the University of Florida. I would also like to thank Dr. Elizabeth Debski for consenting to serve as the outside examiner for my defense.

Many people have come and gone from the Frolenkov lab during my tenure and they have all contributed in one way or another. I owe a huge thanks to Cata, Dr. Alejandra Catalina Vélez-Ortega, for invaluable assistance more times than I can count. Cata is a wonderful mentor and I am extremely excited for her future as she establishes her own lab and embarks on her career as a PI. I still cannot believe my good fortune to have been in the lab with Stephanie Edelmann. Stephanie and I always had fun as she shares my sense of humor, my passion for teaching, and my ability to find trouble. I often referred to Stephanie as a chocolate lab, because every new person she comes across is just a friend she has not met yet. There was a void in the lab when she left but it turned out that there was a yellow lab who would come and fill that void with an ebullient

attitude as bright as the sun. Mary Freeman was that yellow lab and it was a marvelous boon to have had her warmth and positivity during some dark times. I also want to thank Dr. Desislava Marinkova for sharing some of her ABR data to bolster my own. To Abbey, Caro, Isabel, Shawn, Shadan and all the others in the lab, past and present, thank you!

Of course, I would be remiss if I did not thank my family and friends: My parents and grandparents, whose influence while growing up cannot be overstated in shaping the way I look at the world. My mother Debbie, who provides love, support, and exasperation in near equal measure. My non-consanguineal family (both those I have 'adopted' and those who have 'adopted' me) who have been there through thick and thin. Especially my best friend Kristy, her husband, and their two amazing children, whose imprint on my life is indelible. Meine deutschen Freunden, die immer so liebevoll sein. Deutschland ist die Heimat meines Herzens und hoffentlich wird es eines Tages meine Heimat in Wahrheit sein. To include all of my friends would be a Herculean task. Instead I will express my gratitude that my friends know how much I value them without needing the validation of being mentioned in a document destined to be read by only 6 people.

Having saved the best for last, I want to thank my wonderful husband, Tyler Robert Grossheim. The constancy of his love, companionship, wit, and humor has buoyed my spirits during difficult periods and been my bulwark against despair. Together with the unconditional love of our furry, four-legged compatriot Chewy, he has brought joy and contentment to my life. Hand in hand we confidently head into the future, invigorated, and excited to face the challenges ahead.

Adventure awaits.

TABLE OF CONTENTS

LIST OF TABLES

LIST OF FIGURES

).

CHAPTER 1. **INTRODUCTION TO HEARING AND HEARING LOSS**

1.1 Overview of Hearing

Sound is the term we use for the interpretation by our brains of pressure waves in the air. As with the detection of any external stimuli, the stimulus must reach the receptive field of a receptor and be of sufficient magnitude to be transduced into an action potential. However, the magnitudes of these pressure waves are usually quite small and thus the mechanosensitive receptors detecting them must be extremely sensitive. Unfortunately, this incredible sensitivity means the receptors must be protected from a harsh external environment lest they overwhelm our somatic senses or become damaged. How do we protect these delicate receptors while simultaneously ensuring that these miniscule pressure waves reach them? Nature has provided a marvelous solution which possesses an elegant beauty on par with its complexity.

1.1.1 Outer and middle ear

The visible outer ear found on either side of the head consists of the auricle (or pinna), auditory canal and tympanic membrane (or eardrum) (Figure 1.1A). The auricle is composed of elastic cartilage covered by skin and serves to funnel sound pressure waves into the auditory canal where they travel about 2.5 cm through the temporal bone to impinge upon the tympanic membrane. The tympanic membrane is a thin (~0.1 mm) tissue separating the outer and middle ear (Van der Jeught et al., 2013).

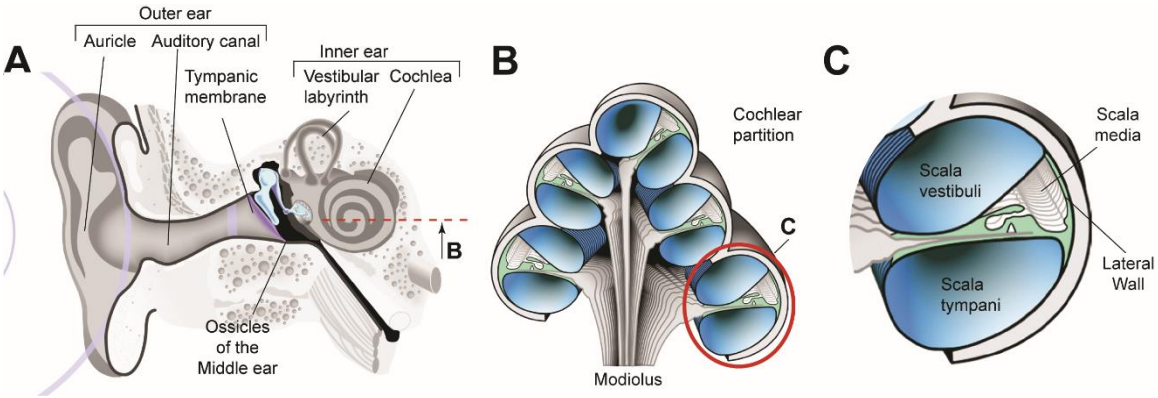

Figure 1.1. Overview of the ear

(Modified from Frolenkov et al, 2004). A, Diagram of the three regions of the ear with prominent features of each labeled. B, Cross-section of the cochlea (from red dashed line in A). C, Enlarged region of cochlear partition showing the three fluid-filled scalae.

Connected to the basal side of the tympanic membrane is the malleus, the largest of three bones located in the middle ear collectively termed the ossicles. The ossicles span the air-filled middle ear with the malleus articulating with the incus which articulates with the smallest bone in the body, the stapes. The base, or footplate, of the stapes rests against a membrane called the oval window which separates the middle and inner ear. This connection permits the transmission of pressure wave generated vibrations of the tympanic membrane though the ossicles in the middle ear to the inner ear where the sensory cells are located. Further, since the oval window is ~6x smaller than the tympanic membrane, the transmission of the vibrations amplifies the pressure (p=F/A) applied at the oval window which is essential to transition from the air-filled middle ear to the fluid-filled inner ear (Mancheno et al., 2017).

1.1.2 Inner ear: cochlea

Located within the densest bone in the body, the inner ear is composed of the vestibular labyrinth and the cochlea (Lam et al., 1999). Of these, the concho-spiral shaped cochlea is the structure containing the sensory epithelium involved in hearing. The human cochlea resembles a snail shell with the apex oriented anteriorly and is slightly smaller than a pea, measuring approximately 9 mm in the transverse plane and 7 mm in the sagittal plane (Pelliccia et al., 2014). A transverse cross-section through the cochlea (Figure 1.1B) reveals three chambers around a conically shaped bony structure in the middle termed the modiolus. The modiolus contains cochlear nerve neuronal soma and axons and it anchors the medial end of the basilar membrane at an insertion point termed the spiral limbus. The basilar membrane spans the width of the cochlear partition terminating at the spiral prominence which is its insertion point in the lateral wall. As its name suggests, the lateral wall is the outer edge of the cochlea and the otic capsule, its outer layer, is made up of bone.

The three fluid-filled chambers of the cochlear partition revealed in transverse cross-section are termed the scala vestibuli, scala media and scala tympani (Figure 1.1C). The fluid found in the scalae vestibuli and tympani is termed perilymph and, similar to cerebrospinal fluid, has a high concentration of Na^+. Meanwhile, the scala media contains the endolymph which is a K^+-rich solution with an electrical potential of about +80 mV (Davis et al., 1957). The Reissner's membrane, composed of a layer of epithelial and a layer of mesothelial cells separated by a basement membrane, separates the scala vestibuli from the scala media (Johnsson 1971). The scala tympani is separated from the scala media by the reticular lamina, a barrier formed by apical tight junctions between cells of the

sensory epithelium. The lateral wall's inner layer, which spans the space between the spiral prominence and Reissner's membrane, is the stria vascularis which has three layers of epithelial cells supported by a robust capillary bed. Together with the Reissner's membrane, the stria vascularis creates and maintains the low [Na^+] and high [K^+] of the endolymph necessary for the positive extracellular potential, known as endocochlear potential. (Tasaki and Spyropoulos, 1959; Lee and Marcus, 2003).

1.1.2.1 Organ of Corti

Two types of sensory *hair cells* and over a half a dozen supporting cells make up the sensory epithelium resting atop the basilar membrane (Figure 1.2A). Collectively these cells make up the *organ of Corti* and, extending from the spiral limbus and covering much of their apical surface, is an extracellular matrix of collagens and noncollagenous glycoproteins called the *tectorial membrane* (Goodyear and Richardson, 2002). Although the distal end of the tectorial membrane rests upon the tallest mechanosensitive cellular projections on the apical surface of some of the sensory hair cells, it is only anchored at the medial region of the cochlea. Thus, despite being connected, the amplitude of sound induced vibrational movement of the tectorial membrane differs from that of the organ of Corti and creates a shearing force between them which deflects the aforementioned mechanosensitive cellular projections on the hair cells (Figure 1.2B) (Allen, 1980; Gavara et al., 2011).

The cells of this epithelial tissue, as well as the acellular membranes which support its function, are consistently arranged along the length of the cochlea; however, their physical properties gradually change from the base to the apex of the cochlea. These gradual changes are essential to our ability to discriminate between different frequencies

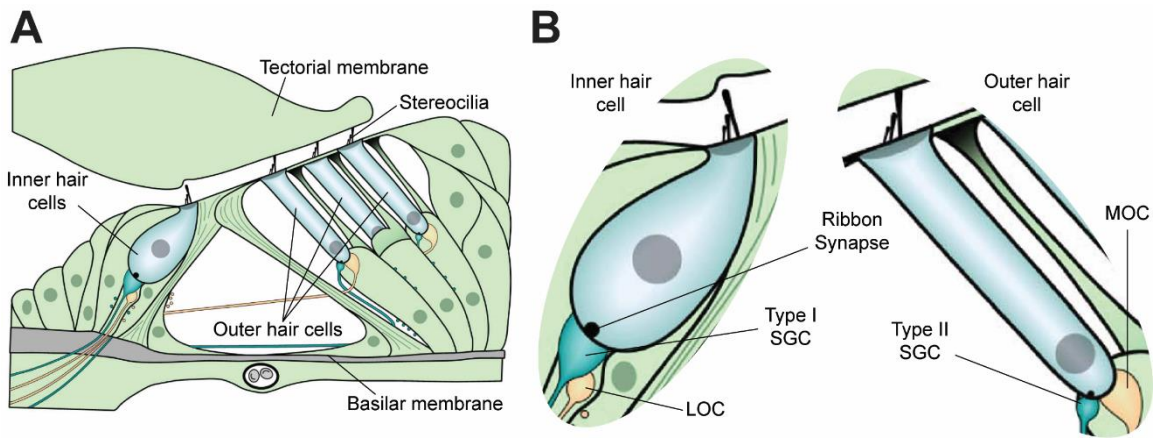

Figure 1.2. Sensory cells of the organ of Corti

(Modified from Frolenkov et al, 2004). A, Diagram of the organ of Corti highlighting the sensory structures required for mechanotransduction. B, Magnified view of inner and outer hair cells showing differences in structure and innervation. SGC: Spiral Ganglion Cells, LOC: Lateral Olivocochlear Cells, MOC: Medial Olivocochlear Cells.

and are analogous to the strings of a harp where slight differences in adjacent strings permit the production of different notes. Similar to the arrangement of strings of a harp from higher to lower pitch notes, the acellular basilar membrane upon which the sensory epithelium rests is narrow and stiff at the base and increases in width and thickness, causing a decrease in stiffness, along its length to the apex of the cochlea (Olson et al., 1991). As a consequence, the traveling waves generated by the vibrations of the stapes on the oval window at the base of the cochlea resonate in a frequency-specific (tonotopic) manner at unique locations along the length of the basilar membrane, a discovery for which Georg von Békésy won a Nobel Prize in 1951. The cellular receptors, which are a part of

the sensory epithelium resting on the basilar membrane, transduce the mechanically generated, sound-induced vibrations into action potentials in afferent neurons of the cochlear nerve by releasing neurotransmitter.

1.1.2.2 Mechanoelectrical transduction in cochlear hair cells

In mammals there are four rows of sensory hair cells running the length of the organ of Corti. The hair cells located in the row nearest the modiolus are termed the *inner hair cells* (IHC) and are morphologically distinct from the hair cells in the other rows which are termed *outer hair cells* (OHC) (Figure 1.2B and 1.3A). The moniker "hair cell" derives from the presence of stereocilia on the apical surface of the cells (Figure 1.3). The stereocilia are very precisely arranged into bundles, most often with three rows of stereocilia. Within a row the stereocilia are of equivalent height but they vary in height between rows. The rows are numbered starting with the tallest row, which is located laterally, and each successive row in the direction of the modiolus is shorter than the preceding one (Figure 1.3B).

As previously described, oscillations in the basilar membrane create a shearing force on OHC stereocilia bundles by the connection of their tallest (1^{st}) row stereocilia with the tectorial membrane (Figure 1.2B). The stereocilia bundles of IHCs, however, do not make contact with the tectorial membrane and are instead deflected by fluid flow from perturbation of the endolymph (Ciganovic et al, 2017).

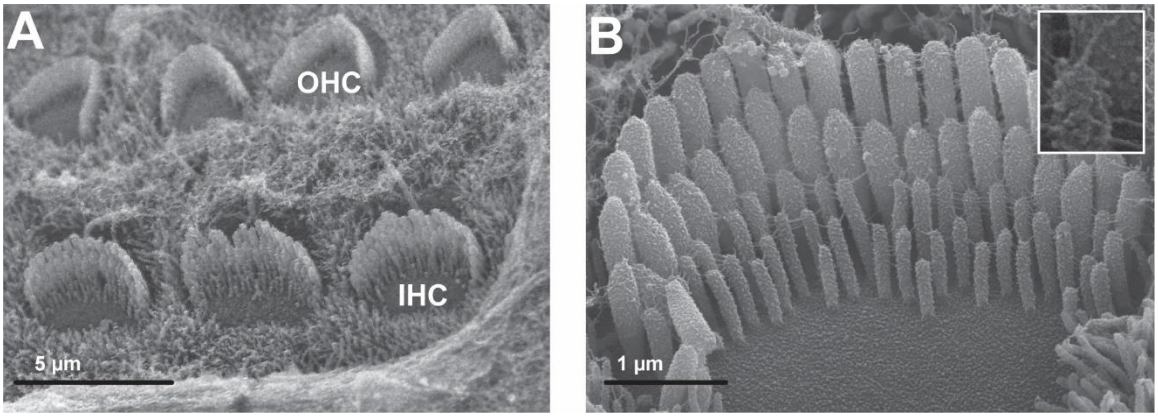

Figure 1.3. View of the mechanosensory bundles on organ of Corti

A, Scanning electron microscopy (SEM) image of IHC and OHC stereocilia bundles from a juvenile (postnatal day 4) mouse cochlear explant. B, Higher magnification image from the explant in A showing an IHC bundle with inset showing links between stereocilia including the tip-link associated with the MET channel.

1.1.2.2.1 MECHANOELECTRICAL TRANSDUCTION

The shorter stereocilia within a bundle possess a mechanoelectrical transduction (MET) channel at their tips and are referred to as *transducing stereocilia* (Beurg et al., 2009). Associated with the MET channel is an extracellular proteinaceous connection, called a *tip-link*, which connects the top of the shorter stereocilia laterally to the side of an adjacent, taller stereocilia (Figure 1.3B inset and Figure 1.4A) (Pickles et al., 1984; Osborne et al., 1984; Assad et al., 1991; Pickles and Corey, 1992). Deflection of the bundle increases tension on tip-links, transmitting the force to the associated MET channels which are non-selective cation channels highly permeable to Ca^{2+} (Corey and Hudspeth, 1979; Lumpkin et al., 1997). There is a large chemiosmotic force for the influx of K^+ and Ca^{2+}

through open MET channels of transducing stereocilia due to the negative intracellular potential of hair cells (approximately -50mV) and the positive extracellular potential of the endolymph (Ricci and Fettiplace, 1998). Thus, deflections of the bundle from sound induced vibrations cause depolarization of the hair cell (Figure 1.4)

1.1.2.2.2 INNER HAIR CELLS

The sensory cells which are primarily involved in afferent signaling are the IHCs. In order to fulfill this role, the IHCs possess ribbon synapses, a specialized type of neuronal synapse where the presynaptic cell has a unique structure called a synaptic ribbon which positions hundreds of synaptic vesicles in close proximity to the presynaptic membrane (reviewed in Nouvian et al., 2006). Depolarization of the IHC via bundle deflection causes Ca^{2+} influx through the activation of voltage-gated Ca^{2+} channels at the base of the IHC. Upon binding to otoferlin this entry of Ca^{2+} causes the release of the synaptic vesicles from the synaptic ribbon and exocytotic delivery of glutamate into the synaptic cleft (Ottersen et al., 1998; Ruel et al., 1999). The presence of thousands of synaptic vesicles in the IHCs permits high frequency neurotransmitter release to persist over long durations (Glowatzki and Fuchs, 2002).

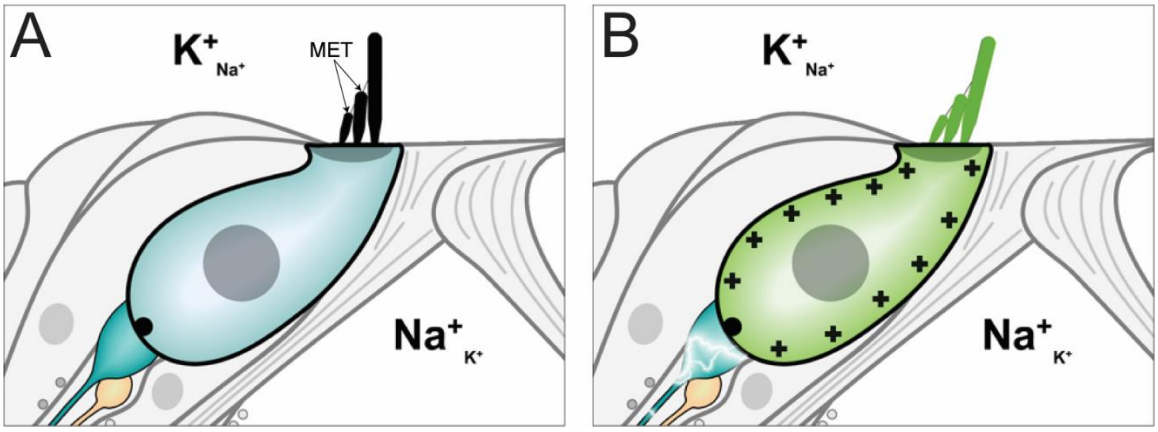

Figure 1.4 – Illustration of mechanoelectrical transduction in an IHC

(Modified from Frolenkov et al., 2004). A, Unstimulated IHC and synapse with afferent Type I SGC, MET channels at tips of transducing stereocilia are closed. B, Deflection of the IHC stereocilia bundle increase tension at the tip-links and gates MET channels, depolarizing the cell and releasing glutamate at the synapse which excites the SGC.

1.1.2.2.3 OUTER HAIR CELLS

Although at casual inspection OHCs are morphologically similar to IHCs there are distinct differences which support their function as contractile cells. The maintenance of cell shape in OHCs resembles that of erythrocytes with an actin and spectrin mesh at the plasma membrane of the lateral wall instead of the central cytoskeleton found in the non-contractile IHCs and most other cells (Holley and Ashmore, 1990; Byers and Branton, 1985; Shen et al., 1986). Additionally, within the plasma membrane of the lateral wall is a protein with piezoelectric properties called *prestin* (Iwasa, 1993; Zheng et al., 2000, Dong et al., 2002; Dallos et al., 2008). Bundle deflections which depolarize the OHCs drive a

conformational change in prestin which causes a contraction of the cell while repolarization has the opposite effect (Brownell et al., 1985; Kachar et al., 1986; Ashmore, 1987). As a result of these voltage dependent changes in cell shape, termed *electromotility*, and the connection of the OHCs to the basilar membrane at their base and the reticular lamina at their apex, the OHCs serve as cochlear amplifiers by intensifying the sound-induced vibrations of the basilar membrane more than 100-fold (Dallos and Harris, 1978; Brown et al., 1983). This amplification is essential to overcome the attenuation of sound-induced vibrations in a viscous fluid and allows the IHCs to detect sounds of lower intensity. Indeed, the vast majority of clinical cases of hearing impairment worldwide are caused by a loss of cochlear amplification due to the malfunction, or loss, of OHCs.

1.1.2.3 Differential innervation of IHCs and OHCs

In addition to the morphological differences between the inner and outer hair cells their individual functions are further supported by their distinct innervation (Figure 1.2B). The afferent neurons which innervate the hair cells are located in the modiolus and are called *spiral ganglion cells* (SGC). The SGCs are a part of cranial nerve VIII, the vestibulocochlear nerve, and are present in two varieties: type I and type II. IHCs are innervated by type I SGCs which constitute 90-95% of all SGCs. These bipolar neurons are arranged so that each IHC is innervated by multiple type I SGCs (Liberman 1980; Liberman et al., 1990). In contrast, the type II SGCs are pseudounipolar neurons and are therefore able to synapse with multiple OHCs (Brown, 1987). There is speculation that these afferents act as cochlear nociceptors in response to noxious acoustic stimuli; however, there is still uncertainty regarding the function of the type II SGCs (Weisz et al., 2009).

The efferent nerves which innervate the cochlea are also present in two types: lateral olivocochlear (LOC) and medial olivocochlear (MOC). The cholinergic MOC neurons, with myelinated axons, synapse directly with numerous OHCs while the thin, unmyelinated axons of the LOC do not synapse directly with sensory cells but instead innervate the dendrites of type I SGCs (Figure 1.2B).

The MOC may act as a protective reflex to protect against acoustic trauma. It has been demonstrated to inhibit cochlear amplification by signaling the OHCs through nicotinic acetylcholine receptors at the MOC synapse which leads to the activation of calcium sensitive potassium channels causing the OHC to hyperpolarize (Blanchet et al., 1996, Dallos et al., 1997; Evans et al., 2000). Interestingly, the inhibition of cochlear amplification by the OHCs is not due to a loss of electromotility (Frolenkov et al, 2000) but rather due to an increase in OHC stiffness (Dallos et al., 1997) from alterations of the cytoskeleton (Matsumoto et al., 2010; Zhang et al., 2003; Kalinec et al., 2000) as a result of the increased intracellular [Ca^{2+}] (Frolenkov et al., 2003). Additionally, the MOC has been shown to improve auditory signal-to-noise ratios (Andéol et al., 2011; Liberman et al., 1996) and a very interesting hypothesis suggests that this may be the true evolutionary origin of the MOC function and the protective effects are incidental (Smith and Keil, 2015).

Studying the effects of the LOC has proved more difficult as electrical stimulation of their unmyelinated fibers also stimulate the MOC. Adding to the challenge are the multiple neurotransmitters in LOC neuronal processes: GABA, Dopamine, Enkephalin, CGRP, Dynorphin, and Acetylcholine in the axon terminals of LOC (Ruel et al., 2007; Eybalin and Pujol, 1984; Hoffman et al., 1985; Sliwinska-Kowalska et al., 1989) The combination of excitatory and inhibitory signaling molecules has been shown to both

potentiate and inhibit Type I SGC signaling (reviewed in Nouvian et al., 2015). This suggests a role in fine tuning the dynamic range of afferent signaling by IHCs through the alteration of Type I SGC excitability. An increased susceptibility to noise-induced trauma from selective lesioning of LOC fibers suggests that the LOC may also serve a protective role from acoustic insult (Darrow et al., 2007)

1.2 Stereocilia

Despite their name, stereocilia are actually modified microvilli and are filled with a core of densely packed actin filaments which give them rigidity (DeRosier et al., 1980). They are rod-like structures with a uniform diameter for most of their length. Stereocilia taper at their base where they protrude from the apical surface of the cell and bundle deflections cause the stereocilia to pivot at this point (Figure 1.4B) (Karavitaki and Corey, 2010). In addition to the aforementioned tip-links, stereocilia within a bundle are connected to one another by three other types of links named for their location: top, side, and ankle. Compositionally each type of link is distinct, and they are not all present at all stages of development (reviewed in Richardson and Petit, 2020). The tip-link is a calcium sensitive, protein complex of two non-classical cadherins: cadherin-23 at the top and protocadherin-15 at the bottom of the tip-link (Kazmierczak et al., 2007).

1.2.1 Actin core

The actin core contains thousands of highly crosslinked, parallel filaments running the length of the stereocilium and which are composed of equivalent amounts of two isoforms of actin: β_{cyto}-actin and γ_{cyto} actin (Figure 1.5A) (Perrin et al., 2010). Multiple crosslinkers, each with their own geometry, cause the filamentous actin (F-actin) to be

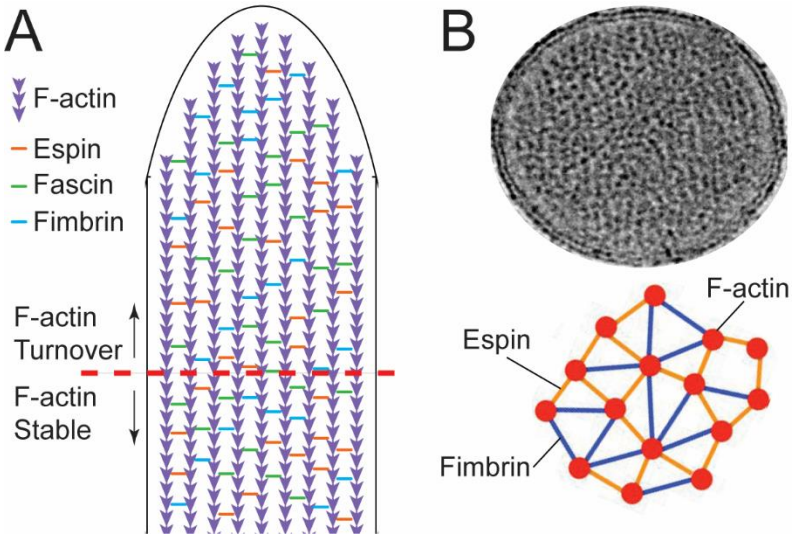

Figure 1.5. F-actin within the stereocilia.

A, Illustration of the crosslinked parallel actin filaments which make up the actin core of stereocilia. The 'barbed' ends of the F-actin are just under the plasma membrane at the tip of the stereocilia where turnover occurs. The main part of the stereocilia shaft is stable with remarkably little turnover of actin. B, Modified from Krey et al., 2016. Transverse section through a wild-type stereocilium showing tightly packed F-actin with a diagram illustrating how crosslinkers of different length generate a paracrystalline array.

arranged in a paracrystalline array (Figure 1.5B) (Krey et al., 2016). F-actin is polarized and normally undergoes a process called *treadmilling* which is an equilibrium state whereby polymerization by the addition of actin monomers, typically occurring at the 'barbed' end, occurs at an equal rate with depolymerization at the 'pointed' end (Fujiwara et al., 2002). By this mechanism stable length actin filaments can be maintained while

replacing older actin monomers with newer ones. In stereocilia, the F-actin is all oriented with the barbed ends at the top of the stereocilia and the pointed ends at the base (Flock and Cheung, 1977) but it is remarkably stable for most of its length and does not undergo treadmilling (Zhang et al., 2012; Narayanan et al., 2015; Drummond et al., 2015).

1.2.1.1 Stability

In mammals, hair cells are terminally differentiated cells which do not regenerate and, under healthy conditions, their stereocilia persist for the life of the animal. Despite conventional wisdom, and the evidence of treadmilling in other actin-based structures, the actin in a mature and fully grown stereocilia appears to turnover only at the tips. A number of studies have confirmed this observation through a variety of means including: multi-isotope imaging mass spectrometry, the use of GFP-actin in photobleaching experiments, and isoform specific conditional excision of either β_{cyto} or γ_{cyto} actin (Zhang et al., 2012; Narayanan et al., 2015; Drummond et al., 2015). These studies have demonstrated that little to no actin turnover occurs in stereocilia shafts even over time courses lasting several months (Figure 1.5A). In solution, actin depolymerization has been shown to be slowed by the presence of crosslinkers in a concentration dependent manner (Schmoller et al., 2011). Therefore, it may be that the dense network of crosslinkers in stereocilia, estimated to be present at every 10^{th} actin subunit, is responsible for the extreme stability of these actin filaments (Shin et al., 2013). Interestingly, in contrast to the static actin filaments of the stereocilia shaft, the crosslinkers themselves appear to turnover in minutes for OHC stereocilia and hours for IHC stereocilia (Roy and Perrin, 2018). Additionally, some

stereocilia membrane proteins are also dynamic such as the plasma membrane Ca^{2+}-ATPase (PMCA2) which exhibits turnover in 5-7 hours (Grati et al., 2006).

1.2.1.2 Turnover

Experiments which demonstrated the remarkable stability of the majority of the actin in stereocilia also point to a dynamic environment of actin turnover at the tips of stereocilia (Figure 1.5A). This region of actin turnover is fairly uniform in size among the tallest row stereocilia but is much more variable, and often larger, in the transducing stereocilia (Narayanan et al., 2015). This leads one to wonder whether local changes in ion concentrations caused by the opening and closing of the MET channels at the tips of the transducing stereocilia are responsible for the observed actin turnover. Results from experiments in our lab which blocked the MET channels supports this hypothesis and raise interesting questions regarding the possibility that this represents a mechanism to maintain the sensitivity of, and even repair damage to, the MET machinery at the tips of these shorter stereocilia (Vélez-Ortega et al., 2017).

1.2.2 Rootlets

In addition to the crosslinked filaments of the actin core, another, distinctly arranged, collection of actin filaments called the *rootlet* is an integral component of stereocilia (Tilney et al., 1980). Unlike the well characterized rootlets of cilia, there is still much we do not know about the rootlets of stereocilia. The rootlet appears to anchor the stereocilia to the *cuticular plate* which is a large bowl-shaped region at the apex of hair cells composed of a mesh of actin filaments with no directionality (DeRosier and Tilney,

1989). The rootlet is present both in the center of the shaft of stereocilia and extending down into, and occasionally all the way through, the cuticular plate and the length of a rootlet is proportional to the height of its stereocilium (Figure 1.6A) (Furness et al., 2008).

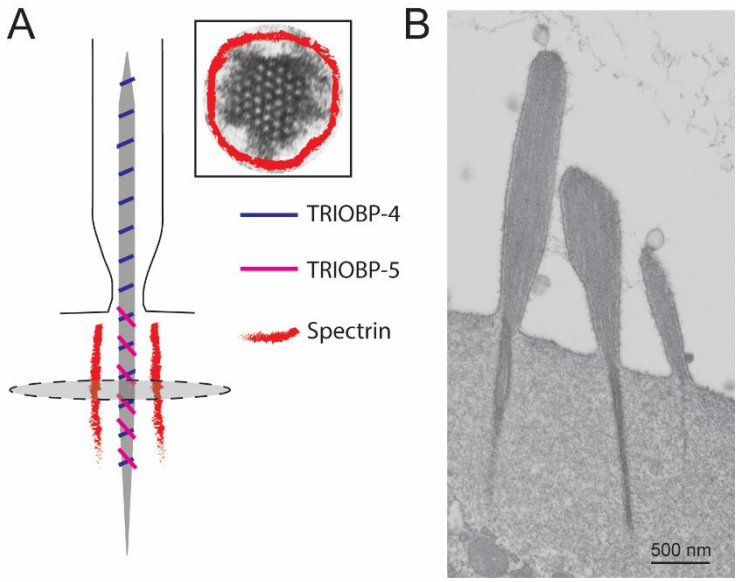

Figure 1.6. Illustration and micrograph of stereocilia rootlets

A, Illustration of a stereocilia rootlet with localization of selected associated proteins. Inset (Modified from Itoh and Nakashima, 1980) shows micrograph of tightly packed actin filament organization from cuticular rootlet. Spectrin is present at the apex in a ring around the filaments of the cuticular rootlet. B, Micrograph of stereocilia from a cochlear explant cultured for 2 days from a P4 mouse showing a well-developed cuticular rootlet but no supracuticular rootlet.

It is believed that the rootlet is the structure which permits the stereocilia to pivot at its base when deflected but the exact mechanism by which this occurs is unclear (Flock et al., 1977). F-actin within rootlets are spaced more closely than the F-actin making up the

rest of the stereocilia and this likely precludes the presence of any crosslinking proteins between filaments (Itoh and Nakashima, 1980). Instead, the F-actin of rootlets appear to be bundled together by a protein, TRIOBP, which seems to wrap around the bundle (Kitajiri et al., 2010). Without crosslinkers restricting movement it may be that the actin filaments within the rootlet have the ability to slide relative to one another like a bundle of sticks wrapped with twine (Tilney et al., 1983)..

1.2.2.1 Cuticular rootlet

The lower portion of the rootlet, located within the cuticular plate, is visible in mice within a few days after birth. The F-actin of cuticular rootlets are bundled by two isoforms of TRIOBP (TRIO and F-actin Bundling Protein): TRIOBP-4 and TRIOBP-5 (Kitajiri et al., 2010; Katsuno et al., 2019). Additionally, the actin crosslinker spectrin is found in a ring surrounding the cuticular rootlets of 1st and 2nd row stereocilia (Figure 1.6A inset) (Furness et al., 2008; Liu et al., 2019). Transmission electron microscopy (TEM) examination of the rootlet shows a narrow region between the densely packed F-actin of the rootlet and the actin mesh of the cuticular plate which is less dense than surrounding actin mesh (Furness et al., 2008). Small thin fibrils in this region appear to connect the F-actin of the cuticular rootlet to the surrounding cuticular mesh (Arima et al., 1987; Itoh and Nakashima, 1980; Furness et al., 2008). It is not clear if these thin fibrils connect the F-actin of the rootlet to the spectrin ring around them or if they are in fact spectrin. Pejvakin (PJVK), RIPOR2 and other unidentified proteins are associated with the cuticular rootlet, but their function is entirely unknown as of yet (Reviewed in Pacentine et al., 2020).

1.2.2.2 Supracuticular rootlet

Although rootlets appear continuous along their length, there is evidence to suggest that the F-actin of the upper, or *supracuticular*, rootlet is separate from the F-actin of the cuticular rootlet. Other than actin, the only protein associated with the cuticular rootlet which is also present in the supracuticular rootlet past the taper region of the stereocilia is TRIOBP-4 (Figure 1.6A) (Kitajiri et al., 2010; Katsuno et al., 2019). The supracuticular rootlet also develops much later than the cuticular rootlet and even as late as P6 the supracuticular rootlet is not visible or is very short (Figure 1.6B). It appears that the supracuticular rootlet begins to develop at the base of the stereocilia, growing up into the shaft. Until the supracuticular rootlet forms, the actin core in the lower part of stereocilia is uniform in appearance. The supracuticular rootlet is fully formed by about P16 in mice and the results from the actin incorporation studies mentioned previously rule out the possibility of the polymerization of new F-actin to make the supracuticular rootlet; however, the mechanism by which the existing F-actin at the center of the actin core is recruited into the developing supracuticular rootlet is unknown. Interestingly, TRIOBP-4 localizes to the shaft of stereocilia well before the supracuticular rootlet is actually visible (Katsuno et al, 2019).

1.3 Hearing loss

The ability to hear, while obviously not always a necessity, is nonetheless a strong evolutionary advantage. Interestingly, the ability to regenerate auditory hair cells, an ability shared by other members of the phylum *Chordata*, is a trick which mammals seem to have forgotten. Therefore, it is not terribly surprising that a lifetime of acquired injuries and acoustic insults universally lead to a decline in acuity with age. If anything, it is

actually more surprising that humans can continue to hear for more than a century without this regenerative capacity.

1.3.1 Threshold shifts

The scale used to quantitatively reference the intensity of a sound pressure level (SPL) is the decibel (dB) (Institute of Electrical Electronics Engineers, 1993). The decibel is a logarithmic scale with 0 dB SPL set at 20 μPa and every 20 dB representing a 10-fold increase in pressure (International Electrotechnical Commission, 1994-07). Although 0 dB SPL is commonly referred to as the human hearing threshold, our hearing sensitivity is frequency dependent and the actual threshold varies significantly within the human perceptual range of 20 to 20,000 Hz. Often, hearing loss is frequency specific and in age-related hearing loss reduced sensitivity begins at the higher frequencies so reliably that it is nearly unheard of for even a young adult in their 20's to be able to hear frequencies at 20 kHz.

Testing hearing thresholds in humans is usually relatively straightforward and involves the production of pure tones for a variety of frequencies and recording the minimum decibel level at which the subject reports being able to hear the sound. Studies of hearing thresholds in non-human animals requires a bit more work. The most common test used emulates the test described above but uses subcutaneous electrodes to measure sound evoked auditory brainstem responses (ABR). Frequency specific hearing thresholds are obtained by finding the lowest intensity tone which generates a characteristic electrical response.

1.3.1.1 Permanent v temporary hearing loss

Some age-related hearing loss can be compensated for with the use of hearing aids; however, because we cannot regenerate our hair cells, it never recovers. Not all hearing loss is permanent though (Figure 1.7). Noise-induced hearing loss (NIHL) can either be temporary or permanent and the clinical distinction between the two is determined by whether or not elevated hearing thresholds return to a normal range within a 2-week timeframe.

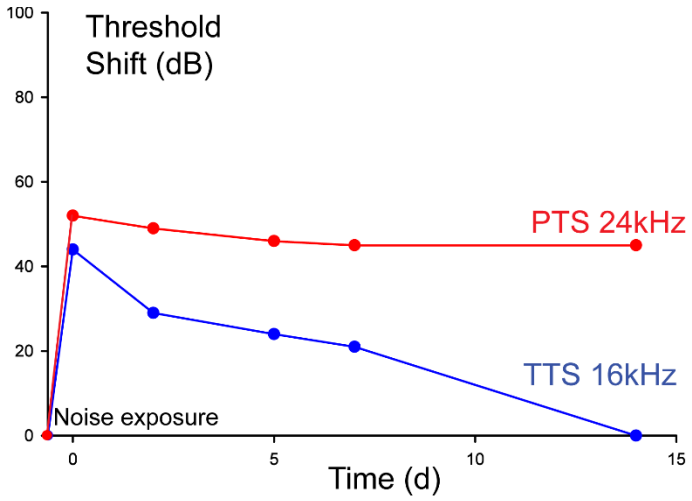

Figure 1.7. Example of auditory threshold shifts after noise exposure

Immediately after acoustic trauma auditory thresholds are elevated (measured in decibels). If hearing returns to normal within 2 weeks, it is considered a temporary threshold shift (TTS). If, however, there is a persistent increase in the hearing threshold it is considered a permanent threshold shift (PTS).

1.3.2 Noise exposure

How loud is too loud? The answer depends on the type of exposure and is often given in dBA, a weighted scale which focuses on frequencies in the middle range of human hearing. According to the National Institution for Occupational Safety and Health (NIOSH) division of the Centers for Disease Control (CDC), continuous exposure to 85 dBA for 8 hours causes NIHL and is the recommended exposure limit. Hearing protection, or a reduction in the noise exposure, is recommended at or above this limit. Up to approximately 120 dBA, it is thought to be possible for exposure to more intense noise to be safe by reducing the exposure time with an exchange rate of 3-dBA. This means reducing the exposure time in half for each increase of 3 dBA in noise intensity: 4 hours for 88 dBA, 2 hours for 91 dBA, etc. However, research in the past decade has uncovered a permanent component to "temporary" hearing loss, which will be discussed in more detail in section 1.3.4.2. This finding suggests that these guidelines may be based on erroneous assumptions which need to be reexamined (Kujawa and Liberman 2009).

The prevalence, and disabling effects, of hearing loss makes it an obvious area of interest for study. Numerous population studies have examined trends in NIHL among workers in various industries, soldiers, the elderly, and other groups. Research studies have sought to elucidate the anatomical and physiological consequences of noise exposure in hopes that a better understanding may lead to the development of therapeutic options to restore lost hearing or prevent damage from becoming permanent. Unfortunately, the degree of variability between studies in terms of the age and species of animal model used as well as the frequency range, intensity, and duration of the noise exposure is such that direct comparisons between studies is difficult. Instead, the results of the studies must be

examined for similarities and differences in temporary NIHL and permanent NIHL based on the location, extent and type of damage done.

1.3.3 Outer and middle ear pathologies

The exposure to moderately loud noises for extended durations can cause NIHL but does not damage the outer or middle ear. However, intense impulse, or blast, exposure can rupture the tympanic membrane and dislocate, or even break, the ossicles of the middle ear (Roberto et al., 1989). This type of injury is common among soldiers exposed to shockwaves from explosions or from firing their own weapons without proper ear protection (Breuck et al., 2014; Weyer et al., 2011). Depending on the severity of the damage, this type of injury may heal on its own with minimal medical treatment or require surgical intervention (Sridhara et al., 2013). Generally, this type of hearing loss is at least partially recoverable, especially if the damage is confined to the outer and middle ear structures.

1.3.4 Inner ear pathologies

Impulse noise exposure of 120 dBA or higher can damage the inner ear as well and in extreme cases entire sections of the organ of Corti can be detached from the basilar membrane (Roberto et al., 1989). However, for the vast majority of people this type of exposure is fairly rare. Instead, a more insidious culprit is to blame: long term exposure to moderate noise. Many common activities far exceed 85 dBA including: using a hair dryer, highway driving with the windows down, riding the subway, attending a concert, going out to the movies, and listening to headphones. These types of exposure are insidious because they are ubiquitous, culturally normative, and often are not perceived as painful

or even uncomfortable despite their damaging effects. Considering the words of the researcher A. James Hudspeth in an article published in November of 1985 in the journal *Science*, "With over a million essential moving parts, the auditory receptor organ, or cochlea, is the most complex mechanical apparatus in the human body," it is hardly surprising that damage to this exquisitely sensitive machinery takes a variety of forms (Hudspeth, 1985).

1.3.4.1 Metabolic effects

An interesting consequence of the extreme sensitivity of hair cells to vibration is that their environment is hypoxic relative to other tissues in the body (Kawakami et al., 1991). Capillaries and other blood vessels must be kept at a distance from the hair cells to prevent vibrations from the movement of blood gating the MET channels of the transducing stereocilia and depolarizing the hair cells (Axelsson et al., 1990; Nakashima et al., 1991). The cells of the organ of Corti are well adapted to this environment and under normal conditions it is not a problem. Acoustic trauma, however, causes a transient reduction in cochlear blood flow and which decreases the partial pressure of oxygen in the cochlea (Shin et al., 2019; Misrahy et al., 1958b). As a result of noise-induced hypoxia, neuronal signaling is reduced and normal cochlear metabolism is disrupted reducing sensitivity and elevating hearing thresholds (Misrahy et al., 1958a). As described below, acoustic trauma generates other pathological conditions within the inner ear, and it is unclear to what extent each pathology contributes to NIHL. However, increasing cochlear hypoxia without acoustic trauma, by reducing cochlear blood flow, also causes temporary threshold shifts (Misrahy et al., 1958a; Attias et al., 1990). The mechanism(s) by which

these metabolic disruptions affect hearing thresholds is debated and most likely multifactorial, but increased glutamate metabolism and elevated levels of reactive oxygen species (ROS) are prime suspects (Ji et al., 2019; Yamane et al, 1995). While the reduced cochlear blood flow from noise exposure is transient, the metabolic effects may lead to permanent damage depending on the intensity and duration of exposure.

1.3.4.2 Excitotoxicity

Excitotoxicity is a pathological phenomenon by which neurons are damaged by excessive postsynaptic activation by an excitatory neurotransmitter, glutamate in the inner ear. The ribbon synapses of IHCs which are essential for sustained neurotransmitter release at a high frequency also make their associated afferent neurons susceptible to excitotoxicity (Otterson et al., 1998; Glowatzki and Fuchs, 2002). Type I SGCs possess both non-selective cation ionotropic (AMPA, Kainate and NMDA) and metabotropic glutamate receptors (reviewed in Puel, 1995) In addition to the apparent neuroprotective effects of LOC innervation of the SGC dendrite, the presence of certain types of metabotropic glutamate receptors may help protect against excitotoxicity, although not all studies agree (Friedman, et al., 2009; Puel et al., 1995; Peng et al., 2004). Despite this, sustained excitation of the ionotropic glutamate receptors during noise exposure allows the entry of Na^+ from the perilymph into the dendrite of the type I SGC which results in an increase in osmotic pressure causing swelling which can eventually rupture the cell membrane (Robertson, 1983; Spoendlin, 1971). Although this swelling at the terminals of SGCs following even mild acoustic trauma with temporary threshold shifts (TTS) has been recognized for nearly 50 years, in the last decade studies have shown that this damage is permanent and increases prevalence of age-related hearing loss (Kujawa and Liberman,

2006). The swollen terminals retract and the SGC eventually dies (Kujawa and Liberman, 2009). Hearing thresholds measured by ABR are normal because each IHC synapses with multiple type I SGCs and not all of them become swollen (Furman et al., 2013). Although hearing thresholds are restored, the quality of the perceived sound, and the signal-to-noise ratio, are reduced in a phenomenon labeled "hidden hearing loss" (Schaette and McAlpine, 2011).

1.3.4.3 Cell death

Overstimulation from noise exposure can be damaging to the hair cells as well and HC death is often a prominent feature in instances of NIHL with permanent threshold shifts (PTS), especially among the OHCs (Wang et al., 2002; Hu et al., 2002; Wei-ju et al., 2010). Ischemia from noise-induced reductions in cochlear blood flow increases ROS production from oxidatively stressed mitochondria in cells with high energy demands like OHCs (Yamane et al., 1995; Ohlemiller et al., 1999). Additionally, noise exposure leads to an increase in intracellular [Ca^{2+}] in OHCs through prolonged activation of MET channels (Fettiplace and Nam, 2019; Szűcs et al., 2006) and possibly from the release of Ca^{2+} from subsurface cisternae (Sziklai et al., 2001; Lioudyno et al., 2004). Elevated intracellular [Ca^{2+}] in OHCs becomes sequestered in the mitochondria which also causes an increase in ROS production (Fettiplace and Nam, 2019). ROS induced mitochondrial permeability transition contributes to cell death from both necrosis and apoptosis (Hunter et al., 1976; reviewed in Crompton, 1999). In these cases of OHC loss after noise exposure the patient can still hear but, without the cochlear amplification provided by OHCs, their hearing threshold for the resonant frequencies of those missing OHCs will be elevated by about 40 dB (Dallos and Harris, 1978).

1.3.4.4 Stereocilia bundle damage

As the mechanosensitive apparatus of hair cells, the presence of stereocilia on the apical surface of a hair cell is as important to hearing as the presence of the hair cell itself. This has led to a great deal of interest in the effects of noise exposure on stereocilia and studies have been conducted in several different animal models. In addition to *in vivo* experiments of noise exposure, *in vitro* experiments have been carried out observing the effects of mechanical overstimulation on hair cell bundles in tissue explants. As with the variability found in noise exposure experiments, the *in vitro* studies vary in terms of the species of animal used, age at time of excision, time in culture, type of hair cell, and location of hair cell within the tissue as well as the type of stimulus used, its intensity and duration.

Due to their association with the MET channels at the tips of transducing stereocilia, tip-links are an integral part of the proper functioning of hair cells (Figure 1.4) (Pickles et al., 1984; Beurg et al., 2009). Damaging noise exposure can break tip-links *in vivo* (Pickles et al., 1987; Kurian et al., 2003; Husbands et al., 1999) *In vitro* tip-links can be ablated through the use of a calcium chelator such as BAPTA which eliminates mechanotransduction in affected hair cells (Assad et al., 1991) However, even in mammals tip-links regenerate and restore mechanoelectrical transduction within hours of being broken (Zhao et al, 1996; Indzhykulian et al., 2013). Despite their fragile appearance and calcium dependence, tip-links appear to be fairly resilient structures and are generally only mechanically broken when the stimulation has been sufficient to disrupt bundle morphology by breaking the other links connecting stereocilia (Clark and Pickles, 1996). Bundle dysmorphia following noise exposure causing both TTS and PTS has been well

characterized by scanning electron microscopy (SEM) and light microscopy (Liberman and Beil, 1979; Nikaido, 1992; Wang et al., 2011). Additionally, reversible changes in bundle stiffness without any apparent change in bundle morphology have been observed after mechanical overstimulation *in vitro* (Duncan and Saunders, 2000; Saunders and Flock, 1986). This generated much speculation regarding the possibility of damage to the underlying actin core of stereocilia which requires different imaging techniques to explore.

Examination of the actin core by fluorescent imaging of rhodamine-conjugated phalloidin, which preferentially binds to F-actin, has found areas of reduced fluorescent signal termed "gaps" in the stereocilia of guinea pigs exposed to severe acoustic trauma (Avinash et al., 1993). In another study with similar noise exposure, antibody staining revealed the accumulation of globular monomeric actin (G-actin), the actin crosslinker espin, and the F-actin severing protein cofilin in these phalloidin-less "gaps" which presumably lack F-actin (Belyantseva et al., 2009). Despite the compelling nature of this data, visualization of these gaps through fluorescent microscopy only provides tantalizing suggestions of the ultrastructure of the actin core of these stereocilia following acoustic trauma.

Examination of the F-actin within stereocilia by TEM imaging of ultrathin sections is able to reveal a more complete picture of the effects of noise exposure. In rabbit and cat models of PTS, months after the noise exposure, TEM micrographs of longitudinal sections, as well as serial reconstruction of transverse sections, though hair cells and their stereocilia reveal large regions of depolymerized actin, stereocilia displaced from their rootlets and broken at the base, lying on the cuticular plate (Figure 1.8A) (Engström et al., 1983; Liberman, 1987). Similar pathologies were found in alligator lizard cochlea

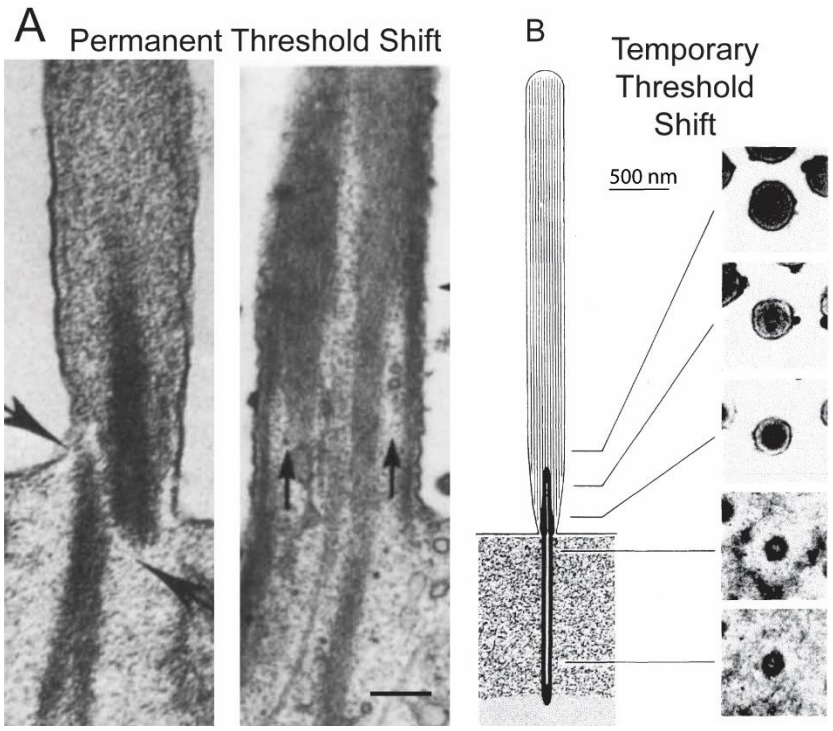

Figure 1.8. TEM images of damage to the actin core of stereocilia from acoustic trauma.

A, Damage to the stereocilia ultrastructure from intense noise exposure causing PTS. Left: (modified from Engström et al., 1983) Displaced OHC stereocilium with fractured rootlet (arrows) from rabbit. Right: (modified from Liberman, 1987) Regions of F-actin depolymerization (arrows) in an IHC stereocilium from cat. B, Damage to the stereocilia ultrastructure from moderate noise exposure causing TTS. (Modified from Liberman and Dodds, 1987) Illustration of a stereocilium with a shortened supracuticular rootlet reconstructed from transverse serial sections.

immediately after noise exposure which would have caused PTS in a mammalian species and also showed disorganized F-actin suggesting a loss of crosslinks in the actin core

(Tilney et al., 1982). The only other study examining the F-actin ultrastructure within damaged stereocilia was a TTS experiment which looked at serial reconstruction of transverse sections and found no abnormalities except for a slight decrease in the height of the supracuticular rootlet in the stereocilia of noise exposed cats (Figure 1.8B) (Liberman and Dodds, 1987).

1.4 Research hypothesis

This project began when I examined resin embedded tissue samples from *in vitro* overstimulation experiments carried out in mice by Dr. Ruben Stepanyan during his postdoctoral work in the lab. I quickly discovered stereocilia with large gaps in the actin core which bore a resemblance to the gaps in phalloidin staining seen in the stereocilia of noise exposed guinea pigs (Figure 1.9) (Belyantseva et al., 2009).

A supposition of that paper was that γ_{cyto}-actin, although not required for stereocilia development, is an essential component of stereocilia F-actin repair. In vitro work with guinea pig and chick hair cells using a fluid-jet to deliver damaging stimulation resulted in a decrease in bundle stiffness which was recoverable. This led us to wonder if there was a connection between these gaps and reversible changes in bundle stiffness. *We hypothesized that mechanical and acoustical overstimulation generates repairable breaks in an otherwise stable actin core.*

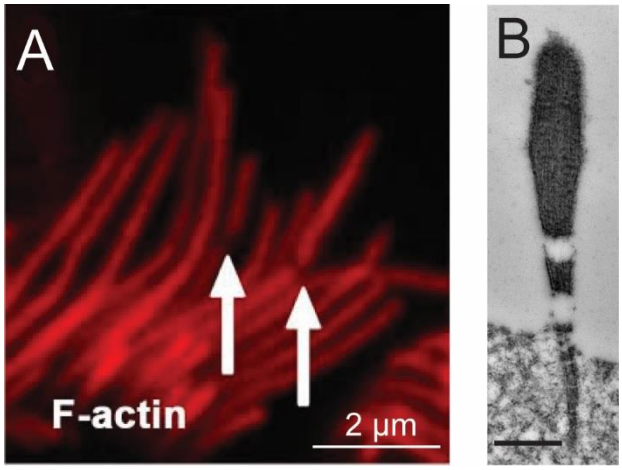

Figure 1.9. Gaps in the F-actin of overstimulated stereocilia.

A, (modified from Belyantseva et al., 2009) Gaps in the phalloidin staining of F-actin in guinea pig IHCs after intense noise exposure. B, TEM micrograph of gaps in the F-actin of a mouse stereocilium mechanically overstimulated *in vitro*. Overstimulation experiment was conducted by Dr. Ruben Stepanyan. Scale bar is 500 nm.

First, we confirmed that we could use a fluid-jet to generate a repairable decrease in bundle stiffness in cultured explants. Second, we sought to confirm that breaks in the actin core from fluid-jet overstimulation were the cause of the decrease in bundle stiffness and that the breaks could be repaired. Finally, we attempted to demonstrate a translational connection between these repairable breaks found *in vitro* and temporary noise-induced hearing loss.

Chapter 2 outlines the materials and methods utilized in this study. Chapter 3 presents the experimental results and analysis. Lastly, a discussion of the results and future directions for other researchers is set forth in Chapter 4.

CHAPTER 2. **MATERIALS AND METHODS**

2.1 Organ of Corti explants

Cochlear explants were used to examine the effects of fluid-jet overstimulation on stereocilia ultrastructure. Due to the need to study changes in the stereocilia 24 hours after fluid-jet overstimulation cultured explants were utilized for the *in vitro* experiments. Unfortunately, hair cell viability is too brief in organ of Corti explants to use older pups and so explants were isolated at postnatal days 3 (P3) through P5 from male and female CD1 wild-type mice (Charles River Laboratories, Wilmington, MA) and Sprague-Dewley rats (RRID:RGD_734476, Charles River Laboratories). All animal procedures were approved by the University of Kentucky Institutional Animal Care and Use Committee (protocol # 903M2005).

2.1.1 Dissection

Pups were decapitated after several minutes of anesthesia in a cold box and the scalp was removed. The skull and brain were transected along the midsagittal plane and then again along a coronal plane immediately posterior to the eyes yielding two halves. Subsequent microdissection with forceps was carried out in a plastic Petri dish containing refrigerated Leibovitz's L-15 medium (Gibco). The temporal bones were uncovered in each half by excising the brain and meninges from the skull and then the developing bony labyrinth was removed to fresh L-15 medium in a separate Petri dish. The cochlear duct was exposed by removing the incompletely ossified otic capsule and then, holding the basal turn with the forceps, it was pulled in one smooth motion from the modiolus. Conveniently at this age, holding the basal turn at the spiral limbus and pulling away the stria vascularis

in a single smooth motion exposes the organ of Corti by tearing away at the spiral prominence and also removing the Reissner's membrane.

2.1.2 Tissue culture

For imaging purposes explants were cultured in glass-bottom Petri dishes (MatTek Corporation) using a culture medium of Dulbecco's Modified Eagle's Medium (DMEM) (Gibco) with 7% fetal bovine serum (FBS) (Atlanta Biologicals) and 10 µg/mL ampicillin (Calbiochem). The explant was transferred from the L-15 medium by use of a glass pipette. A light positive pressure was applied to the pipetteman during transfer so that the surface tension of the medium held the explant at the very tip of the pipette. Touching the tip of the pipette to a small (200 µL) bubble of culture medium on the glass-bottom Petri dish expelled the explant with minimal transfer of L-15. The explant was then centered in the dish and uncoiled as much as possible. In order to aid adherence, the scant volume of culture media was carefully spread to the edge of the glass-bottom keeping the explant in place by the surface tension of the media. To minimize evaporation of the small volume of media the dish was sealed with Parafilm® M (Bemis Company, Inc.). Dishes were placed in an incubator at 37°C and 5% CO_2 for approximately 12 hours to allow attachment of the explant (Figure 2.1). At this point an additional 2 mL of fresh culture media was added to the dish and the explants were returned to the incubator without Parafilm for 1-2 days.

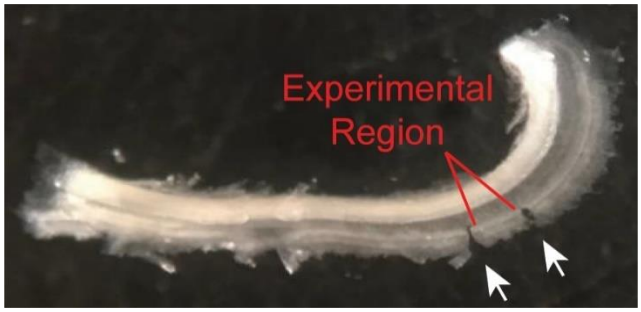

Figure 2.1. Image of a cochlear explant

Cochlear explant from a P3 mouse. Arrows indicate where OHCs have been been removed by suction through a micro pipette. This served to demarcate the experimental region, where IHC stereocilia bundles would be overstimulated. Hair cells outside the experimental region, as well as OHCs within the region, served as unstimulated controls.

2.2 In vitro overstimulation

Tissue cultures were removed from the incubator and the tectorial membrane was painstakingly removed. In order to provide optimal imaging conditions, the culture medium was replaced with clear L-15 medium at 37°C prior to viewing under the microscope.

2.2.1 Light microscope set up

Imaging was carried out at room temperature (RT) using an upright Nikon microscope with a 60x Olympus water-immersion objective (1.0 NA, 2.0 mm working distance). The microscope was equipped with DIC and 1.6x secondary magnification lens.

2.2.2 Micro pipettes

10 cm long borosilicate glass capillaries (World Precision Instruments) were placed into a P-2000 infrared laser puller to make micro pipettes. Pipettes with a small diameter (~ 4-6 µm) were used for fluid-jet stimulation of hair cell bundles. Larger diameter pipettes (~ 8-10 µm) were used as suction pipettes to remove detritus from the surface of stereocilia bundles, to remove individual cells and to clear blockages in the fluid-jet pipette during the procedure.

2.2.3 Demarcation of experimental area

Once the area of interest was located and optics were adjusted to optimal resolution, a region of ~ 20 IHCs was selected as the experimental region. In order to locate this region for later imaging the experimental region was demarcated by using the larger diameter suction micro pipette to remove a group of OHCs and supporting cells on either side of the experimental region (Figure 2.1 and Figure 3.2a). Subsequently the suction pipette was used to clear any extracellular debris very gently from the surface of the IHC stereocilia bundles in both the experimental region and from several IHCs in the control region on either side. This also served as a control against preservation artefact and ensured that damage to the IHC stereocilia in the experimental region could be attributed solely to the fluid-jet overstimulation.

2.2.4 Fluid-jet stimulation

Fluid-jet stimulation was delivered to each IHC stereocilia bundle in the experimental area using the smaller diameter pulled micro pipettes filled with the L-15 medium bath solution. A High-Speed Pressure Clamp (HSPC-1, ALA Scientific) was used

to generate pressure at the back of the micro pipette. The pipette was oriented over the modiolus with the tip of the pipette centered 4-6 µm from the 1st row stereocilium at the bundle vertex. In this position, positive pressure applied through the micro pipette would generate a fluid-jet to push the bundle in the direction of transduction and negative pressure applied through the micro pipette would pull the bundle in the opposite direction. The pressure applied to generate the fluid-jet was controlled using a MultiClamp 700B amplifier and pClamp 10 software (Molecular Devices).

2.2.4.1 Test deflections

With the goal of determining the effects of overstimulation on bundle stiffness it was decided to examine the degree of bundle deflection in response to brief low pressure stimulations as had previously been done in the lab (Kitajiri et al., 2010). Deflections in the direction of transduction defined as a positive deflection. Starting with the pressure set at -10 mmHg, the bundle was stimulated with pressure increasing in a stepwise manner at 5 mmHg increments to a maximum pressure of 25 mmHg. These test deflections were delivered immediately before (Figure 2.2A) and after damaging overstimulation (Figure 2.2B).

2.2.4.1 Overstimulation

Damaging deflections were generated by fluid-jet overstimulation of the bundles at higher pressure after the test deflections. A cycle of positive and negative deflections was delivered 20 times. The pressure of positive deflections was 50 mmHg and the pressure of negative deflections was -50 mmHg and each had a duration of 1 second with 0.5 seconds

between deflections. The test deflection was repeated after overstimulation before moving to the next bundle.

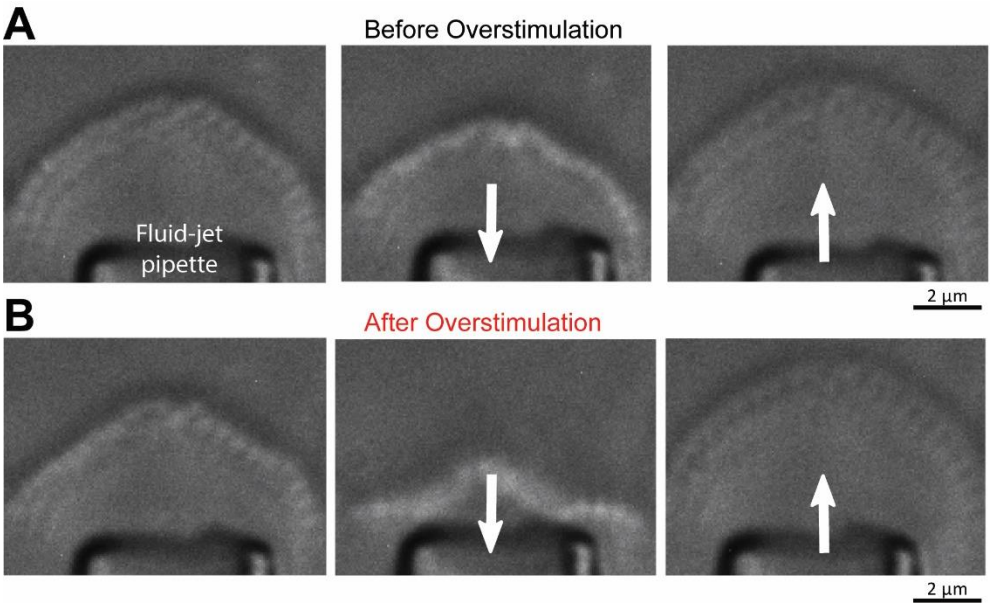

Figure 2.2. Testing bundle stiffness with a fluid-jet.

A, Images from video recordings of deflections of an IHC bundle with a low-pressure fluid-jet before overstimulation. Left panel shows bundle at rest. Middle panel shows bundle deflection in response to -10 mmHg fluid-jet. Right panel shows bundle deflection in response to +25 mmHg fluid-jet. B, Images from the same bundle immediately after overstimulation. Left panel shows bundle at rest. Middle panel shows bundle deflection in response to -10 mmHg fluid-jet. Right panel shows bundle deflection in response to +25 mmHg fluid-jet.

2.2.4.1.1 RECOVERY

The explant was immediately removed from the microscope after deflections of the last bundle in the experimental region. The L-15 media was replaced with culture media in samples designated for recovery and they were returned to the incubator for 24 hours. At the end of the recovery time they were removed from the incubator and the culture media was replaced with clear L-15 media for imaging. The explant was returned to the microscope and the experimental region was located and each IHC bundle in the experimental region again received test stimulations.

2.2.5 Video recording of stimulation

To measure bundle deflections, we recorded the bundle during low pressure test deflections generating an AVI video at 30 frames per second. Each IHC within the experimental region was designated by number in the file names so that recordings for each bundle could be compared before overstimulation, after overstimulation, and after 24 hours recovery.

2.3 Video analysis

The AVI video files were opened in ImageJ software (ver. 1.5x) and converted to greyscale before being saved as a TIFF stack. The MetaMorph for Olympus Imaging Series v.7.7 (Molecular Devices) was then used to open the TIFF stack. The stack was examined visually for a qualitative assessment to identify a stereocilium which was identifiable throughout the stack during deflections and which was representative of the deflections of the bundle as a whole. The position of the stereocilium was visualized at its largest negative and positive deflections and a line covering the range of deflection was drawn perpendicularly to the hair bundle. The average pixel brightness within a 2-3-pixel range

along this line for each image were saved in a LOG file. Using a custom written algorithm, written in MATLAB (MathWorks) and originally developed to measure OHC electromotility (Frolenkov et al., 1997), the frame-by-frame position of the stereocilium was computed from the LOG file generated by the MetaMorph program.

2.3.1 Measuring bundle deflections

The data from the MATLAB program was exported to an Excel (Microsoft) file and a line graph was created to visualize the position of the stereocilium (y-axis) in each frame (x-axis) throughout the test deflections (Figure 2.3). For each deflection, a baseline position for the stereocilium was determined by averaging 15 consecutive data points immediately preceding the deflection. Similarly, the position of the stereocilium during each deflection was determined by averaging 15 consecutive data points in the middle of the deflection. The deflection distance was calculated by subtracting the position value during the deflection from the baseline position value and converting to μm based upon the field of view of the microscope lens as determined by a stage micrometer. The deflection distance was plotted at each pressure level of the test deflections for the same stereocilium before overstimulation, immediately after overstimulation and after 24 hours recovery in the incubator (Figure 3.1a).

2.3.2 Estimating stiffness

Bundle stiffness was estimated as the resistance of the bundle to deflection by the fluid-jet. To quantify bundle stiffness, a linear fit was applied to the bundle deflection distances at pressure levels from -5 mmHg to +15 mmHg during the test deflections and the inverse of the slope of the linear fit was calculated. Stiffness was estimated for each

bundle before overstimulation, after overstimulation and after 24 hours recovery. The averages for each treatment group across bundles were reported relative to control (Figure 3.1b).

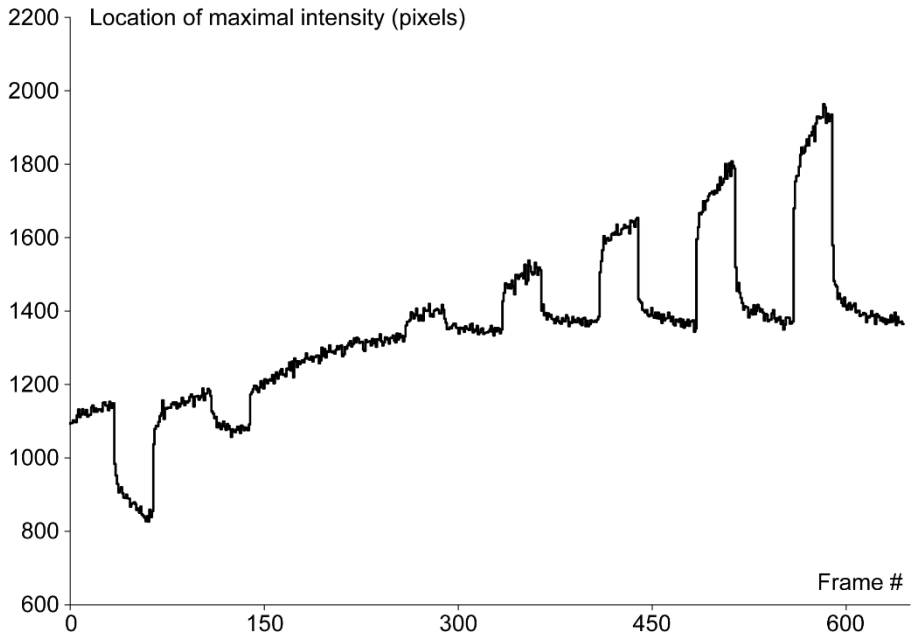

Figure 2.3. Measuring bundle deflection from fluid-jet stimulation.

Representative graph of bundle deflections by fluid-jet. Video recording at 30 fps was made of stereocilia bundle deflections in response to fluid-jet stimulation. A line scan of the path of deflection of a stereocilium recorded the average pixel brightness within a 2-3 pixel range along this path. The frame-by-frame position of the stereocilium was subsequently computed and plotted in a graph.

2.4 Scanning Electron Microscopy (SEM)

To determine whether fluid-jet overstimulation resulted in a loss of tip-links, two organs of Corti explants were examined by SEM. Tip-link counts from bundles in the

experimental region which had been subjected to fluid-jet overstimulation were averaged and compared to the average tip-link counts from unstimulated control bundles outside the experimental region. Unfortunately, visualization of tip-links via SEM precludes the possibility of comparing an individual bundle before and after overstimulation due to the tissue preparation prior to SEM imaging.

2.4.1 Glutaraldehyde and Paraformaldehyde fixative

Fresh fixative was prepared for each experiment and the same fixative was used with all samples for electron microscopy. A stock solution of 0.1935 M Sodium Cacodylate buffer was made by dissolving 8.285 g of Sodium Cacodylate Trihydrate (Electron Microscopy Sciences - EMS) in 190 mL of ddH_2O with 200 µL of a 2 M $CaCl_2$ solution. The pH of the solution was adjusted to 7.42 with 0.1 N HCl and the final volume adjusted to 200 mL with ddH_2O.

For the fixative, 2 mL of 25% Glutaraldehyde and 2.5 mL of 16% Paraformaldehyde were added to 15.5 mL of the stock Sodium Cacodylate buffer. Glutaraldehyde and Paraformaldehyde (EMS) were high purity EM grade. Fixative is 2.5% Glutaraldehyde and 2% Paraformaldehyde in 0.15 M Sodium Cacodylate buffer.

2.4.2 SEM sample prep

To examine the overstimulation-induced changes in the IHC bundles before any repair processes could occur, Organ of Corti explants were fixed immediately upon being taken off the light microscope stage to stop cellular activity and preserve tissue structure. The L-15 media was almost completely removed and replaced with fixative and the dish was sealed with Parafilm and stored at 4°C overnight. The explants were rinsed 3x with

ddH_2O to remove an unbound fixative and then carefully detached from the glass-bottom Petri dish. SEM samples must be imaged in a vacuum which is incompatible with a wet sample. However, the evaporation of water from the sample creates a great deal of morphological distortion in the transition from a liquid state to a gas state due to its surface tension at the phase boundary between the two states. To avoid this, the sample must first be dehydrated by exchanging the water for Ethanol (EtOH) in which water is miscible.

2.4.2.1 Dehydration

To dehydrate the explant, it was first transferred into 3 mL of ddH_2O in a scintillation vial. Increasing amounts of EtOH (200 proof) were gently added in 6 steps (Table 2.1) to make an 80% EtOH solution. The tissue was incubated for 30 minutes at RT between each step. After the final 30-minute incubation in 80% EtOH the solution was almost completely removed from the vial and replaced with 20 mL of 200 proof EtOH and the explant was stored overnight at RT. The next day the EtOH in the vial was replaced with fresh EtOH from a new unopened bottle of 200 proof EtOH.

Although the surface tension of EtOH is much less than half that of water, drying the explant by evaporation of the EtOH would still distort nanoscale morphological features such as tip-links. To minimize the presence of artefacts the tissue samples underwent Critical Point Drying (CPD) with CO_2. For this process, the EtOH, which is miscible in both water and CO_2, served as a transitional fluid.

Table 2.1 Ethanol Series used for tissue dehydration for SEM prep.

Step #	EtOH Volume Added	EtOH Concentrations
1	158 µL	5%
2	175 µL	10%
3	417 µL	20%
4	1.25 mL	40%
5	2.5 mL	60%
6	7.5 mL	80%

2.4.2.2 Critical point drying

The explants were transferred from the scintillation vial into metal mesh boats under EtOH to prevent drying. The chamber of the CPD machine (EMS 850, Electron Microscopy Sciences) was filled halfway with EtOH and the boats containing the explants were placed inside and the lid securely closed. The chamber was cooled as CO_2(g) was added from a cylinder at high pressure. Most of the CO_2(g) was forced into a liquid phase under these conditions and began mixing with the EtOH. Over the course of a couple of hours the EtOH/CO_2 solution was slowly drained from the bottom of the chamber as CO_2 was constantly added while a constant temperature and pressure in the chamber was maintained. The concentration of CO_2 increased as the concentration of EtOH decreased until all of the EtOH was removed. The addition of CO_2 to the chamber was stopped and excess CO_2 was drained until the chamber was about half full of liquid CO_2 and half full of CO_2(g). At that point the exhaust valve was closed, and the temperature slowly increased inside the chamber. The increased temperature increased the pressure until the critical point was reached at about 35°C and 1200 psi. At the critical point, the density and surface tension of liquid CO_2 are indistinguishable from those of CO_2(g) and the specimen transitions from ‘wet’ to ‘dry’ without being subject to any surface tension from crossing

a phase boundary. The temperature of the chamber was maintained as the pressure was slowly released to below 1000 psi to prevent the transition of the CO_2 to a liquid phase.

2.4.2.3 Sputter coating

The boats with the dried explants were removed from the chamber of the CPD and the explants were gently taken and carefully pressed onto a conductive carbon adhesive tab on an aluminum pin mount. The pin mounts were then placed into motorized mount in a Sputter Coater (Q150T, Quorum Technologies, Guelph, Canada) and the air was evacuated from the chamber. A small amount of Ar(g) was introduced to the chamber and electric field applied to a thin Pt disc situated above the samples. The electric field in the Ar created a plasma which removed Pt from the disc and deposited it onto the samples while the motorized mount spun to ensure an even coating. The amount of Pt deposited onto the samples was determined by monitoring the piezoelectric properties of a quartz crystal in the chamber and was stopped when the thickness of the coating was 5 nm. Finally, N_2(g) was used to return the chamber pressure to atmosphere.

2.4.3 SEM Imaging

The mounted and Pt coated samples were placed into the chamber of a scanning electron microscope (Helios Nanolab 660, FEI, Heillsboro, OR). Air was evacuated from the chamber and an electron beam was delivered to the sample with an accelerating voltage of 10 kV and a 6.3 pA current. To achieve optimal visualization of surface topography the Through Lens Detector (TLD) was used to collect secondary electrons arising from inelastic collisions of the electron beam with the sample surface. To improve the signal-to-noise ratio the sample was imaged at a working distance of 4 mm from the pole piece of

the final lens and the micrograph was generated in a raster pattern with a dwell time of 30 µs.

2.4.4 Tip-link counts

The SEM micrographs were opened in Fiji (ImageJ2 ver 1.52n) and examined for tip-links. A link which connected the top of a transducing stereocilia to the side of the taller stereocilia immediately adjacent to it was considered a tip-link. Tip-link counts were recorded as tip-links per stereocilia pair.

2.5 In vivo noise exposure

Male and female young adult (~3 weeks old) CD1 wild-type mice were anesthetized and exposed to mild acoustic trauma. Auditory thresholds at specific frequencies were measured before noise exposure, and at multiple timepoints up to 2 weeks after exposure, to determine the degree of hearing loss, and recovery, resulting from the noise exposure protocol. All animal procedures were approved by the University of Kentucky Institutional Animal Care and Use Committee (protocol # 903M2005).

2.5.1 Anesthesia

A stock solution of Avertin (concentration 1.6g/mL) was made by dissolving 25 g of 2,2,2, Tribromoethanol (Sigma-Aldrich) in 15.5 mL Tert-amyl alcohol on a heated plate with magnetic stirrer overnight in a dark bottle. The Avertin working solution was made by adding 500 µL of Avertin stock to 39.5 mL normal saline in a 50 mL conical tube wrapped in aluminum foil to exclude light. The tube was placed inside a box on an orbital shaker overnight and the solution was filter sterilized through a 0.2-micron filter. Working

solution was stored in a foil wrapped container at 4°C. Mice were weighed immediately prior to intraperitoneal injection of a 0.4 mg/g dose of Avertin.

2.5.2 Auditory Brainstem Responses (ABR)

Anesthetized mice were placed on stage heated to body temperature and subdermal needle electrodes were positioned in the posterior cranial region. The nose cone of an MF-1 speaker (Tucker-Davis Technologies) was centered and positioned in front of the mouse at a distance of 1 inch from the midpoint between the mouse's ears. A System 3 Auditory Workstation (Tucker-Davis Technologies) was used with the BioSigRP software to measure ABRs. Brief, 5 ms, tone-burst stimuli were delivered with 20 Hz alternating polarity at 8, 16, 24 and 32 kHz and response signals were averaged 512 to 1024 times to generate an artefact-free waveform. Hearing thresholds were determined by finding the lowest stimulus level which evoked a recognizable characteristic waveform response.

2.5.3 Noise Exposure

Except for the control mice, all young adult mice were exposed to the same mild acoustic trauma. The anesthetized mouse and MF-1 speaker were positioned as described in section 2.5.2. A broadband (white) noise was delivered for a duration of 30 minutes at an intensity of 100 dB SPL.

2.5.3.1 Recovery

After noise exposure, mice which were in a recovery cohort were returned to their cages. Prior to being returned to animal housing they were observed for recovery from

anesthesia. Recovery mice in the imaging study were euthanized 24 hours after noise exposure as described below in section 2.5.4.

2.5.4 Dissection

Young adult mice were euthanized by gradual displacement of chamber air with compressed CO_2 delivered through a precision flowmeter. After unconsciousness, the flowrate was increased for 1 minute before the mouse was removed and immediately decapitated. Dissection then preceded as described in section 2.1.1 up to the removal of the bony labyrinth from the temporal bone.

2.6 TEM and Focused Ion Beam Scanning Electron Microscopy prep

Tissue preparation for transmission electron microscopy is similar to that for scanning electron microscopy in that fixation and dehydration are essential. However, instead of drying the sample after dehydration as is done for SEM, the dehydration fluid is exchanged for a resin which is then polymerized into a hard, plastic block. The block is then trimmed to expose the region of interest of the embedded tissue sample.

2.6.1 Fixation

The same fixative was used for all electron microscopy samples as described above in section 2.4.1. In addition, to better visualize actin filaments within the stereocilia, tissue samples for the TEM, and Focused Ion Beam Scanning Electron Microscopy (FIB-SEM), were post-fixed in a 1% Tannic Acid solution buffered with Sodium Cacodylate buffer which was made fresh immediately prior to use.

2.6.1.1 Explants

Organ of Corti explants were fixed immediately upon being taken off the light microscope stage to stop cellular activity and preserve tissue structure. The L-15 media was almost completely removed and replaced with fixative and the dish was sealed with Parafilm and stored at 4°C overnight. The explants were then rinsed 3x with Sodium Cacodylate buffer and post-fixed in 1% Tannic Acid for 1 hour. The explants were rinsed 3x with ddH_2O prior to cryoprotection with glycerol.

2.6.1.2 Young adult cochlea

In the older mice the lateral wall of the cochlear partition is connected to the ossified bone of the otic capsule and removal prior to fixation damages the organ of Corti. To fix the tissue, the round window membrane was removed with the stapes and the membrane of the oval window was removed with forceps. A small piece of bone was carefully removed from the apex of the cochlea exposing the cochlear partition. The tissue was then fixed by gentle perfusion using a fine needle and alternating delivery through the round and oval windows. The cochleae were transferred to a vial, submerged in a small volume of fixative, and stored at 4°C overnight. Unbound fixative was removed by perfusion of Sodium Cacodylate buffer before perfusion of 1% Tannic Acid for post-fixation. After 1 hour the cochleae were rinsed by perfusion with ddH_2O and were stored in ddH_2O at 4°C until final microdissection. During excision of the tissue from the cochlea the tectorial membrane was removed and the organ of Corti was cut into 4 pieces: Base, Mid-base, Mid-apex, and Apex. Our imaging study focused on the hair cells in the Mid-apex which tonotopically corresponds to the 8 to 16 kHz region where hearing thresholds recovered.

2.6.2 Cryoprotection

Out of a desire to reduce the presence of artefacts within tissue from sample preparation, cultured and young adult organ of Corti samples were dehydrated via freeze substitution. Preparatory to this technique the tissues were cryoprotected with 30% glycerol (EMS). Due to tissue thickness differences between neonatal and mature organ of Corti, the graded series of increasing glycerol concentrations to reach 30% were different for each tissue type. In the final step tissue samples were transferred to a small plastic petri dish of 30% glycerol with 3 mm Cu grids (described in section 2.6.3) and stored overnight at 4°C.

2.6.2.1 Explants

Prior to cryoprotection, fixed explants were gently detached from the glass-bottom Petri dish and transferred to a scintillation vial. The ddH_2O was replaced with increasing concentrations of glycerol in a graded series as indicated (Table 2.2).

Table 2.2 Glycerol series used for cryoprotection of in vitro explants.

Step	Glycerol Concentration	Incubation Time	Incubation Temperature
1	5%	2 hours	RT
2	10%	2 hours	RT
3	30%	Overnight	4°C

2.6.2.1 Young adult cochlea

The ddH_2O was replaced with increasing concentrations of glycerol in a graded series as indicated (Table 2.3).

Table 2.3 Glycerol series used for cryoprotection of in vivo tissue samples.

Step	Glycerol Concentration	Incubation Time	Incubation Temperature
1	5%	2 hours	RT
2	10%	2 hours	RT
3	15%	2 hours	RT
4	20%	2 hours	RT
5	25%	2 hours	RT
6	30%	Overnight	4°C

2.6.1 Freeze substitution and Uranyl Acetate staining

Freeze substitution was carried out in a Leica EM AFS2 freeze substitution machine after the following preparations. Tissue samples in 30% glycerol were placed on submerged 3 mm 200 hexagonal mesh Cu grids (EMS) with hair cells facing up. Approximately 5 mL of a 1% Uranyl Acetate in Methanol (MeOH) solution was placed in a small plastic cup which normally holds the embedding block molds for the EM AFS2. The cup was dipped into liquid nitrogen (LN) in a Styrofoam container until the Uranyl Acetate solution inside was frozen at which point the cup was submerged in the LN. The chamber temperature of the Leica EM CPC plunge freezer was chilled to approximately -150°C by adding LN to the compartment beneath the chamber. Chlorotrifluoromethane (Freon 13) gas was slowly added to a metal cylinder in the center of the chamber where it was condensed and kept in its liquid state by the low temperature. Freon 13 was selected as a cryogen because it lacks a Leidenfrost point which would cause uneven freezing of the sample. The small plastic cup with frozen Uranyl Acetate at the bottom was filled with LN and set inside the chamber next to the cylinder of liquid Freon.

To minimize thermal transfer, coated forceps were used to pick up the Cu grid and remove the tissue sample from the 30% glycerol. Bibulous filter paper was used to carefully

remove excess fluid from the grid leaving only a small amount surrounding the tissue sample. The grid with the tissue sample was quickly plunged into the liquid Freon to rapidly freeze the sample in vitreous ice. After about 30 seconds the grid and frozen tissue were swiftly placed on top of the frozen Uranyl Acetate under LN in the small plastic cup situated next to the liquid Freon. The small plastic cup was quickly transferred to the chamber of the EM AFS2 which was prechilled to -90°C and filled with N_2(g) to minimize water vapor contamination. The chamber lid was closed and covered to avoid precipitation of the photo-sensitive Uranyl Acetate. The chamber was maintained at -90°C which quickly evaporated the LN from the cup but kept the tissue sample frozen while the Uranyl Acetate solution melted.

The chamber was maintained at -90°C for 32 hours and then slowly warmed at about 4°C per hour to -45°C. During this time, the MeOH of the Uranyl Acetate solution slowly exchanged with the ice thus dehydrating the sample. Additionally, electron dense uranyl ions bonded to glycoproteins and nucleic acid staining the tissue membranes and improving contrast in EM imaging. Scintillation vials with MeOH were added to the chamber and given 1 hour to chill to -45°C. The tissue samples were rinsed 3x with MeOH by transferring between scintillation vials.

2.6.2 Lowicry resin

Lowicryl HM-20 (EMS) is a very low viscosity, clear methacrylate resin ideal for low temperature embedding. It consists of a monomer and a crosslinker which are combined in different proportions depending on the desired hardness of the final plastic block. For this study moderately hard blocks were desired, and the resin was prepared with 14.9% crosslinker and 85.1% monomer by weight. An initiator was used, measured to be

0.5% by weight, to accelerate the polymerization of the resin at the end of the protocol. The monomer, crosslinker and initiator were mixed together by bubbling N_2(g) through the solution for 5 minutes which also served to remove O_2 from the solution which could interfere with polymerization.

Lowicryl resin is miscible with MeOH and a 50% Lowicryl and 75% Lowicryl solution were made with MeOH and placed into the chamber to chill to -45°C. Tissue samples were transferred from the MeOH to the 50% Lowicryl solution and incubated for a minimum of 2 hours. This was repeated with the 75% Lowicryl solution before the tissue samples were transferred to a scintillation vial with pure resin and left to incubate for a minimum of 18 hours. Fresh Lowicryl resin was made and placed in the chamber to chill to -45°C. The tissue samples were moved to the fresh resin and incubated for another 24 hours at -45°C before being transferred to block molds. As much as possible the tissue was positioned in the mold so that the region of interest would be oriented perpendicular to the block face. The chamber was closed with a lid containing longwave UV emitting LEDs and the samples were left to settle for 1 hour before UV irradiation. The Lowicryl resin in the block mold was polymerized by longwave UV irradiation for a total of 128 hours while the chamber temperature was increased to RT in steps (Table 2.4) after which the blocks were removed from the mold and prepared for TEM or FIB-SEM imaging as described below.

2.7 Transmission Electron Microscopy

SEM is used to image a sample by detecting electrons which come off the surface of the sample similar to viewing an object under a stereoscope from the photons reflected

Table 2.4 Temperature changes during UV polymerization of Lowicryl resin blocks

Step	Beginning Temperature	Ending Temperature	Duration
1	-45°C	-45°C	27 hours
2	-45°C	0°C	9 hours
3	0°C	0°C	40 hours
4	0°C	20°C	4 hours
5	20°C	20°C	48 hours

off the object. TEM utilizes a higher energy electron beam (~100 kV accelerating voltage) to penetrate a sample and an image is generated by detecting the electrons which pass through the sample similar to viewing a tissue slide in a light microscope. The benefit of TEM is unparalleled resolution but there are some significant drawbacks outlined below.

2.7.1 Sectioning

In order to penetrate the sample and be detected the accelerating voltage of the electron beam must be higher in a TEM than in an SEM but the sample has to also be much thinner. Resin blocks were trimmed with a razor blade to expose the tissue and to shape the block face into a trapezoid ~ 1 mm wide. Using an ultramicrotome (UC6, Leica, Wetzlar, Germany) and a Tungsten Carbide knife (EMS) the block face was smoothed in 1 µm steps for ultrathin sectioning. Ultrathin sections (~90 nm thickness) were cut using a DiATOME Ultra 45° diamond knife. Sections were floated onto 3 mm 200 mesh hexagonal Cu grids and dried, section side up, in a glass Petri dish lined with filter paper (Whatmann) on a warm hot plate.

2.7.2 Imaging

The Lowicryl resin sections are more fragile than epoxy resin sections and required carbon coating prior to imaging to stabilize the section in the electron beam. The Pt disc of the sputter coater (Q150T, Quorum Technologies, Guelph, Canada) was removed and replaced with a carbon filament holder. The grids were placed section side up on a plastic Petri dish lined with filter paper adhered to a rotating platform in the coater chamber. After closing the lid, the chamber was evacuated, and a current was briefly applied to a carbon filament which deposited a thin layer of carbon on the grid. Chamber pressure was returned to atmosphere with N_2(g) and the grids were removed to be imaged. TEM imaging was done at 100 kV accelerating voltage on either a Phillips Tecnai 12 or a Hitachi Model H-7600.

2.7.3 Limitations

Although TEM can provide superior resolution the technique posed a number of problems for this project. The concho-spiral shape of the tissue meant that it rarely laid flat in the block and in most cases the area of interest moved and changed angles as the block was sectioned. The region of interest, the stereocilia bundle of an IHC, is ~ 20 μm^2 in a tissue spanning hundreds of microns and the lowest magnification was 800x which often resulted in long periods of time simply finding the area to image. The resin sections were weakest at the interface of the tissue which often meant the sections would be torn at the region of interest. The sections had to be supported by the 3 mm Cu grid and the region of interest was frequently resting on a supporting bar of the grid unable to be imaged. Even when the region of interest was able to be imaged, the stereocilia were rarely in a useful orientation; the success rate was ~5-20%. Attempts to adjust the angle of sectioning proved

fruitless as nanoscale adjustments were not possible on the ultramicrotome and any angle adjustment required re-facing the block. As a consequence, the next useable section was several microns deeper into the block than the one from which the adjustment was made and a new bundle, with a different orientation, was being imaged. While practice and skill did sometimes help with tissue orientation during sectioning and quickly locating the region of interest during imaging, finding useable, longitudinally sectioned stereocilia was purely a matter of luck.

2.8 Focused Ion Beam – Scanning Electron Microscopy

Many of the challenges of the TEM are eliminated in the FIB-SEM. The image resolution is not as good as a great TEM image but in this study that was easily offset by the ability to more reliably gather large numbers of useable images as serial sections. The SEM made it easier to discern the orientation of the stereocilia at the block face and they were never obscured by grid bars. The motorized stage allowed for smaller and more precise adjustments in the angle of imaging and sectioning. The FIB provided more controlled sectioning and the ability to serial section in 20 nm steps to generate a stack of images through a bundle. This made it possible to reconstruct a 3D image of the bundle and it also meant that stereocilia which were not perfectly oriented could be followed from one image to the next in a stack and provide useful data. Although the set-up to start imaging a new block could take several hours, once imaging began the amount of useable data for this study far exceeded what could be accomplished with the TEM.

2.8.1 Block prep

Prior to using the FIB-SEM the resin block had to be prepared by first trimming the front of the block to expose the tissue. Then, using the Tungsten Carbide knife and

ultramicrotome, the upper surface of the block had to be trimmed so that the apex of the hair cells was ~20 µm under the surface. The block was then adhered with epoxy to a low profile 45° / 90° pin mount and sputter coated with a 25 nm thick layer of Pt.

2.8.2 Serial sectioning

The block was placed into the FIB-SEM chamber and a Navigation Camera photo was taken to position the stage to image the block face with the electron beam and find the tissue using a 2 kV accelerating voltage and 0.2 nA current with the TLD capturing secondary electrons. Once the hair cells were located the block was repositioned to the eucentric height to put the region of interest at the coincidence point of the two beams which was confirmed by very brief imaging of the block with the ion beam at 30 kV and 7.7 pA to minimize damage. The stage angle was then adjusted so that the block face was parallel to the ion beam and the position saved as the milling position. The ion beam current was increased to 21 nA and a milling pattern was run which smoothed the block face at the hair cells to a depth of about 200 µm. The stage was tilted to bring the block face perpendicular to the electron beam and the Z height adjusted to a working distance of 2 mm. The lens mode was switched to magnetic immersion for improved resolution and In Column Detector (ICD) was used to collect backscattered electrons. Backscattered electrons are electrons from the beam which have undergone an elastic collision with an atom in the sample and bounced back along the beam path. Larger, more electron dense atoms are more likely to generate backscattered electrons and as a result the uranyl ions in the tissue stand out from the surrounding low-density resin. The stereocilia of a hair cell of interest was centered and brought into focus and the stage position saved as the imaging position.

The stage was returned to the saved milling position and, using the ion beam with a 47 nA current, 10 µm wide trenches were milled on either side of the region of interest. During serial sectioning the trenches serve to protect the block from re-deposition and excessive charging from the ion beam. The stage was then rotated 180° and tilted to bring the block face perpendicular to the ion beam. The current was adjusted to 21 nA and the top of the block was smoothed, removing about 5 µm of the resin above the tissue. The stage was again returned to the saved milling position and a small injection needle was positioned near the surface of the block. The injection needle delivered gases from heating $C_9H_{16}Pt$ which were broken down by the ion beam depositing a 500 nm thick protective layer of Pt on the surface of the block above the region of interest. The stage was moved to the saved imaging position and measurements were taken for final preparations before serial sectioning (Figure 2.4A). The stage was brought back to the saved milling position and then rotated and tilted to bring the block face perpendicular to the ion beam once again. Using the ion beam a small, 3µm deep fiducial pattern was milled just outside the serial sectioning region. The stage was returned to the milling position and the Slice and View (FEI) automation program was opened.

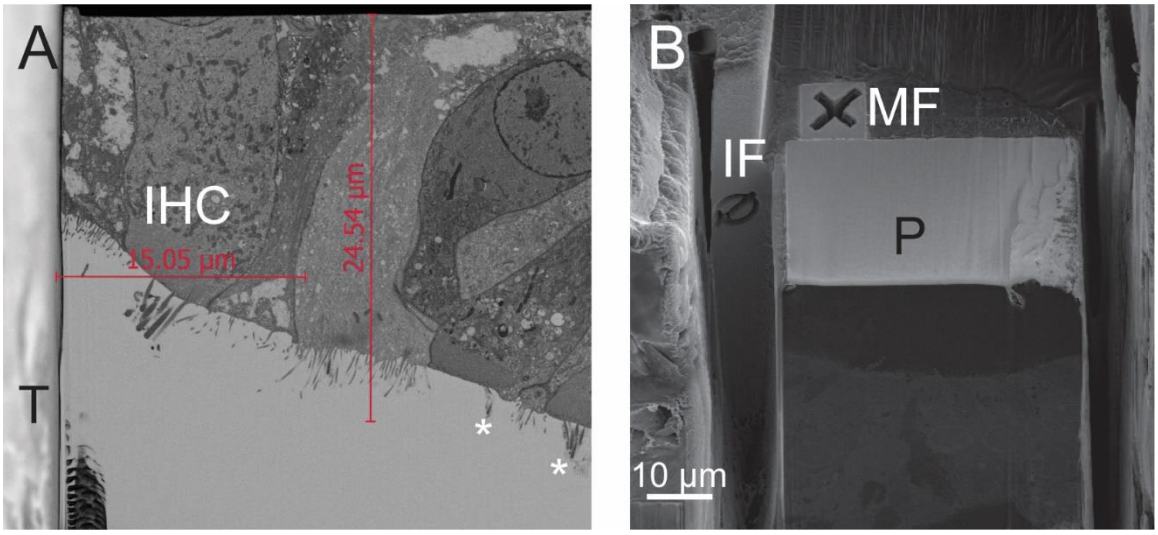

Figure 2.4. SEM images of the face of a resin block with embedded organ of Corti explant.

A, Image of block face showing organ of Corti. IHC is indicated and asterisks mark the presence of OHC bundles. The vertical line to the left of the IHC is the end of a protective trench (T). Red lines are measurements to determine positional placement. For milling of the imaging fiducial, the SEM measurements are used instead of ion beam imaging in order to minimize damage to the block face. B, Image of a block fully prepped for serial sectioning by the ion beam. A 500 nm thick pad of Pt (P) is deposited on the top of the block above the region of interest. Along with the trenches on either side this helps prevent re-deposition and excessive charging of the sample by the ion beam during milling. A milling fiducial (MF) is created on the top of the block to correct for drift before milling by the ion beam. An imaging fiducial (IF) is created on the block face to the side of region of interest to correct for drift before SEM imaging.

With the block face parallel to the ion beam another fiducial pattern was milled into the upper surface of the region of interest (Figure 2.4B). The serial sectioning region was defined, and its position saved relative to the fiducial pattern on the upper surface. The stage was then moved to the saved imaging position and the beam realigned and stigmation adjusted for optimal focus and resolution. The imaging region was defined, and its position saved relative to the fiducial pattern on the block face. The program was configured to capture backscattered electrons using both the ICD and TLD detectors to create two inverted images of the region each with slightly different quality. Finally, the autofocus was configured and tested before beginning the automated serial sectioning.

The automation began by returning the stage to the saved milling position and adjusting for drift using the fiducial. The ion beam then removed 20 nm of the block face from the serial sectioning region. The stage was moved to the saved imaging position and adjusted for drift using the fiducial. The electron beam imaged the apex of the hair cell at the block face by collecting backscattered electrons from a raster pattern. Once imaging of the region was complete, the stage was returned to the milling position and another 20 nm of the block face was removed by the ion beam and a new image of the block face was taken. This process was repeated over and over, generating a stack of serial images in 20 nm steps.

2.9 Image analysis of stereocilia ultrastructure

Data analysis required careful analysis of the serial FIB-SEM section images. Images were loaded into Fiji and saved as a TIFF stack. Stereocilia were counted and examined for any ultrastructure damage. Observed damage could be categorized as: a break

in the actin core, a displacement of a stereocilium from its cuticular rootlet, a shattered supracuticular rootlet or a hollow supracuticular rootlet.

Stereocilia with breaks were counted and recorded according to which row they were located in. The breaks were characterized by their size and their location relative to the cuticular plate. To measure this, the pixel size for the image stack as it was recorded by the SEM was saved under the image properties in Fiji. The size of a break (Figure 2.5A) was measured by drawing a line at the widest point of the break connecting the lower and upper edges. The location of the break relative to the cuticular plate (Figure 2.5B) was measured by drawing a line from the base of the stereocilia to the bottom edge of the break. When a stereocilium was displaced from its cuticular rootlet the displacement distance was measured by drawing a line from the center of the rootlet to the center of the stereocilium.

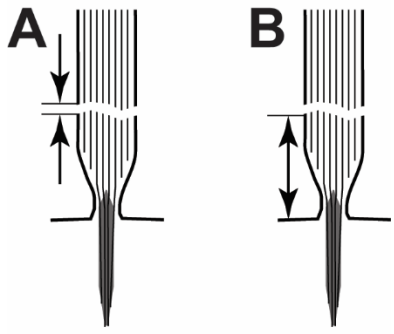

Figure 2.5. Illustration showing measurement of break characteristics in a stereocilia with a break in the F-actin.

A, The size of breaks were measured longitudinally at the widest point of the break.

B, The location of breaks were determined by measuring the distance from cuticular plate to the lower edge of the break.

2.10 3D reconstruction of serial FIB-SEM image stack

A custom-written MATLAB script was used to register and align the image stack from serial FIB-SEM sectioning of a hair cell bundle and saved as a new stack. The new stack was opened in Fiji and inverted. The stack was then median filtered and the Z-project function in Fiji was used to generate a maximum intensity projection of the stack.

CHAPTER 3. **RESULTS**

3.1 *In vitro* fluid-jet overstimulation causes a recoverable decrease in bundle stiffness

Transient decreases in bundle stiffness following *in vitro* fluid-jet overstimulation have previously been reported (Saunders and Flock, 1986; Duncan and Saunders 2000). However, those studies only speculated as to the underlying cause of the bundle stiffness changes. Our study is the first to examine the ultrastructure of the stereocilia F-actin in response to *in vitro* mechanical overstimulation. We restricted our study to IHC stereocilia for a number of logistical reasons: There are three rows of OHCs for every IHC and stimulating them all was too time prohibitive. The closely spaced rows of OHCs made it difficult to either stimulate a bundle without also inadvertently stimulating the bundle of the OHC in the row behind the targeted bundle or stimulate a bundle without also smashing the pipette into the bundle of the OHC in the row in front of the targeted bundle. It was very often impossible to determine which OHC we were examining when we were imaging with the TEM and we did not transition to the FIB-SEM until late in the project.

We first sought to determine whether we could generate the same repairable bundle stiffness changes in mouse and rat organ of Corti explants. A micro pipette filled with bath solution was positioned in front of IHC bundles and positive and negative pressure was applied to the back of the pipette which deflected the bundle (Figure 2.2a). Brief test deflections were carried out in both directions in a stepwise fashion beginning with a fluid-jet pressure of -10 mmHg and increasing the pressure by 5 mmHg with each deflection ending at +25 mmHg. We did a frame-by-frame analysis of video recorded during these tests to measure how far the bundle was deflected at each pressure level (Figure 3.1A).

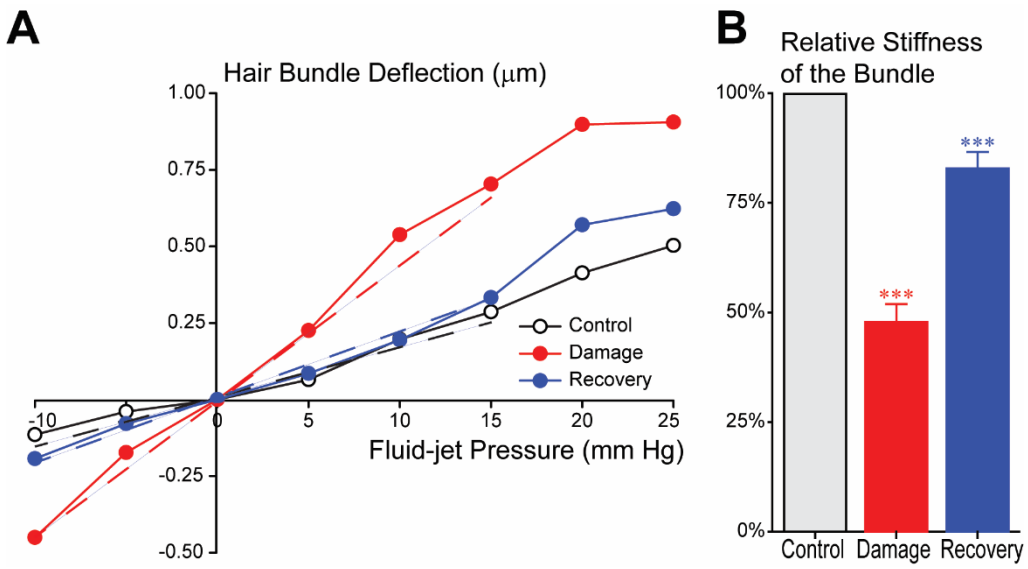

Figure 3.1. Fluid-jet overstimulation results in a recoverable loss of bundle stiffness

A, Representative pressure displacements from video analysis of bundle movement in response to test stimuli before overstimulation, immediately after overstimulation and after 24-hour recovery. B, Percent change in the relative stiffness of the bundle estimated by calculating the inverse slopes of linear fits of pressure displacement graphs, shown as dashed lines in A. Bars show mean ± SEM values of combined data of 17 cells from 3 explants. (***) indicates a P value < 0.001 determined by a Student's t-test.

For the damaging overstimulation we alternated between positive and negative deflections each lasting 1 second. We also increased the fluid-jet pressure to +50 mmHg and -50 mmHg. Immediately after overstimulation we repeated the test deflections (Figure 2.2b) and were able to measure an increase in bundle deflection at each pressure level (Figure 3.1A). We then estimated bundle stiffness using the inverse slope of the

displacement measurements and found a 52% reduction in bundle stiffness after mechanical overstimulation (Figure 3.1B).

To determine whether bundle stiffness would recover we returned the explants to the incubator for 24 hours. We then repeated the test deflections and measured the displacement of the stereocilia (Figure 3.1A) and found that bundle stiffness had recovered to 84% of normal (Figure 3.1B).

3.2 The reduction in bundle stiffness after overstimulation is not due to a loss of links.

In discussing the decreased bundle stiffness observed after fluid-jet overstimulation in guinea pig, Saunders and colleagues suggested that it was caused by damage to either the "rootlet region" or the links connecting stereocilia (Saunders and Flock, 1986).

Previously published results from experiments done in cultured, young postnatal mice in our lab showed that the use of BAPTA to remove most of the links between IHC stereocilia resulted in a small change in bundle stiffness (Kitajiri et al., 2010). Separate experiments in our lab (Indzhykulian et al., 2013), as well as other studies, have shown that tip-links are repairable within the 24 hours (Jia et al, 2009; Zhao 1996). Therefore, it is possible that loss of bundle stiffness we have observed in our current study is a result of the fluid-jet overstimulation breaking the links between stereocilia and that bundle stiffness returned within 24 hours because the links were repaired. However, it has also been reported that tip-links remain intact after noise exposure unless the other links between the stereocilia are also broken and the normal bundle morphology is lost (Clark and Pickles, 1996).

Although hair cell bundle morphology appeared unchanged in our experiment, we wanted to more closely examine whether fluid-jet overstimulation had an effect on the links between stereocilia. Therefore, we prepared explants for SEM by applying a Glutaraldehyde and Paraformaldehyde fixative to the explant immediately after removing it from the microscope stage. The tissue was then dehydrated with a graded series of Ethanol (Table 2.1) and critical point dried with CO_2 before being mounted and sputter coated with 5nm of Pt.

We compared bundles in the experimental region which had been overstimulated with those in the control region which had not (Figure 3.2A). We examined the links between stereocilia and observed no apparent differences between damaged and control bundles (Figure 3.2B). Due to the difficulty in quantifying side-links and top-links, which are often obscured from view, we focused on tip-links. In order to account for variations in the number of stereocilia from one bundle to the next, we quantified tip-links per stereocilia pair. We found a very slight 2% difference between the control and damaged bundles (Figure 3.2C) which was not significant ($p>0.28$) and concluded that the changes in bundle stiffness we observed were not caused by a loss of the extracellular links between stereocilia.

3.3 Mechanical overstimulation results in damage to the F-actin of stereocilia

Since we were unable to attribute the loss of bundle stiffness to a loss of links, we next decided to look at damage to the stereocilia in the bundles. Overall bundle morphology was unchanged as seen by SEM (Figure 3.2B) but damage to the F-actin of the stereocilia could change the mechanical properties of the bundle. Supporting this idea are studies showing damage to the F-actin at the base of stereocilia following noise exposure

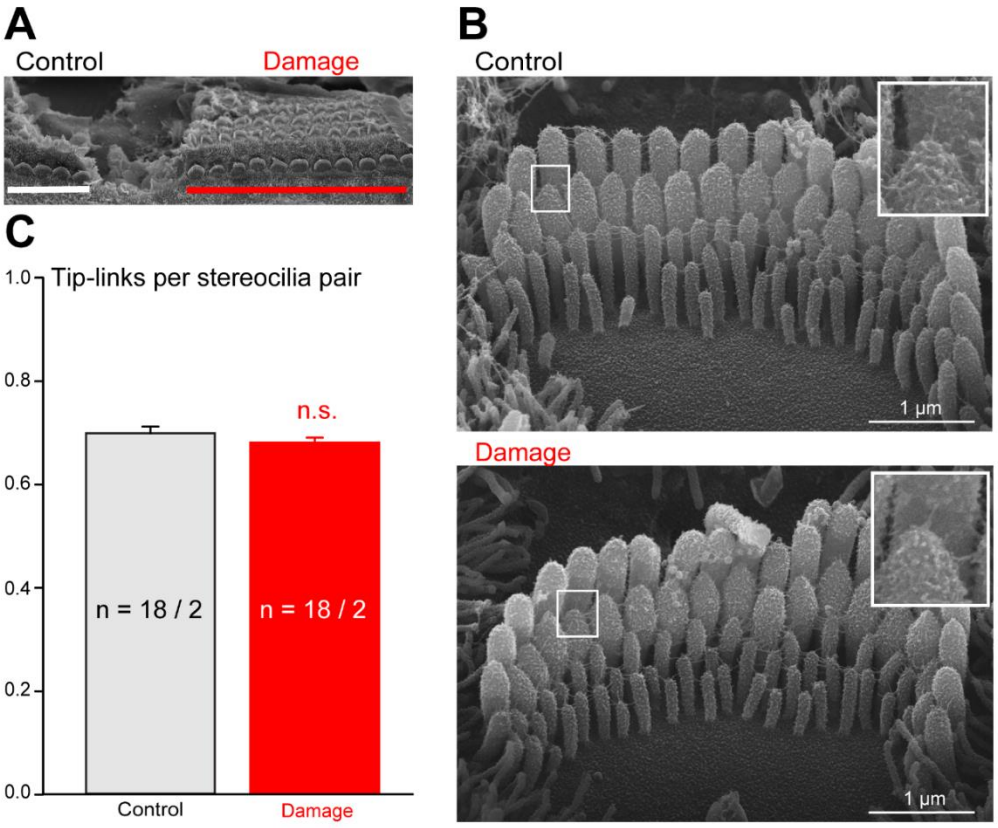

Figure 3.2. Fluid-jet overstimulation does not cause a loss of links between stereocilia

A, SEM micrograph showing the removal of hair cells to demarcate the experimental region (red) from the flanking control region (white). B, Representative SEM images of IHC stereocilia bundles from a cochlear explant. Upper panel is a control bundle from an unstimulated region of the explant. Lower panel is a bundle after fluid-jet overstimulation. Insets show tip-links between second and first row stereocilia at higher magnifications. C, Percentage of stereocilia pairs with intact tip-links. Bars show mean ± SEM values of combined data of 18 cells from 2 explants each. (n.s.) indicates no significance determined by a Student's t-test.

(Engström et al, 1983; Liberman, 1987). However, these studies were examining the effects of PTS months after noise exposure. Only one study (Liberman and Dodds, 1987) looked at short term damage in TTS from noise exposure, in a mammal, and found no change in stereocilia ultrastructure aside from a slight shortening of the supracuticular rootlet. No previous study has examined the F-actin ultrastructure after *in vitro* overstimulation.

To examine the immediate effects of overstimulation we quickly fixed the explants after removing them from the microscope stage. We then post-fixed in tannic acid, to improve the visualization of actin, before dehydration by freeze-substitution followed by resin embedding in Lowicryl. The explants were imaged using either TEM or FIB-SEM.

The stereocilia from control IHCs appeared normal (Figure 3.3A) with parallel actin filaments. The supracuticular portion of the rootlets are not developed at this age (P4+2) but the cuticular rootlets are well developed and aligned with their stereocilium. In contrast, 43% of the stereocilia we imaged which had been overstimulated had submicron breaks in the F-actin at their base (Figure 3.3B red arrows). Unlike our findings with the links, the presence of these breaks in the damaged stereocilia, which we did not find in any control stereocilia, was highly significant ($P < 0.001$) and could explain the decrease in bundle stiffness observed after fluid-jet overstimulation. FIB-SEM serial sectioning allowed us to follow a break throughout the entire diameter of stereocilia (Figure 3.4) and we determined that the breaks do not completely transect the stereocilia. They are generally confined to a localized area near the periphery of the actin core and the stereocilia can remain supported by the unbroken F-actin.

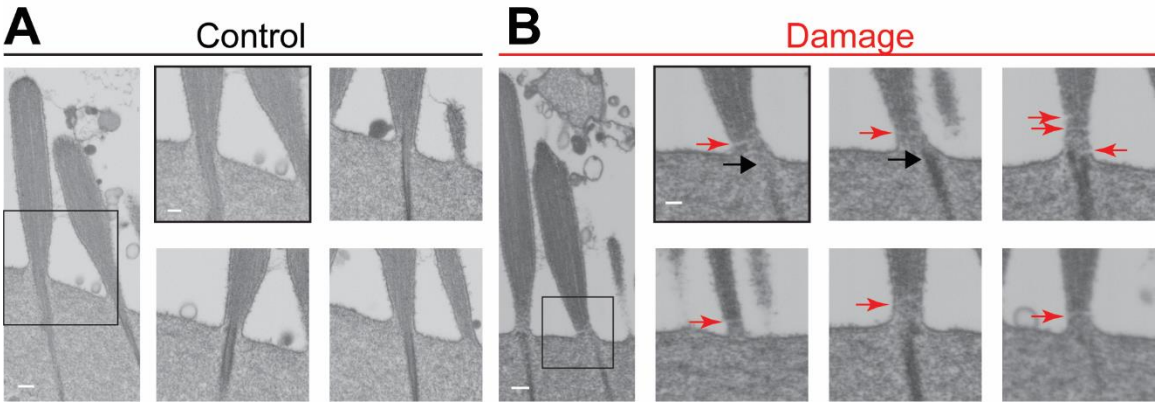

Figure 3.3. Fluid-jet overstimulation causes breaks in the F-actin of stereocilia in vitro

A, B, Representative FIB-SEM images of IHC stereocilia from cochlear explants. A, Stereocilia from unstimulated control bundles showing normal F-actin in the shafts and cuticular rootlets. B, Stereocilia from overstimulated bundles fixed immediately after overstimulation. Red arrows indicate breaks in the actin core. Black arrows indicate displacement of the stereocilium from its cuticular rootlet. Scale bars are 200 nm (larger images) and 100 nm (smaller images). Age of explants: A, P4+2, B, P4+1

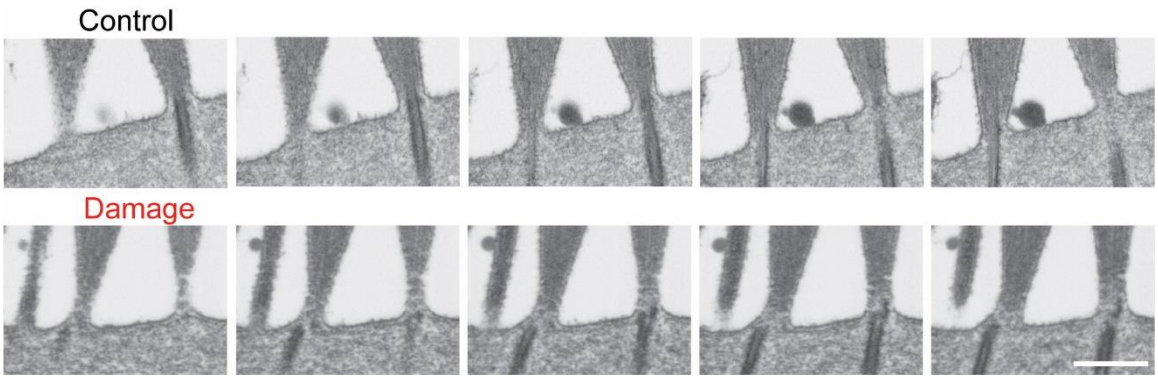

Figure 3.4. Breaks in the F-actin from overstimulation do not transect the stereocilia

FIB-SEM 20 nm serial sections of unstimulated control (top) and overstimulated damage (bottom) stereocilia showing that breaks in the F-actin do not transect the entire width of the stereocilia. Scale bar is 500 nm.

3.4 The submicron breaks in the F-actin are localized at the base of stereocilia

Next, we went through the images to analyze the characteristics of the breaks. We examined the ultrastructure of 228 stereocilia from 11 overstimulated IHC bundles. On average we found breaks in the F-actin of 38% of the stereocilia in a bundle (Figure 3.5A). We also examined the ultrastructure of 756 stereocilia which had not been overstimulated (269 from 24 IHC bundles and 487 from 27 OHC bundles) and found no breaks in the F-actin.

We measured the size of the breaks longitudinally using the line measurement tool in ImageJ. The breaks were very small ranging in size from 11 to 71 nm with an average size of 27 nm. We also separated the breaks by row to see if the height of the stereocilia

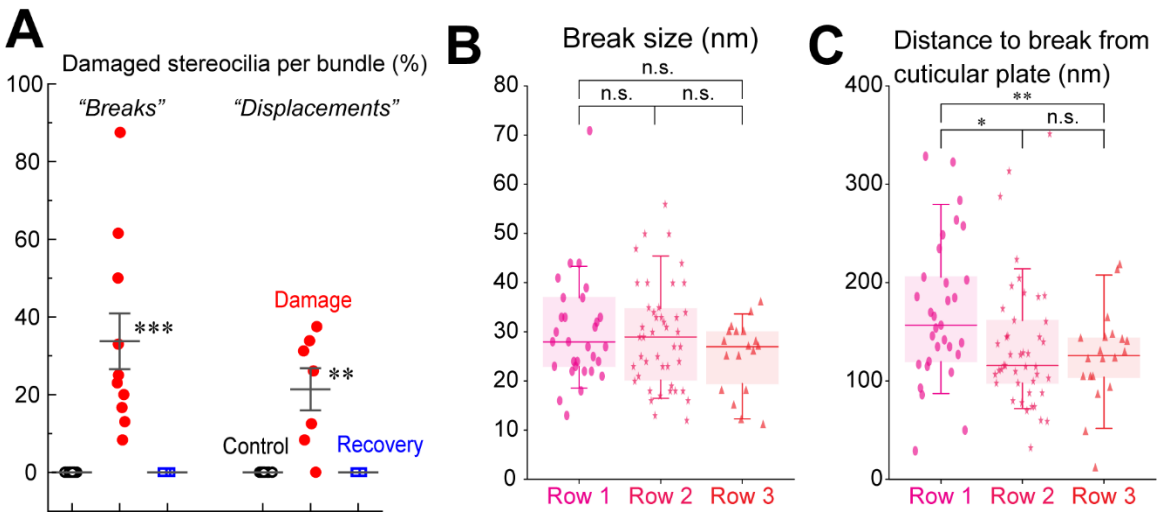

Figure 3.5. Characterization of F-actin breaks in overstimulated stereocilia in vitro.

A, Scatter plot diagram of the percentage of stereocilia with F-actin breaks per bundle. Bars show mean ± SEM value of combined data of 228 stereocilia from 11 cells. (***) indicates a P value < 0.001 determined by a Student's t-test. B, Scatter plot graphs of individual break sizes (nm) by row with overlay boxes showing the median value, 10th, 25th, 75th, and 90th percentiles. (n.s.) indicates no significance determined by a Student's t-test. C, Scatter plot graphs of individual break distances by row with overlay boxes showing the median value, 10th, 25th, 75th, and 90th percentiles. (n.s.) indicates no significance, (*) indicates a P value < 0.05, (**) indicates a P value < 0.01 determined by a Student's t-test.

made any difference in the size of the breaks but found no significant difference. (Figure 3.5B). We then quantified the location of the breaks by measuring from the inferior edge of the break to the cuticular plate. On average the breaks were located only 165 nm from the cuticular plate with the closest being 11 nm and the further 978 nm from the cuticular

plate. Unlike with the size of the breaks, the height of the stereocilia appeared to play a factor in the location of the break. The breaks in the 1st row stereocilia were located significantly further from the cuticular plate than those in the 2nd ($P < 0.05$) and 3rd ($P < 0.01$) rows (Figure 3.5C). Note that because some of the data came from TEM images it was often not possible to determine which row a stereocilia belonged to and therefore not all breaks could be included in the row by row comparisons.

3.5 Damage from overstimulation caused stereocilia to be displaced from their cuticular rootlets

In addition to the breaks in the F-actin of the stereocilia core we also found a significant ($P < 0.01$) number of stereocilia which were displaced from their cuticular rootlets (Figure 3.3B black arrows). This pathology was present in an average of 21% of the stereocilia within an overstimulated IHC bundle but was not present in any unstimulated bundles. In the unstimulated bundles, the center of the cuticular rootlet is aligned with the center of the stereocilium (Figure 3.3A, Figure 3.6A, and Figure 3.7A). However, when the bundle has been overstimulated by a fluid-jet a stereocilium can become displaced and no longer aligned with its cuticular rootlet (Figure 3.6B). In some instances, the stereocilium can become completely dissociated from its cuticular rootlet (Figure 3.3B black arrows and Figure 3.7A). We measured the size of the displacement as the distance from the center of the rootlet, at the cuticular plate) to the center of the base of the stereocilium. Similar to our findings with the location of breaks within the actin core of stereocilia, the size of the displacement was significantly larger in taller stereocilia (Figure 3.7B). The average size of the displacement was only 41 nm and 83% of all

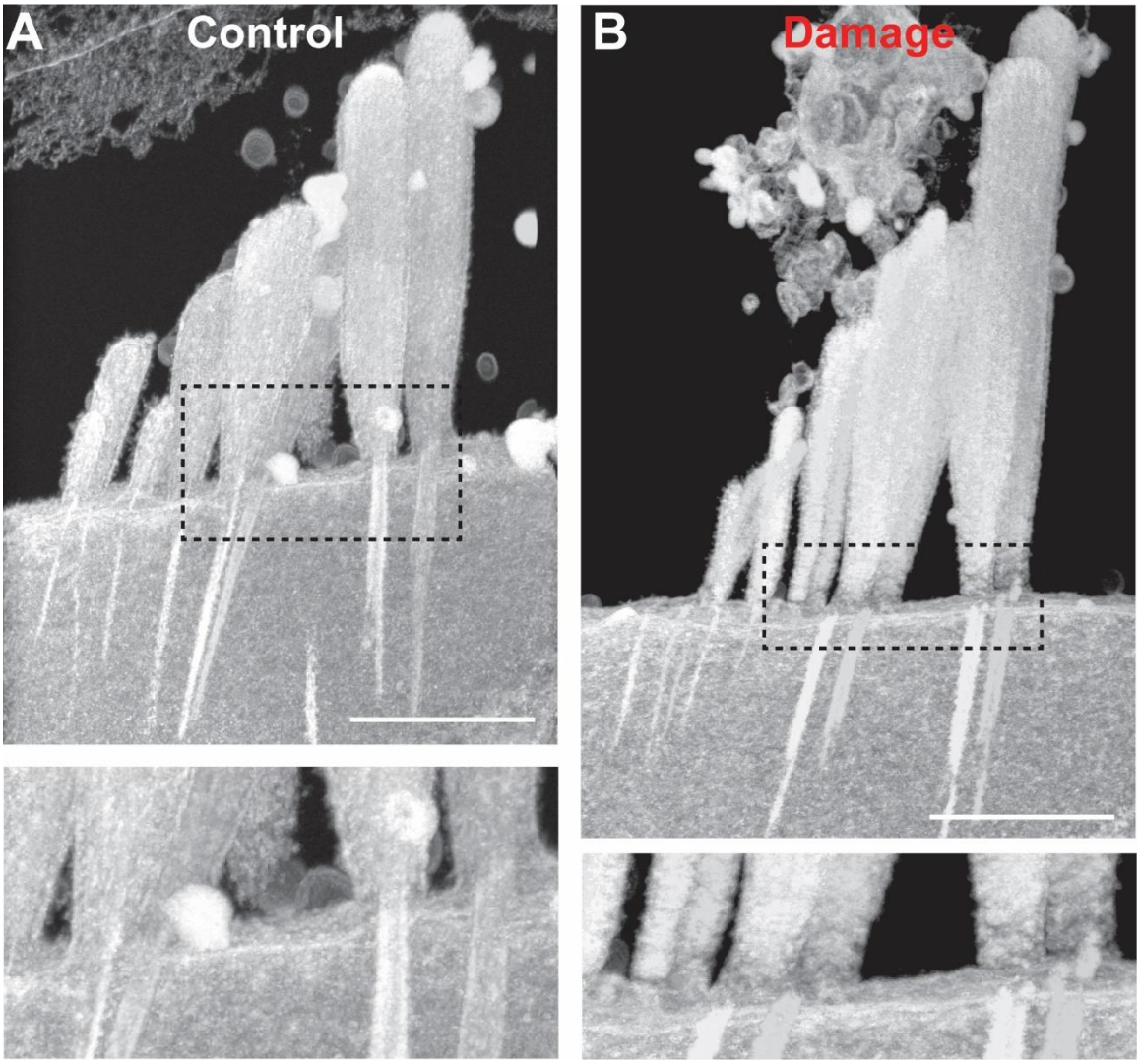

Figure 3.6. Overstimulation causes displacement of the stereocilium from its cuticular rootlet.

A, B, Representative 3D reconstructions created from FIB-SEM serial sections of portions of IHC stereocilia bundles. Boxes indicate the region of the higher magnification shown in the lower panels. A, Unstimulated control bundle with no stereocilia displacement. B, Damage bundle which has been overstimulated by fluid-jet causing some stereocilia to be displaced from their associated cuticular rootlet. Scale bars are 500 nm.

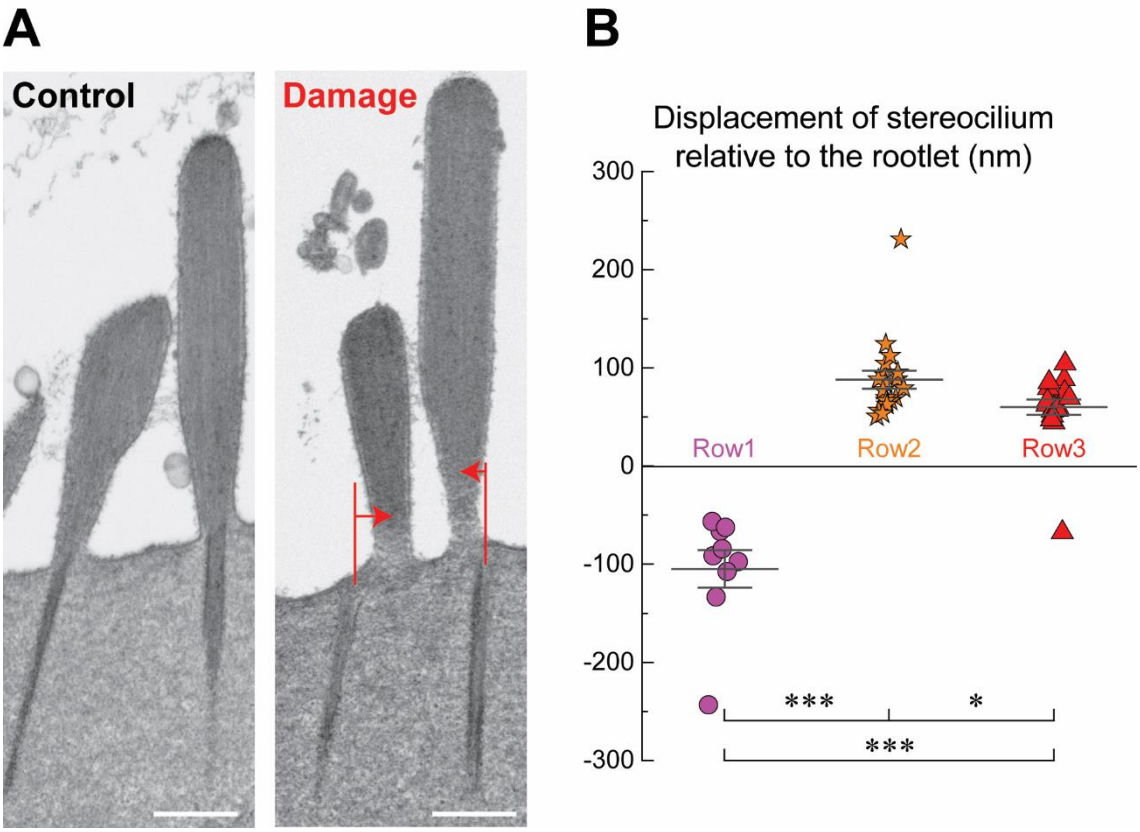

Figure 3.7. The amount of stereocilia displacement depends on the height of the stereocilia.

A, Representative FIB-SEM images of IHC stereocilia from unstimulated control bundle (left) without displacement and from overstimulated damage bundle (right) showing stereocilia displaced from their rootlets after fluid-jet overstimulation. Interstereocilia spacing is reduced as displaced stereocilia are pulled closer together by the extracellular links connecting them. B, Scatter plot of the displacements of individual stereocilium relative to their cuticular rootlet by row. Bars show mean ± SEM of combined data. Displacements were measured from the center of the cuticular rootlet to the center of the stereocilia base. Positive values indicate displacement of the stereocilia towards the taller row stereocilia and negative values

indicate displacement towards the shorter row stereocilia. (*) indicates a P value < 0.05, (***) indicates a P value <0.001 determined by Student's t-test.

displacements were under 100 nm in size but there were two much larger displacements measuring 243 nm and 232 nm found in 1st and 2nd row stereocilia respectively. We also noticed that these displacements were accompanied by a decrease in the interstereocilia spacing (Figure 3.7A). This suggests that there is tension in the extracellular links between the stereocilia in a bundle and that once the stereocilia were not anchored to by their cuticular rootlet the links pulled the stereocilia closer together.

3.6 Damage to the stereocilia is repaired within 24 hours corresponding to the recovery of bundle stiffness

Next, we explore whether the damage to the stereocilia ultrastructure from fluid-jet overstimulation is repairable. Bundle stiffness recovered 24 hours after overstimulation (Figure 3.1B) and so we would expect for the damage to the F-actin to also recover within 24 hours. We examined 74 stereocilia from 6 IHC bundles which had been overstimulated and then given 24 hours to recover in the incubator at 37°C before being fixed. Just as in the stereocilia from the unstimulated bundles we found no breaks in the F-actin and no displaced stereocilia (Figure 3.8).

We concluded that the submicron breaks in the actin core, as well as the displacement of stereocilia from their associated cuticular rootlets, recover within 24 hours after the damage. These breaks and displacements of stereocilia seem to be the primary cause of the decrease in bundle stiffness observed immediately after fluid-jet overstimulation. This conclusion is supported by the repair of stereocilia F-actin and the

realignment of stereocilium with their cuticular rootlets concomitant with the recovery of bundle stiffness within 24 hours after overstimulation.

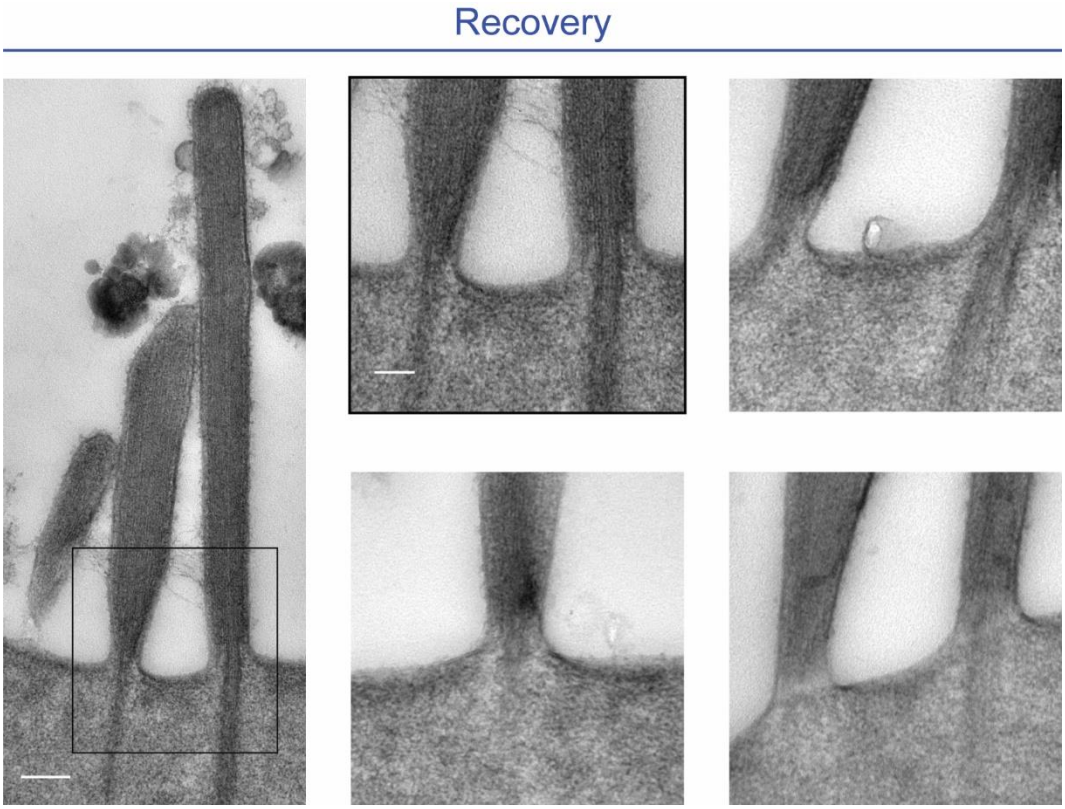

Figure 3.8 Repair of stereocilia damage occurs within 24 hours of damage

Representative TEM images of stereocilia from overstimulated bundles given 24 hours in the incubator at 37°C after overstimulation before being fixed. Scale bars 200 nm (larger images) and 100 nm (smaller images).

3.7 Damage to the stereocilia ultrastructure from noise exposure causing TTS is mostly repaired after 24 hours

The results of our *in vitro* experiments suggested that mechanical overstimulation can cause repairable damage to the F-actin of stereocilia in the rootlet region which

corresponds to changes in bundle stiffness. This comported with the findings of transient decreases in bundle stiffness in chick (Duncan and Saunders, 2000) and guinea pig (Saunders and Flock, 1986) hair bundles after fluid-jet overstimulation. However, with the exception of an observation of a small amount of shortening of the supracuticular rootlet (Liberman and Dodds, 1987), damage to the F-actin of stereocilia was only demonstrated in noise exposure sufficient to cause PTS (Engström et al., 1983; Liberman, 1987; Tilney et al., 1982).

Therefore, we next sought to examine whether temporary NIHL from moderate noise exposure could involve the same type of damage we observed in response to *in vitro* fluid-jet overstimulation. Following our labs established protocols for TTS we exposed mice aged P19-22 to a broadband noise at 100 dB SPL for 30 minutes. Auditory brainstem responses (ABRs) demonstrated elevated threshold shifts immediately after noise exposure. As expected in temporary NIHL, by 2 weeks post noise exposure the threshold shifts had recovered in a frequency specific manner. Thresholds for frequencies above 16 kHz remained elevated by more than 20 dB SPL while thresholds for frequencies at or below 16 kHz were only slightly elevated from pre-noise exposure measurements, consistent with normal age-related hearing loss (Figure 3.9).

We limited our inquiry to the mid-apex of the organ of Corti which corresponds tonotopically to the 8 to 16 kHz region of hearing in which threshold shifts after noise

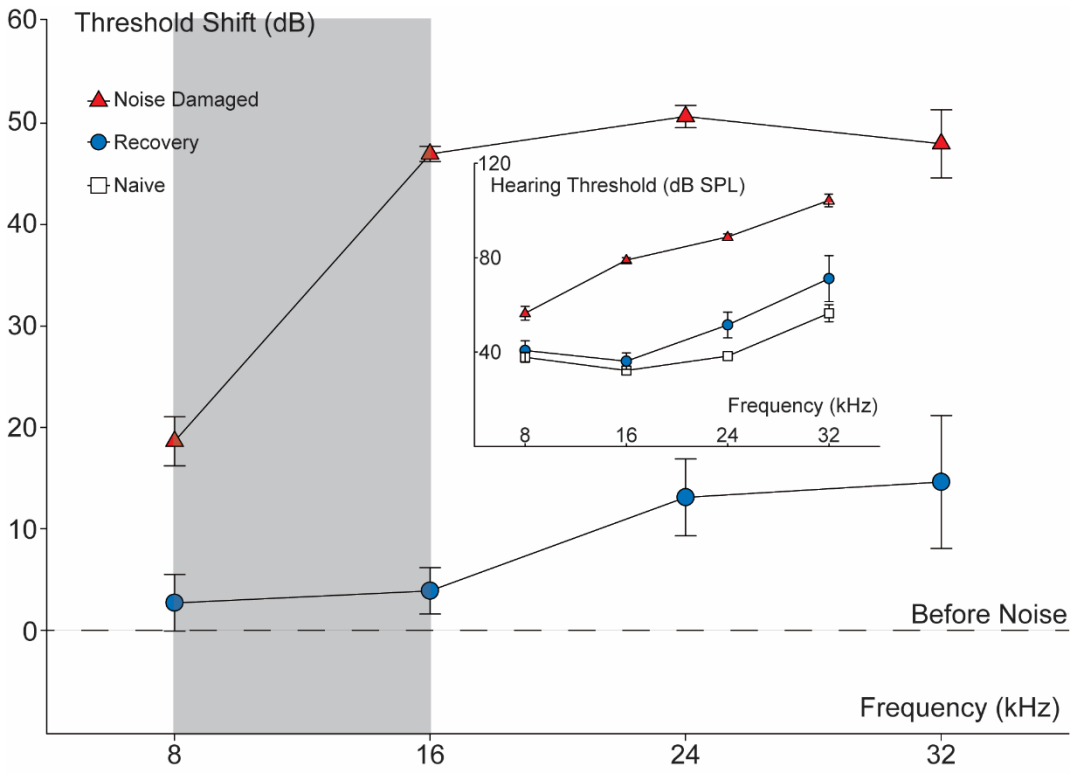

Figure 3.9 Auditory Brainstem Responses demonstrate temporary threshold shifts after moderate acoustic trauma

Mice were exposed to 100 dB SPL of broadband noise for 30 minutes. Immediately after noise exposure hearing thresholds were elevated at all frequencies compared to thresholds determined prior to noise exposure. The threshold shift was slightly less than 20 dB at 8 kHz but was near 50 dB for all other frequencies tested. The threshold shifts at lower frequencies, corresponding to the mid-apex region of the organ of Corti were temporary and recovered by 2 weeks after acoustic insult. Threshold shifts at higher frequencies did not recover completely and showed a permanent threshold shift of ~15 dB. Inset shows hearing threshold values at each frequency for naïve (square), noise-damaged (triangle), and recovery (circle). Bars show mean ± SEM

for combined data from 6 mice and includes data collected by Dr. Desislava Marinkova.

exposure recovered. To try to ensure that any damage we observed after noise exposure was the result of mechanical trauma rather than any cellular processes, we euthanized the mice immediately after noise exposure.

Although our *in vitro* experiments focused on damage to IHCs we first looked for damage among OHC stereocilia following noise exposure. This was due to the well-established susceptibility of OHCs to damage from noise exposure. Additionally, within the frequency range we examined, the threshold shifts we observed after noise exposure were within the ~40 dB range expected with a loss of OHC function.

We examined the ultrastructure of 126 OHC stereocilia from naïve mice, 262 OHC stereocilia from noise exposed mice sacrificed immediately after noise exposure and 93 stereocilia from noise exposed mice given 24 hours recovery time prior to euthanasia. As in our control *in vitro* samples we did not find breaks in the F-actin core of OHC stereocilia in naïve mice with no noise exposure (Figure 3.10A). In the OHC stereocilia of mice sacrificed immediately after noise exposure we found submicron breaks resembling those we observed *in vitro* after fluid-jet overstimulation (Figure 3.10B red arrows).

The breaks were found in 27% of stereocilia per bundle in the OHCs of noise exposed mice (Figure 3.10D). Although this occurrence is less frequent than the occurrence of the breaks found in IHC stereocilia after fluid-jet overstimulation *in vitro,* the difference in occurrences was not significant ($P > 0.5$).

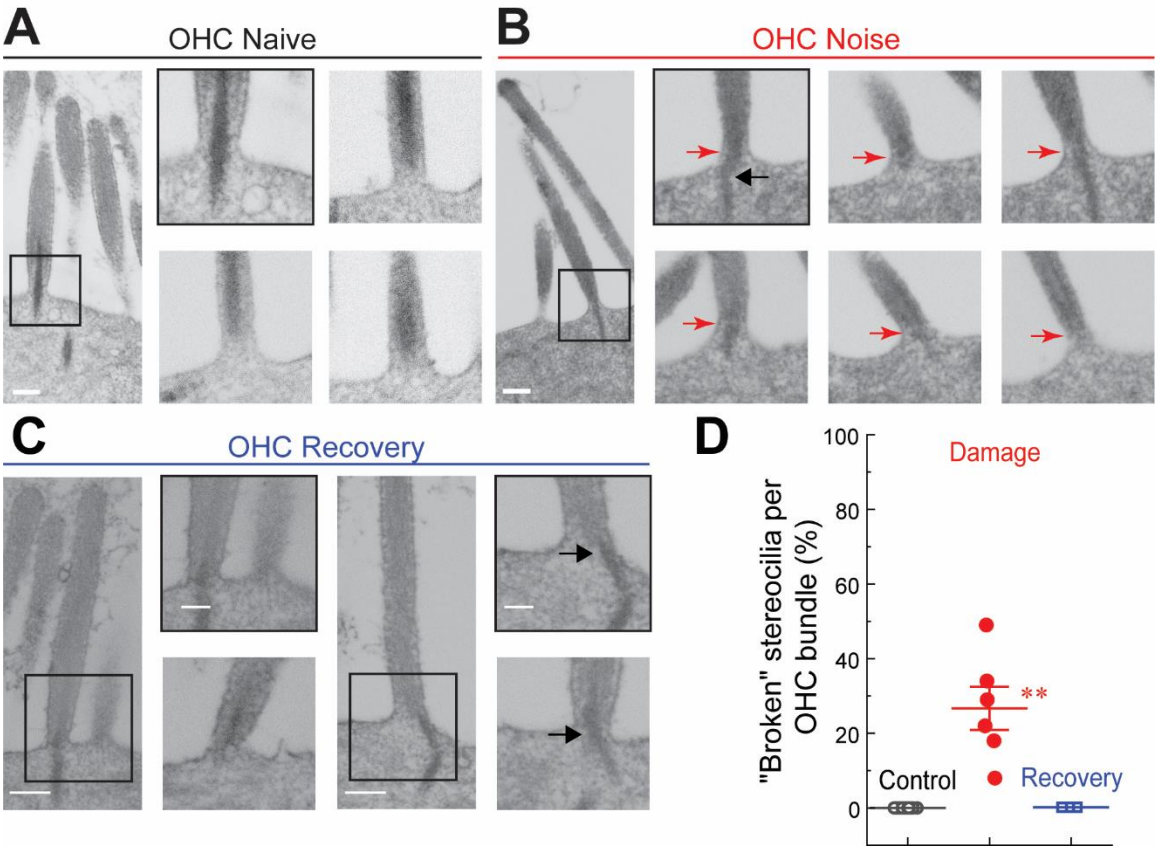

Figure 3.10. Damage to OHC stereocilia in TTS after noise exposure

A-C, Representative FIB-SEM images of OHC stereocilia. A, Stereocilia from naïve control bundles. B, Stereocilia from noise damaged bundles. Red arrows indicate breaks in the F-actin core. Black arrows indicate stereocilia displacement. C, Stereocilia from noise damaged bundles given 24 hours recovery time prior to euthanasia. Black arrows indicate stereocilia displacement. Scale bars are 200 nm (larger images) and 100 nm (smaller image). D, Scatter plot graph of damaged stereocilia with breaks in the F-actin core per bundle. Bars are mean ± SEM. (**) indicates P value < 0.01 as determined by Student's t-test.

There was a very significant difference ($P < 1 \times 10^{-6}$) in the size of the breaks compared we what found *in vitro.* The average size of the breaks in the noise exposed OHC stereocilia was only 20 nm which sometimes made visualizing them difficult. However, since we did not do overstimulation of OHC stereocilia *in vitro* it is difficult to make an informed comparison given the structural differences between IHC and OHC stereocilia. Additionally, we found that the breaks in these OHC stereocilia were located significantly ($P < 1 \times 10^{-12}$) closer to the cuticular plate (70 nm on average) than those in the fluid-jet overstimulated IHCs (165 nm on average). As with the difference in break sizes however, it is not possible to meaningfully compare these results due to the differences in structure. Similar to our *in vitro* experiments, there were no significant differences found among the rows in terms of break sizes (Figure 3.11A) or distance of the break from the cuticular plate (Figure 3.11B). Recovery of the stereocilia core in OHCs appears to be complete within 24 hours after noise exposure as we found no breaks in the F-actin in those OHC stereocilia (Figure 3.10C).

We also noticed stereocilia which were displaced from their rootlets (Figure 3.10B black arrow). However, there were some notable, but not always significant, differences between the displacements in OHCs *in vivo* and those found in IHCs after *in vitro* fluid-jet overstimulation. First, they occurred less frequently and were only found in 17% of stereocilia per bundle in the noise-exposed mice and there did not appear to be any recovery from the displacements after 24 hours (Figure 3.10C black arrows). Second, the displacements were found only in the 3rd row stereocilia and the displacement distance was significantly ($P < 0.001$) smaller in the *in vivo* OHCs (54 nm on average) than the displacements in the 3rd row of IHC stereocilia *in vitro* (68 nm on average).

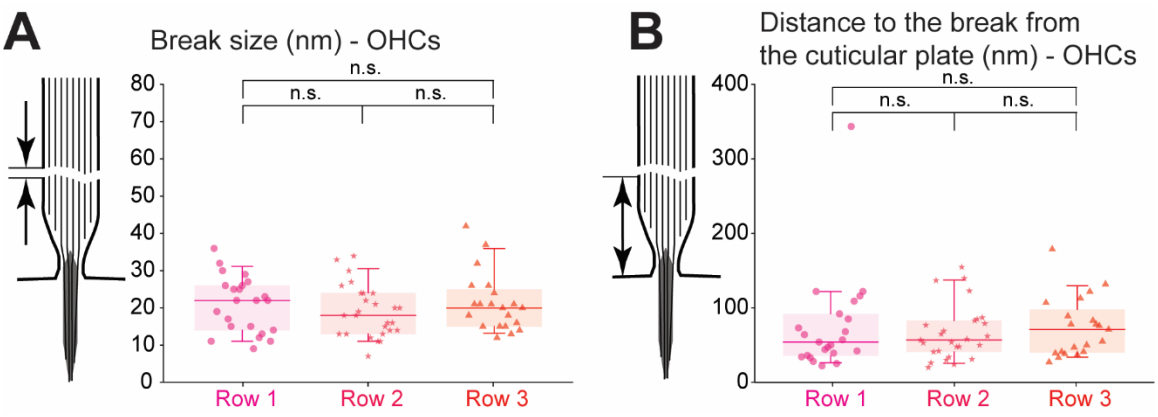

Figure 3.11. Row by row comparison of break characteristics in bundles of OHC stereocilia after noise exposure

A, Scatter plot graphs of individual break sizes (nm) by row in noise exposed OHCs with overlay boxes showing the median value, 10th, 25th, 75th, and 90th percentiles. (n.s.) indicates no significance determined by a Student's t-test. C, Scatter plot graphs of individual break distances by row in noise exposed OHCs with overlay boxes showing the median value, 10th, 25th, 75th, and 90th percentiles. (n.s.) indicates no significance, determined by a Student's t-test.

3.8 IHC stereocilia have a different ultrastructure pathology after noise exposure causing TTS than is seen in OHCs or in *in vitro* overstimulation of IHCs.

Our final analysis was of the *in vivo* IHC stereocilia. We examined 57 IHC stereocilia from naïve mice, 165 IHC stereocilia from noise exposed mice sacrificed immediately after noise exposure, and 154 IHC stereocilia from noise exposed mice given a 24-hour recovery time before euthanasia. We found that there were some striking ultrastructure pathologies of *in vivo* IHC stereocilia after noise exposure that were not seen in the overstimulated *in vitro* IHC stereocilia. The similarities between the two are that

control stereocilia appeared normal (Figure 3.12A) and that the stereocilia of noise exposed mice had breaks in the F-actin at their base (Figure 3.12B red arrows).

The prevalence of the breaks was slightly less than after *in vitro* overstimulation averaging 20% of stereocilia per bundle (Figure 3.12D) but the difference was not significant (Figure 4.1A). The break characteristics were similar between *in vitro* and *in vivo* damaged IHCs with the exception of their locations (Figure 4.1B and Figure 4.1C). The breaks in the *in vivo* IHC stereocilia immediately after noise exposure were significantly ($P < 0.001$) closer to the cuticular plate (96 nm on average) than in the *in vitro* damage IHC stereocilia (145 nm on average). There were no significant differences in terms of break sizes (Figure 3.12G) and locations (Figure 3.12H) between rows of stereocilia in the *in vivo* noise damaged IHCs which was the same as the *in vitro* overstimulated IHC stereocilia.

Although the breaks were largely very similar between the damage *in vivo* and *in vitro* IHC stereocilia, the breaks *in vivo* did not appear to recover by the 24-hour timepoint (red arrows in Figure 3.12C and Figure 3.12D). The exception to this was in the 3rd row stereocilia which had no breaks 24 hours after noise exposure. Interestingly, although the differences were not significant, the breaks are larger after 24 hours (32 nm on average) and it is visually apparent compared to the stereocilia immediately after noise (26 nm on average). Additionally, after 24 hours the breaks are located a bit further from the cuticular plate (120 nm on average) compared to the stereocilia immediately after noise (96 nm on average). Another notable difference was a dearth of displaced stereocilia after noise exposure. We found only 3 displaced stereocilia in noise exposed IHC bundles and none were found in bundles given 24 hours to recover.

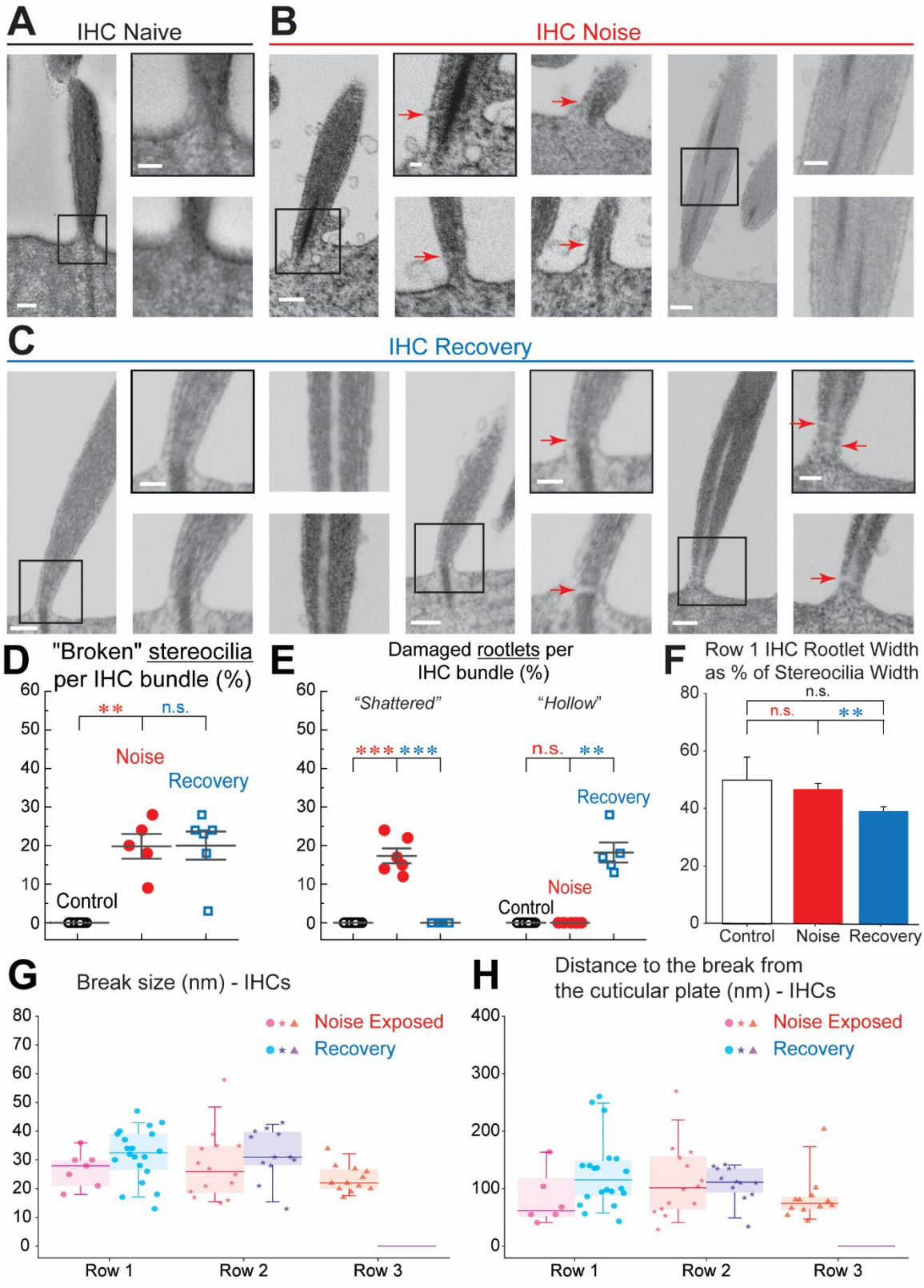
A
IHC Naive
B
IHC Noise
C
IHC Recovery
D
"Broken" stereocilia per IHC bundle (%)
**
n.s.
Noise
Recovery
Control
E
Damaged rootlets per IHC bundle (%)
"Shattered"
"Hollow"
*****
n.s.
**
Recovery
Noise
Control
F
Row 1 IHC Rootlet Width as % of Stereocilia Width
n.s.
n.s.
**
Control
Noise
Recovery
G
Break size (nm) - IHCs
Noise Exposed
Recovery
Row 1
Row 2
Row 3
H
Distance to the break from the cuticular plate (nm) - IHCs
Noise Exposed
Recovery
Row 1
Row 2
Row 3

Figure 3.12 Damage to IHC stereocilia in vivo from noise exposure causing TTS

A-C, Representative TEM and FIB-SEM images of IHCs from young adult mice. A, Representative TEM images of IHC stereocilia from naïve control bundles. B, Representative FIB-SEM images of IHC stereocilia from noise damaged bundles with red arrows indicating breaks in the F-actin. C, Representative FIB-SEM images of IHC stereocilia from noise damaged bundles given 24 hours recovery time with red arrows indicating breaks in the F-actin. Scale bars are 200 nm (larger images) and 100 nm (smaller images). D, Scatter plot graph of damaged stereocilia with breaks in the F-actin core per bundle. Bars are mean ± SEM. (**) indicates P value < 0.01, n.s. indicates no significance as determined by Student's t-test. E, Scatter plot graph of damaged supracuticular rootlets with "shattered" phenotype seen in Noise stereocilia in B on the left and "hollow" seen in Recovery stereocilia in C on the right. Bars are mean ± SEM. (***) indicates P value < 0.001, (**) indicates P value < 0.01, n.s. indicates no significance as determined by Student's t-test. F, Bar graph comparing the percentage of the stereocilia taken up by its rootlet at the base of the IHC stereocilia. Bars are mean ± SEM. (**) indicates P value < 0.01, n.s. indicates no significance as determined by Student's t-test. G Scatter plot graphs of individual break sizes (nm) by row in noise exposed and recovery IHCs with overlay boxes showing the median value, 10^{th}, 25^{th}, 75^{th}, and 90^{th} percentiles. H, Scatter plot graphs of individual break distances by row in noise exposed and recovery IHCs with overlay boxes showing the median value, 10^{th}, 25^{th}, 75^{th}, and 90^{th} percentiles.

The most striking difference in the ultrastructure pathology occurred with the supracuticular rootlets of the taller row IHCs *in vivo*. There were two different abnormal structural variations observed which we termed "shattered" and "hollow" based on their appearance (Figure 3.12B and Figure 3.12C). There was remarkable consistency in the presentation of these two variations: the "shattered" supracuticular rootlets were only found in IHC stereocilia immediately after noise exposure and the "hollow" supracuticular rootlets were only found in IHC stereocilia 24 hours after noise exposure (Figure 3.12E). Moreover, these structural variations in the supracuticular rootlet were present in every single 1st row stereocilia imaged. Additionally, two 2nd row stereocilia in recovery samples had the "hollow" supracuticular rootlet. Finally, we also noticed that the "hollow" rootlets appeared thinner at the base of the stereocilia where normal rootlets are the thickest (Furness et al., 2008). We compared the widths of the rootlets at the base of 1st row stereocilia as a percentage of the width of the base of the stereocilia. We confirmed that the "hollow" supracuticular rootlets are significantly ($P < 0.01$) narrower (39% on average) relative to the width of the stereocilia at the base than the "shattered" supracuticular rootlets (47% on average) (Figure 3.12F).

From our *in vivo* experiments we concluded that damage to the stereocilia ultrastructure is a component of temporarily elevated auditory thresholds after moderate noise exposure. Our results show that there are processes which effect repair for this type of damage after acoustic trauma. The repair is not complete 24 hours after noise exposure, but we expect the recovery is complete once hearing thresholds have recovered.

CHAPTER 4. **DISCUSSION**

The hair cell stereocilia bundles are the most visually striking feature of the auditory sensory system and there continues to be many unanswered questions regarding their structure and function. As the mechanosensitive apparatus of the hair cells, the importance of healthy stereocilia has long been acknowledged and changes in the morphology of the stereocilia bundle is considered to be a hallmark of both temporary and permanent hearing loss (Liberman and Beil, 1979; Nikaido 1992; Wang et al., 2011). Additionally, *in vitro* studies of bundle dynamics have demonstrated decreases in bundle stiffness following mechanical overstimulation (Szymko et al., 1995; Saunders et al., 1986) which in other studies has been found to be reversible (Duncan and Saunder, 2000; Saunders and Flock, 1986).

However, while the loss of bundle stiffness is suggestive of stereocilia bundle damage, and the recovery of stiffness is suggestive of repair, no one has looked at damage to the stereocilia ultrastructure from mechanical overstimulation. Examination of the ultrastructure after acoustic trauma has almost exclusively been limited to PTS. Indirect examination of damage to the actin core using fluorescent labeling of F-actin (Avinash et al., 1993; Belyantseva et al., 2009) and direct examination of the ultrastructure (Engström et al, 1983; Liberman, 1987; Thorne et al., 1986; Tilney et al., 1982) have shown damage to the F-actin of stereocilia and their rootlets after acoustic trauma. Each of those studies showed significant pathologies in stereocilia structure but only examined acoustic trauma sufficient to cause PTS and therefore found no evidence of repair. Only a single study looking at TTS in cats (Liberman and Dodds, 1987) has explored stereocilia ultrastructure with TEM following moderate acoustic trauma and showed only the presence of shortened

supracuticular rootlets and evidence suggesting that the shortening of the rootlet was partially recoverable.

We hypothesized that damage to the F-actin of stereocilia and rootlets is the underlying cause of changes in bundle stiffness and morphology following mechanical and acoustical overstimulation and that observations of recovery from these pathologies indicates the presence of an unknown mechanism for repair. Our results include the first observation of F-actin damage following mechanical overstimulation *in vitro* and demonstrate that this damage is quickly repaired within 24 hours (Figures 3.3 through 3.8). Additionally, we were able to show that damage similar to that seen in our *in vitro* experiments is also found in the stereocilia of IHCs located in the frequency region of the organ of Corti which exhibited TTS after moderate acoustic trauma, and that the supracuticular rootlet may play a role in the repair of this damage (Figures 3.9 through 3.12). Damage to the F-actin of stereocilia, and the repair of that damage, is a novel component of temporary noise-induced hearing loss.

4.1 How does mechanical overstimulation cause a decrease in bundle stiffness?

Our results suggest that observed decreases in bundle stiffness from mechanical overstimulation *in vitro* (Szymko et al., 1995; Saunders et al., 1986; Duncan and Saunders, 2000; Saunders and Flock, 1986) may be the result of damage to F-actin at the base of stereocilia. Each of these studies proposed that the decreases in bundle stiffness were due to either damage to the F-actin at the base of the stereocilia or damage to the interconnecting links between the stereocilia.

In 2000 Duncan and Saunders, working with fluid-jet overstimulation of isolated chick hair cells, concluded that the bundle stiffness change was not caused by broken links but rather damage to the actin core or rootlet. This conclusion was based upon studies showing that ablation of links between stereocilia resulted in a reduction in relative and asymmetric motion of the stereocilia (Duncan et al., 1998; Eisen at al., 1999) which they did not observe. Our results also support the conclusion of Duncan and Saunders that the decrease in bundle stiffness after mechanical overstimulation is not caused by a loss of interstereocilia links within the bundle (Figure 3.1 and 3.2). The contribution of a loss of links was always an attractive hypothesis because we know that the tip-links are part of the mechanoelectrical transduction apparatus of stereocilia (Pickles et al., 1984; Beurg et al., 2009) and that they can be broken by noise exposure (Pickles et al., 1987; Kurian et al., 2003; Husbands et al., 1999). Additionally, other studies have observed that the links between stereocilia are an important component of bundle stiffness in both chick (Bashtanov et al., 2004) and mammalian (Goodyear et al, 2005; Beurg et al., 2008) sensory hair cells. We also know that tip-links can regenerate which fits with the observed transient nature of the reduction in bundle stiffness (Zhao et al, 1996; Indzhykulian et al., 2013). Despite this, our results in this study demonstrate that mechanical overstimulation sufficient to cause a significant decrease in bundle stiffness did not result in a significant, or even noticeable, decrease in the number of stereocilia links as determined by counting tip-links in SEM micrographs of the bundles. This finding agrees with previous observations that mechanical overstimulation sufficient to disrupt bundle morphology is generally required to break tip-links (Clark and Pickles, 1996).

Although Duncan and Saunders proposed that the decrease in bundle stiffness which they observed following fluid-jet overstimulation was caused by damage to the F-actin of the stereocilia, they did not examine the ultrastructure of the stereocilia and it has remained educated conjecture up until now. Indeed, no previous study has examined the F-actin of stereocilia after fluid-jet overstimulation. By using TEM and FIB-SEM to examine the F-actin ultrastructure of stereocilia after fluid-jet overstimulation *in vitro*, we have been able to provide evidence for this hypothesis by showing that damage to the F-actin at the base of stereocilia is only present after overstimulation when bundle stiffness is decreased. This supports the contribution of the highly crosslinked paracrystalline F-actin core to the rigidity of stereocilia (DeRosier et al., 1980; Tilney et al., 1980; Krev et al., 2016) and suggests that this rigidity is a significant contributor to the overall stiffness of the stereocilia bundle.

It is not surprising that we found damage to the F-actin core at the tapered base of the stereocilia (Figure 3.5), the pivot point (Flock et al., 1977) where the greatest amount of mechanical stress from overstimulation would be found. The stereocilia rootlet has been shown to be essential for bundle stiffness (Hudspeth, 1983; Howard et al., 1988; Pickles, 1993). Further evidence supporting the role of rootlets in bundle stiffness came from a previous study in our lab in which mice unable to develop rootlets, due to TRIOBP-4 and TRIOBP-5 deficiencies, were compared to wild-type mice and the stereocilia bundles of the mice without rootlets were found to be less stiff (Kitajiri et al., 2010). The mechanical stress was further exacerbated in our *in vitro* experiments due to the young postnatal mouse explants we used not yet having a fully mature rootlet. Without a supracuticular rootlet the fluid-jet overstimulation frequently caused displacement of stereocilia from their

anchoring cuticular rootlets (Figures 3.5 through 3.7). Given that the breaks in the F-actin core did not completely transect the stereocilia (Figure 3.4) it is entirely possible that the change in bundle stiffness is caused more by the displacement of the stereocilia from their anchoring rootlets (Tilney et al., 1983) than by the small breaks in the F-actin core. Although it is not possible to culture explants from older mice, repeating the fluid-jet experiments on freshly isolated organ of Corti tissue of older mice with more mature stereocilia containing a supracuticular rootlet could be illuminating. One might suspect that the decrease in bundle stiffness following fluid-jet overstimulation would be less severe in more adult bundles, in which the stereocilia with a supracuticular rootlet are less often displaced by overstimulation. Regardless of the degree each contributes to the end result, the breaks in the F-actin core of the stereocilia as well as the displacement of the rootlets correlate to the observed decrease in bundle stiffness and strongly supports our hypothesis.

Based on our findings in this study we can also say that there is a repair mechanism which is capable of restoring the normal structure of the F-actin core at the base of stereocilia (Figures 3.5 and 3.8). Additionally, the restoration of the normal stereocilia ultrastructure by this repair mechanism occurs within 24 hours after damage and corresponds to the recovery of bundle stiffness after overstimulation in this same timeframe. Potential mechanisms for this repair are discussed in section 4.4.

The presence of a repair mechanism was always a logical consequence of bundle stiffness recovery if the loss of stiffness was caused by damage to the F-actin at the base of stereocilia. The confirmation that the observed loss of stiffness was indeed due to F-actin damage, and that this damage is indeed repaired, is a major finding of this study.

4.2 Is repairable damage to F-actin in stereocilia a component of the temporary NIHL?

Our results demonstrate that the overstimulation of stereocilia by moderate noise exposure causing temporary threshold shifts damages the F-actin of the stereocilia. Previous studies of damage to the F-actin in stereocilia from noise exposure via fluorescent labeling (Avinash et al., 1993; Belyantseva et al., 2009) and TEM micrographs (Engström et al, 1983; Liberman, 1987; Thorne et al., 1986; Tilney et al., 1982) limited their observations to noise exposure sufficient to cause permanent damage. Although we did not examine recovery past 24 hours, we investigated only the hair cells within the frequency range that exhibits the complete recovery of hearing thresholds within two weeks after noise exposure, suggesting that the damages to the F-actin are completely recoverable in these cells.

The breaks in the F-actin of the stereocilia seen immediately after noise exposure are very similar to the breaks in the F-actin of the stereocilia we observed *in vitro* immediately after fluid-jet overstimulation (Figure 4.1). The *in vivo* breaks were not completely repaired by the 24-hour timepoint in which we saw complete repair of the breaks *in vitro*. However, the *in vitro* bundle stiffness had recovered within 24 hours after fluid-jet overstimulation but hearing thresholds are not recovered as quickly after noise exposure. If this damage to the F-actin is a component of the TTS, then it is not surprising that the damage is not repaired as quickly *in vivo* as it is *in vitro*.

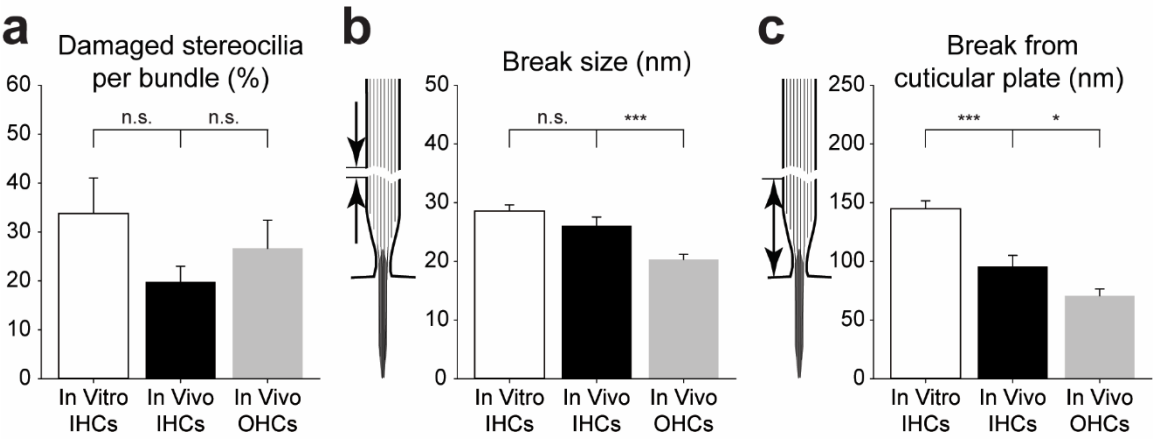

Figure 4.1 Comparisons between in vitro and in vivo breaks in the F-actin of stereocilia

A Percentage of stereocilia with breaks in the F-actin of stereocilia per bundle. B, Size of breaks in the F-actin of stereocilia core. C, Distance of the breaks from the cuticular plate. All graphs show mean ± SEM. (n.s.) indicates no significance, (*) indicates P value < 0.05, (***) indicates P value < 0.001 as determined by Student's t-test.

Further evidence that the damage seen *in vivo* after noise exposure would be repaired after 24 hours comes from studies of bundle dysmorphology in TTS (Nikaido 1992; Wang et al., 2011). Prior to our study this type of damage to the stereocilia ultrastructure had not been visualized, but some type of damage to the F-actin of the stereocilia could be reasonably inferred by the stereocilia disarray seen in previous studies (Nikaido 1992; Wang et al., 2011). The eventual recovery of bundle morphology suggests that the underlying damage has been repaired (Wang et al., 2011).

Additionally, we suggest that the "hollow" supracuticular rootlet we observed 24 hours after noise exposure is part of the repair process. Following the damage to the

supracuticular rootlet which causes the observed “shattered” appearance immediately after noise exposure, the TRIOBP-4 which bundles the F-actin of the supracuticular rootlet may become displaced. The F-actin crosslinkers of the stereocilia core, which are very dynamic (Roy and Perrin, 2018), appear to reorganize the F-actin above the remaining portion of the supracuticular rootlet. Normally TRIOBP-4 is present in the stereocilia shaft, in the region where the supracuticular rootlet will be, long before the supracuticular rootlet has actually formed (Katsuno et al., 2019). At some point during development, the organization of the F-actin in the region of the supracuticular rootlet changes and instead of being crosslinked like the rest of the actin core the filaments are bundled by TRIOBP-4. Although we do not know the signal that causes this change in filament organization, I would speculate that the presence of TRIOBP-4 prior to this reorganization suggests that there is an interaction between TRIOBP-4, the F-actin and the crosslinkers in the region of supracuticular rootlet before the rootlet is formed. This preexisting interaction could be essential to the smooth transition from the paracrystalline organization of the actin core to the tightly bundled actin filaments of the supracuticular rootlet. If TRIOBP-4 indeed becomes displaced with the disruption of the supracuticular rootlet, de novo TRIOBP-4 may diffuse into the area to rebuild the supracuticular rootlet. The paracrystalline F-actin organization which was constructed by rapid turnover of crosslinkers in the absence of TRIOBP-4 may need to be deconstructed and reconstituted in the presence of TRIOBP-4 to replace the damaged supracuticular rootlet. Staining of the stereocilia shaft for the presence of TRIOBP-4 immediately after acoustic overstimulation could determine whether an interaction between TRIOBP-4 and the crosslinkers in the stereocilia F-actin core is part of the mechanism of repair.

Interestingly, *in vivo* damage and recovery was different between the IHC and OHC stereocilia. Although the percentage of stereocilia per bundle which were damaged was similar between the IHC and OHC bundles, the breaks in the OHC stereocilia were significantly smaller and closer to the cuticular plate (Figure 4.1) and lacked the observe damage to the supracuticular rootlet. Additionally, breaks in the OHC stereocilia were completely recovered after 24 hours similar to our *in vitro* experiments in IHCs while the noise-induced breaks in the IHC stereocilia did not recover in this timeframe (Figures 3.10 & 3.12). Unfortunately, as previously described, difficulties in carrying out the *in vitro* experiments on OHC stereocilia bundles as we did with IHC stereocilia bundles keeps us from being able to draw a direct comparison between *in vitro* and *in vivo* experiments in the case of OHC stereocilia. What we do know is that measurements of bundle stiffness in isolated guinea pig cochlea showed that OHC bundles are significantly stiffer than IHC bundles (Strelioff and Flock, 1984). Given the function of OHCs as cochlear amplifiers, with their 1st row stereocilia embedded in the tectorial membrane, it makes sense that their stereocilia would be stiffer. I would hypothesize that during exposure to moderate intensity acoustic trauma the stiffer OHC stereocilia bundles may not experience the same damaging degree of deflection that the more pliant IHC stereocilia bundles suffered. Thus, the breaks found in the OHC stereocilia were smaller and more easily repaired and the supracuticular rootlets were not damaged.

4.3 Our results support findings of TTS in cats from more than 30 years ago

At first glance our results appear to be in conflict with the only other study which has examined stereocilia ultrastructure from moderate noise exposure causing TTS

(Liberman and Dodds, 1987). In their study they found a shortening of the supracuticular rootlet as the sole stereocilia pathology. We believe that the apparent discrepancies between the two studies is illusory and that our findings support those of Liberman and Dodds.

The first apparent discrepancy is that we observed breaks in the F-actin perpendicular to the filaments which Liberman and Dodds did not observe. The most likely culprit is the difference in imaging techniques employed by each study. We were able to observe these breaks by serial sectioning perpendicular to the reticular lamina thereby visualizing a, mostly, longitudinal section through the stereocilia and collecting images every 20 nm with the FIB-SEM. Liberman and Dodds did all of their sectioning parallel to the reticular lamina which would have made it very difficult to see breaks that were in the same plane. Additionally, the limitations of ultrathin sectioning in 1987 means that Liberman and Dodds were making their observations with sections that were 70 to 90 nm thick. This technique permitted Liberman to observe large areas of F-actin damage in PTS (Liberman, 1987) but these breaks are much smaller, averaging just 20 nm in OHCs and 26 nm in IHCs, and it would have been virtually impossible to have imaged them using this technique.

An additional difference between the electron microscopy in our study and theirs is in the choice of staining agents. We used a 1% tannic acid post fix which aids in the visualization of actin filaments (Begg et al., 1978; LaFountain et al., 1977). This may have aided our ability to visualize smaller changes in the F-actin but the effects are likely insignificant compared to the advantage of longitudinal sectioning in our study. We also did not use Osmium Tetroxide or Lead Citrate, both common electron microscopy stains

used by Liberman and Dodds. However, these stains primarily provide contrast and stabilization of lipid and glycoproteins and are unlikely to have contributed to the differences in findings between the two studies.

The other apparent discrepancy is the difference in supracuticular rootlet pathologies between the two studies. We observed “shattered” and “hollow” rootlets and Liberman and Dodds observed “shortened” rootlets. Although we cannot prove a connection between these pathologies, we can infer a plausible hypothesis by comparing the study designs beginning with the assumption that the noise exposure used in the two studies created equivalent damage to the stereocilia. Our study confirmed an established noise exposure protocol used in our lab to reliably generate TTS and then used that protocol to noise expose the mice for our imaging study. We euthanized the mice in our imaging study within a minute of ending the noise exposure and therefore did not test them for elevated thresholds. It was in these mice that we observed the “shattered” supracuticular rootlets. By contrast, single unit recordings were sampled in the cats for several hours after noise exposure in the study by Liberman and Dodds. The two cats in which this “shortened” supracuticular rootlet pathology was found were not euthanized until 6 and 13.5 hours after noise exposure. Our second group of noise exposed mice which had the “hollow” supracuticular rootlets were given 24 hours to recover after noise exposure before being euthanized for imaging. We believe these results suggest a continuum between the “shattered” and “hollow” pathologies with the “shortened” pathology as an intermediate.

Immediately after the cessation of noise exposure we observed the “shattered” pathology. As seen in Figure 3.12B, the upper portion of the supracuticular rootlet is shorter and near the periphery of the stereocilia there are areas of increased actin filament density

similar to what one normally sees in the rootlet. This gives the appearance that the supracuticular rootlet has shattered into fragments. In reality, what has likely occurred is that the actin filaments within the stereocilia core were sliding relative to one another (Tilney et al., 1983). The shearing force from the repeated and prolonged intense deflections caused by the noise exposure would likely have broken the crosslinkers between the filaments, disrupting their normal spacing and resulting in the localized areas of increased F-actin density that we observed.

The rapid turnover of the crosslinkers (Roy and Perrin, 2018) would quickly restore the normal appearance of F-actin core. This would explain why these patchy areas of increased filament density were not observed by Liberman and Dodds at their earliest timepoint 6 hours after noise exposure, as well as why they were not observed in our imaging of stereocilia fixed 24 hours after noise exposure. The only difference between the "shortened" appearance of the supracuticular rootlet seen by Liberman and Dodds and the "shattered" appearance of the supracuticular rootlet we observed is that in the 6 hours before Liberman and Dodds applied a fixative to the tissue the F-actin crosslinkers had been restored.

Another interesting finding by Liberman and Dodds was that the supracuticular rootlet was shorter in the cat euthanized 13.5 hours post noise than in the cat euthanized 6 hours post noise. The shorter supracuticular rootlets found 13.5 hours may lend support to our idea that the "hollow" rootlet pathology we observed at 24 hours is the result of F-actin depolymerization prior to the rebuilding of the supracuticular rootlet. The final bit of evidence for this hypothesis is supplied by Liberman and Dodds in the reexamination of serial sections from the PTS study (Liberman, 1987) which showed the presence of

supracuticular rootlets with intermediate heights between those found in acutely damaged and undamaged stereocilia. This shows that the supracuticular rootlet can be rebuilt following noise exposure but that it does not return to a normal height in cases of PTS.

4.4 How does repair occur despite the apparently stable F-actin in the stereocilia core

One of the unique features of stereocilia is their incredibly stable F-actin. Like F-actin in similar cytoskeletal structures such as microvilli and filopodia, the F-actin in stereocilia is polarized with the 'barbed' end located just under the plasma membrane at the tips of stereocilia and the 'pointed' end at the base of the stereocilia (Flock and Cheung, 1977). Typically this would mean that in order to maintain a steady length, polymerization via the addition of G-actin to the existing F-actin would occur at the 'barbed' end at the same rate as depolymerization via the removal of G-actin from the F-actin would occur at the 'pointed' end, a phenomenon termed "treadmilling" (Fujiwara et al, 2002). This would lead to fairly rapid turnover of the F-actin in the stereocilia core if it occurred. However, a great deal of evidence suggests that this does not occur in mammalian stereocilia except within a small region at the tips.

A multi-isotope imaging mass spectrometry examination of the ^{14}N to ^{15}N ratio in frog and mice fed a ^{15}N labeled diet showed that while extensive protein turnover occurs in the body of the hair cell and a the tips of the stereocilia, the majority of protein within the shaft of the stereocilia is stable even over a time course of months (Zhang et al., 2012). To determine whether the portion of the stereocilia shaft protein content which exhibited turnover was actin, conditional cre-mediated recombination was used to knock out the

expression of either β-actin or γ-actin in adolescent mice. Using isoform specific antibodies it was observed that although the deleted isoform was quickly absent elsewhere in the hair cell, including the tips of the stereocilia, it was still present in the shafts of the stereocilia even several months later indicating that actin is the stable protein fraction in stereocilia shafts (Zhang et al., 2012). Further support for the stability of the F-actin core is found in a study which conditionally induced GFP-β-actin expression in adolescent mice. The GFP-β-actin was localized to the tips of the stereocilia and was not present in the stereocilia shafts even with several months of continued expression (Narayanan et al., 2015). In the same study *in vitro* photobleaching of the stereocilia of IHCs in mice expressing GFP-β-actin exhibited a recovery of fluorescence only in the tips and not within the shaft (Narayanan et al., 2015). This trend holds true in the stereocilia of vestibular hair cells as well (Zhang et al., 2012; Drummond et al., 2015). The question becomes how does damaged F-actin in the stereocilia shaft repair when actin turnover only occurs at the tips of the stereocilia?

Although the breaks we observed appear empty we know that it is not just empty space. Noise-induced gaps in the fluorescent labeling of F-actin in guinea pig IHC stereocilia stained strongly for DNase 1 which is a marker for G-actin (Belyantseva et al., 2009). It is possible that the G-actin in these breaks are polymerized into F-actin thus restoring the paracrystalline structure of the actin core. In fact, a photobleaching study of actin turnover in the stereocilia of developing zebrafish supports this idea. In the study, a band in the midsection of stereocilia bundles was photobleached in transgenic zebrafish expressing mCherry labeled β-actin in their stereocilia. Over the course of 30 hours recovery of fluorescence occurred within the photobleached band but the location of the

band remained static (Hwang et al., 2015). Although this kind of actin turnover appears to be limited to the tips of stereocilia in mammals, the mechanism by which it occurs may be the same.

Normally, F-actin is polymerized by joining together a chain of G-actin monomers and although the affinity for actin polymerization and depolymerization is greatest at the 'barbed' and 'pointed' ends respectively, it also happens the other way around (reviewed in Fujiwara et al., 2018). Indeed, under physiological conditions in the presence of ADF depolymerization at the barbed end of F-actin has been demonstrated (Wioland et al., 2017). This makes sense in light of the turnover of actin observed in mammals at the tips of the stereocilia, without concomitant treadmilling of the F-actin in the shafts of the stereocilia, suggests that depolymerization at the 'barbed' end may be very normal even in mammalian stereocilia. Additionally, a study of Drosophila bristles, which contain a highly crosslinked paracrystalline F-actin scaffold similar to stereocilia, showed that the disassembly of the F-actin core within the bristles was inhibited when depolymerization was blocked at the 'barbed' end (Guild et al., 2002). This was done through the use of jasplakinolide which acts to lower depolymerization and increase polymerization of actin subunits (Bubb et al., 1994; Bubb et al., 2000; Holzinger, 2009).

Taken all together, the likely presence of G-actin localized to gaps in phalloidin stained guinea pig IHC stereocilia (Belyantseva et al, 2009) and the F-actin polymerization at the tips of mammalian stereocilia (Zhang et al., 2012; Narayanan et al., 2015; Drummond et al., 2015) and within the shaft of zebrafish stereocilia (Hwang et al., 2015), suggest a potential mechanism for the repair of the breaks we observed at the base of overstimulated stereocilia. The mechanical forces applied to the stereocilia, whether via fluid-jet *in vitro*

or noise exposure *in vivo*, tears apart submicron regions of the stressed F-actin. This leaves behind small fragments of F-actin which could either be reused in a modular fashion as described in Drosophila (Tilney et al., 1996) or depolymerized by ADF/cofilin which has enhanced activity in the presence of crosslinkers such as fascin (Breitsprecher et al., 2011) leaving behind G-actin. The appearance of breaks in these regions seems to favor the depolymerization of F-actin into G-actin as our use of tannic acid to stain F-actin would possibly show evidence of F-actin fragments if they were present. It is also supported by the fluorescent staining of DNase 1 in the gaps of noise exposed guinea pig IHC stereocilia (Belyantseva et al., 2009). If the G-actin in these gaps is not de novo G-actin, but rather G-actin that had previously been a part of the now broken F-actin, reconstruction of the F-actin with this G-actin would not be observable in studies looking for the incorporation of new actin.

Another possible explanation for how this repair could occur without being observed as turnover comes from the location of the breaks at the base of the stereocilia; they were located an average of only 80 nm from the cuticular plate in our *in vivo* experiments. What is often not mentioned when referencing the studies showing actin turnover only at the tips of stereocilia is that turnover at the cuticular plate occurs at the same rate as anywhere else in the cell other than the stereocilia (Zhang et al., 2012; Narayanan et al., 2015; Drummond et al., 2015). It is a reasonable conjecture that the breaks are so close to the cuticular plate that their repair is indistinguishable from the high turnover seen at the cuticular plate.

Finally, the most likely explanation is the simplest explanation. The studies of stereocilia actin turnover in mammalian hair cells limited their inquiry to undamaged

stereocilia; however, with no damaged F-actin requiring repair, no repair mechanisms were active (Zhang et al., 2012; Narayanan et al., 2015; Drummond et al., 2015). If this is correct then repair of the damaged F-actin in the stereocilia would likely either occur in a modular fashion with fragments of F-actin being connected together to form a full filament as described in Drosophila (Tilney et al., 1996) or in a straightforward actin treadmilling fashion as seen in Zebrafish (Hwang et al., 2015). In either case, the repair would involve the rapid turnover of crosslinking proteins which has already been described in healthy stereocilia (Roy and Perrin, 2018). If correct, the mammalian experiments which showed no F-actin turnover except at the tips of the stereocilia could be carried out *in vitro* with fluid-jet overstimulation of the bundles and observation of F-actin turnover during the 24 hour period between damage and full repair.

4.5 Does the supracuticular rootlet play a role in the repair of F-actin damage?

With its densely packed collection of actin filaments, the rootlet is an integral component of stereocilia which anchors the stereocilia to the cuticular plate and provides a pivot point for bundle deflection (Tilney et al., 1980; Flock et al., 1977). Developmentally the cuticular rootlet forms first and the supracuticular rootlet appears later and. Except for TRIOBP-4, the known proteins associated with the F-actin of the cuticular rootlet are distinct from those associated with the F-actin of the supracuticular rootlet (Kitajiri et al., 2010; Katsuno et al., 2019; Reviewed in Pacentine et al., 2020).

Even in the youngest mice we used for our *in vitro* study, the cuticular rootlets were present in all of the bundles we stimulated but none of the stereocilia from our *in vitro* study had supracuticular rootlets. In contrast, the older mice in our *in vivo* experiments had

supracuticular rootlets which were proportional in size to the size of their stereocilia with the 3rd row still mostly lacking a supracuticular rootlet. It may be that the reason breaks were less prevalent *in vivo* is that the presence of the supracuticular rootlet provided a pivot point which relieved the mechanical stress experienced by the stereocilia actin core *in vitro* which did not have a supracuticular rootlet. In addition to the sliding of actin filaments within the core relative to one another (Tilney et al., 1983) the rootlet is capable of bending during deflections (Bathe et al., 2008).

This would also explain why stereocilia displacement was more common, and larger, *in vitro* than *in vivo*. Without a supracuticular rootlet the mechanical stress at the base of the stereocilia could more easily displace the stereocilia from the cuticular rootlet. Additionally, when present, the displacements *in vivo* were limited to the 3rd row stereocilia which does not have a supracuticular rootlet to speak of suggesting that the presence of a larger supracuticular rootlet protects the stereocilia from overstimulation-induced displacement.

The lack of a supracuticular rootlet may also explain why recovery occurred much more quickly *in vitro* than *in vivo* if the supracuticular rootlet is involved in repair. Three lines of evidence suggest that the supracuticular rootlet could be involved in the repair process. First, the recovery of the breaks in the F-actin were significantly faster *in vitro* at the age when the supracuticular rootlet is developing. Interestingly, the actin bundling protein TRIOBP-4 is localized to the supracuticular rootlet region of the stereocilia well before the supracuticular rootlet is actually formed (Katsuno et al., 2019). This suggests that the machinery for building the supracuticular rootlet is in place already and waiting for the signal to go to work. Second, although breaks in the F-actin were found in all 3

rows of IHC stereocilia *in vivo* only the breaks in the 3rd row were fully recovered within 24 hours. In the 3rd row, the supracuticular rootlets are still undeveloped, leading to a recovery time similar to what we saw in the stereocilia in our *in vitro* experiments.

Finally, it is in the non-transducing stereocilia of IHCs that we found the "hollow" supracuticular rootlets 24 hours after noise exposure. Recent evidence from our lab demonstrates that Ca^{2+} influx provides a stabilizing effect on the F-actin core of transducing stereocilia. When this normal Ca^{2+} influx is disrupted, the F-actin begins to depolymerize reducing the height of these stereocilia (Vélez-Ortega et al., 2017). If tension in the tip-link is disrupted *in vivo* (for example, after overstimulation), this process may act to restore tension to the tip-link thus restoring MET channel activity. Once the MET channels are again able to pass Ca^{2+} into the hair cell at rest, F-actin polymerization restores the transducing stereocilia to their normal height. In undamaged stereocilia this dynamic process of F-actin turnover appears to be limited to the tips of the stereocilia, but in damaged stereocilia it could extend further down the shaft to the location of damage. The 1st row stereocilia, lacking MET channels, displays an insensitivity to reductions in Ca^{2+} influx through the MET channels of the transducing stereocilia and, in undamaged stereocilia, the region of F-actin turnover at the tips of stereocilia is smaller in the 1st row stereocilia than in the transducing stereocilia. This could suggest that F-actin turnover in the 1st row stereocilia, even in instances of damage repair, occurs on a different timescale than what is seen in transducing stereocilia. If, as we previously suggested, the "hollow" supracuticular rootlet seen in 1st row stereocilia 24 hours after noise exposure is a dismantling of the supracuticular rootlet which precedes its reconstruction, the different

rates of F-actin turnover in the transducing stereocilia could explain the lack of this "hollow" rootlet appearance in the 2nd row stereocilia.

Further study of the development of the supracuticular rootlet and its possible role in repair is warranted. Observing the formation of the supracuticular rootlet at developmental stages between the ages of our *in vitro* and *in vivo* experiments may shed light on how the cross-linked F-actin of the core is reformed into the bundled actin of the supracuticular rootlet. Additionally, examining the damage from noise exposure at later timepoints more aligned with the recovery of threshold shifts could elucidate the rebuilding of the supracuticular rootlet in the 1st row stereocilia of IHCs.

4.6 Final thoughts

From the results of my dissertation research I can assert the following:

1) I have demonstrated that mechanical stress from fluid-jet overstimulation *in vitro* generates breaks in the F-actin of stereocilia which cause a decrease in bundle stiffness.
2) An unidentified mechanism exists in the otherwise static F-actin of the mouse stereocilia which repairs this mechanical damage within 24 hours thus restoring bundle stiffness.
3) The F-actin at the base of stereocilia in young postnatal mice is more susceptible to damage from mechanical stress than in adolescent mice possibly due to the lack of a developed supracuticular rootlet.

4) The damage to the F-actin of stereocilia from *in vitro* overstimulation appears to share a translational component to moderate noise exposure causing temporary hearing loss.
5) Repair of this noise-induced damage occurs as a component of the restoration of hearing thresholds.
6) The process for repairing damage to the F-actin of stereocilia following moderate acoustic insult requires more time than what was observed *in vitro* and may involve remodeling of the supracuticular rootlet.

The results of this study are, to the best of our knowledge, a novel addition to the scholarship in our field and reveals the existence of an uncharacterized repair process at the base of mammalian auditory stereocilia.

REFERENCES

Allen JB. Cochlear micromechanics--a physical model of transduction. J Acoust Soc Am. 1980;68(6):1660-1670. doi:10.1121/1.385198

Andéol G, Guillaume A, Micheyl C, Savel S, Pellieux L, Moulin A. Auditory efferents facilitate sound localization in noise in humans. J Neurosci. 2011;31(18):6759-6763.

Arima, T., Uemura, T., & Yamamoto, T. (1987). Three-dimensional visualizations of the inner ear hair cell of the guinea pig. A rapid-freeze, deep-etch study of filamentous and membranous organelles. Hearing Research, 25(1), 61-68.

Assad, J., Shepherd, G., & Corey, D. (1991). Tip-link integrity and mechanical transduction in vertebrate hair cells. Neuron, 7(6), 985-994.

Attias, J., Sohmer, H., Gold, S., Haran, I., & Shahar, A. (1990). Noise and hypoxia induced temporary threshold shifts in rats studied by ABR. Hearing Research, 45(3), 247-252.

Avinash, G., Nuttall, A., & Raphael, Y. (1993). 3-D analysis of F-actin in stereocilia of cochlear hair cells after loud noise exposure. Hearing Research, 67(1-2), 139-146.

Axelsson, A., Nuttall, A. L., & Miller, J. M. (1990). Observations of cochlear microcirculation using intravital microscopy. Acta oto-laryngologica 109(3-4), 263–270.

Bashtanov, M., Goodyear, R., Richardson, G., & Russell, I. (2004). The mechanical properties of chick (Gallus domesticus) sensory hair bundles: Relative contributions of structures sensitive to calcium chelation and subtilisin treatment. Journal of Physiology, 559(1), 287-299.

Bathe, M., Heussinger, C., Claessens, M., Bausch, A., & Frey, E. (2008). Cytoskeletal Bundle Mechanics. Biophysical Journal, 94(8), 2955-2964.

Belyantseva, I., Perrin, B., Sonnemann, K., Zhu, M., Stepanyan, R., McGee, J., . . . Ervasti, J. (2009). Gamma-actin is required for cytoskeletal maintenance but not development. Proceedings of the National Academy of Sciences of the United States of America, 106(24), 9703-9708.

Beurg M, Nam JH, Crawford A, Fettiplace R. The actions of calcium on hair bundle mechanics in mammalian cochlear hair cells. Biophys J. 2008;94(7):2639-2653.

Beurg, M., Fettiplace, R., Nam, J., & Ricci, A. (2009). Localization of inner hair cell mechanotransducer channels using high-speed calcium imaging. Nature Neuroscience, 12(5), 553-558.

Blanchet C, Eróstegui C, Sugasawa M, Dulon D. Acetylcholine-induced potassium current of guinea pig outer hair cells: its dependence on a calcium influx through nicotinic-like receptors. J Neurosci. 1996;16(8):2574-2584.

Breitsprecher D, Koestler SA, Chizhov I, et al. Cofilin cooperates with fascin to disassemble filopodial actin filaments. J Cell Sci. 2011;124(Pt 19):3305-3318.

Brown, M. (1987). Morphology of labeled afferent fibers in the guinea pig cochlea. Journal of Comparative Neurology, 260(4), 591-604.

Brown, M., Nuttall, A., & Masta, R. (1983). Intracellular Recordings from Cochlear Inner Hair Cells: Effects of Stimulation of the Crossed Olivocochlear Efferents. Science, 222(4619), 69-72.

Brownell, W., Bader, C., Bertrand, D., & De Ribaupierre, Y. (1985). Evoked mechanical responses of isolated cochlear outer hair cells. Science (New York, N.Y.), 227(4683), 194-196.

Brueck, S., Kardous, C., Oza, A., & Murphy, W. (2014). Measurement of Exposure to Impulsive Noise at Indoor and Outdoor Firing Ranges during Tactical Training Exercises. International Journal Of Occupational And Environmental Health, 20(4), 341.

Bubb MR, Senderowicz AM, Sausville EA, Duncan KL, Korn ED. Jasplakinolide, a cytotoxic natural product, induces actin polymerization and competitively inhibits the binding of phalloidin to F-actin. J Biol Chem. 1994;269(21):14869-14871.

Bubb MR, Spector I, Beyer BB, Fosen KM. Effects of jasplakinolide on the kinetics of actin polymerization. An explanation for certain in vivo observations. J Biol Chem. 2000;275(7):5163-5170.

Byers, T., & Branton, D. (1985). Visualization of the Protein Associations in the Erythrocyte Membrane Skeleton. Proceedings of the National Academy of Sciences of the United States of America, 82(18), 6153-6157.

Carricondo, F., & Romero-Gómez, B. (2019). The Cochlear Spiral Ganglion Neurons: The Auditory Portion of the VIII Nerve. Anatomical Record, 302(3), 463-471.

Ciganović, N., Wolde-Kidan, A., & Reichenbach, T. (2017). Hair bundles of cochlear outer hair cells are shaped to minimize their fluid-dynamic resistance. Scientific Reports, 7(1), 3609.

Clark, J., & Pickles, J. (1996). The effects of moderate and low levels of acoustic overstimulation on stereocilia and their tip links in the guinea pig. Hearing Research, 99(1-2), 119-128.

Corey, D. P., & Hudspeth, A. J. (1979). Ionic basis of the receptor potential in a vertebrate hair cell. Nature, 281(5733), 675–677.

Crompton, M. (1999). The mitochondrial permeability transition pore and its role in cell death. The Biochemical Journal, 341 (pt 2), 233-249.

Dallos, P., & Harris, D. (1978). Properties of auditory nerve responses in absence of outer hair cells. Journal of Neurophysiology, 41(2), 365-383.

Dallos P, He DZ, Lin X, Sziklai I, Mehta S, Evans BN. Acetylcholine, outer hair cell electromotility, and the cochlear amplifier. J Neurosci. 1997;17(6):2212-2226.

Dallos, P., Wu, X., Cheatham, M., Gao, J., Zheng, J., Anderson, C., . . . Zuo, J. (2008). Prestin-Based Outer Hair Cell Motility Is Necessary for Mammalian Cochlear Amplification. Neuron, 58(3), 333-339.

Darrow, K., Maison, S., & Liberman, M. (2007). Selective removal of lateral olivocochlear efferents increases vulnerability to acute acoustic injury. Journal of Neurophysiology, 97(2), 1775-1785.

DeRosier, D., & Tilney, L. (1989). The structure of the cuticular plate, an in vivo actin gel. Journal of Cell Biology, 109(6), 2853-2867.

DeRosier, D., Tilney, L., & Egelman, E. (1980). Actin in the inner ear: The remarkable structure of the stereocilium. Nature, 287(5780), 291-296.

Dong XX, Ospeck M, Iwasa KH. Piezoelectric reciprocal relationship of the membrane motor in the cochlear outer hair cell. Biophys J. 2002;82(3):1254-1259.

Drummond, M., Barzik, M., Bird, J., Zhang, D., Lechene, C., Corey, D., Friedman, T. (2015). Live-cell imaging of actin dynamics reveals mechanisms of stereocilia length regulation in the inner ear. Nature Communications, 6(1), 6873.

Duncan, R., & Saunders, J. (2000). Stereocilium injury mediates hair bundle stiffness loss and recovery following intense water-jet stimulation. Journal of Comparative Physiology A, 186(11), 1095-1106.

Duncan RK, Dyce OH, Saunders JC. Low calcium abolishes tip links and alters relative stereocilia motion in chick cochlear hair cells. Hear Res. 1998;124(1-2):69-77.

Eisen MD, Duncan RK, Saunders JC. The tip link's role in asymmetric stereocilia motion of chick cochlear hair cells. Hear Res. 1999;127(1-2):14-21.

Engström, B., Flock, &., & Borg, E. (1983). Ultrastructural studies of stereocilia in noise-exposed rabbits. Hearing Research, 12(2), 251-264.

Evans, M., Lagostena, L., Darbon, P., & Mammano, F. (2000). Cholinergic control of membrane conductance and intracellular free Ca2 in outer hair cells of the guinea pig cochlea. Cell Calcium, 28(3), 195-203.

Eybalin, M., & Pujol, R. (1984). Immunofluorescence with Met-enkephalin and Leu-enkephalin antibodies in the guinea pig cochlea. Hearing Research, 13(2), 135-140.

Fettiplace, R., & Nam, J. (2019). Tonotopy in calcium homeostasis and vulnerability of cochlear hair cells. Hearing Research, 376, 11-21.

Flock, A., Flock, B., & Murray, E. (1977). Studies on the sensory hairs of receptor cells in the inner ear. Acta oto-laryngologica, 83(1-2), 85–91.

Flock, A., & Cheung, H. (1977) Actin filaments in sensory hairs of inner ear receptor cells. The Journal of Cell Biology, 75(2), 339-343.

Friedman, R., Van Laer, L., Huentelman, M., Sheth, S., Van Eyken, E., Corneveaux, J., . . . Van Camp, G. (2009). GRM7 variants confer susceptibility to age-related hearing impairment. Human Molecular Genetics, 18(4), 785-796.

Frolenkov, G., Kalinec, F., Tavartkiladze, G., & Kachar, B. (1997). Cochlear outer hair cell bending in an external electric field. Biophysical Journal, 73(3), 1665-1672.

Frolenkov GI, Mammano F, Belyantseva IA, Coling D, Kachar B. Two distinct Ca(2+)-dependent signaling pathways regulate the motor output of cochlear outer hair cells. J Neurosci. 2000;20(16):5940-5948.

Frolenkov, G., Mammano, F., & Kachar, B. (2003). Regulation of outer hair cell cytoskeletal stiffness by intracellular Ca 2 : Underlying mechanism and implications for cochlear mechanics. Cell Calcium, 33(3), 185-195.

Frolenkov, G., Belyantseva, I., Friedman, T. Genetic insights into the morphogenesis of inner ear hair cells. Nature Reviews Genetics, 5(7)**,** 489–498 (2004).

Fujiwara, I., Takahashi, S., Tadakuma, H., Funatsu, T., & Ishiwata, S. (2002). Microscopic analysis of polymerization dynamics with individual actin filaments. Nature Cell Biology, 4(9), 666-73.

Fujiwara I, Takeda S, Oda T, Honda H, Narita A, Maéda Y. Polymerization and depolymerization of actin with nucleotide states at filament ends. Biophys Rev. 2018;10(6):1513-1519.

Furman, A., Kujawa, S., & Liberman, M. (2013). Noise-induced cochlear neuropathy is selective for fibers with low spontaneous rates. Journal of Neurophysiology, 110(3), 577-586.

Furness, D. N., Mahendrasingam, S., Ohashi, M., Fettiplace, R., & Hackney, C. M. (2008). The dimensions and composition of stereociliary rootlets in mammalian cochlear hair cells: comparison between high- and low-frequency cells and evidence for a connection to the lateral membrane. The Journal of neuroscience : the official journal of the Society for Neuroscience, 28(25), 6342–6353.

Gavara N, Manoussaki D, Chadwick RS. Auditory mechanics of the tectorial membrane and the cochlear spiral. Curr Opin Otolaryngol Head Neck Surg. 2011;19(5):382-387.

Glowatzki, E., & Fuchs, P. (2002). Transmitter release at the hair cell ribbon synapse. Nature Neuroscience, 5(2), 147-154.

Goodyear, R., Richardson, G., Fekete, Donna M., & Wu, Doris K. (2002). Extracellular matrices associated with the apical surfaces of sensory epithelia in the inner ear: Molecular and structural diversity. Journal of Neurobiology, 53(2), 212-227.

Goodyear RJ, Marcotti W, Kros CJ, Richardson GP. Development and properties of stereociliary link types in hair cells of the mouse cochlea. J Comp Neurol. 2005;485(1):75-85.

Grati, M., Schneider, M.E., Lipkow, K., Strehler, E.E., Wenthold, R.J., & Kachar, B. (2006). Rapid turnover of stereocilia membrane proteins: evidence from the trafficking and mobility of plasma membrane Ca(2+)-ATPase 2. J Neurosci., 26(23), 6386-6395.

Guild, G., Connelly, P., Vranich, K., Shaw, M., & Tilney, L. (2002). Actin filament turnover removes bundles from Drosophila bristle cells. Journal of Cell Science, 115(Pt 3), 641-53.

Hacohen, N., Assad, J., Smith, W., & Corey, D. (1989). Regulation of tension on hair-cell transduction channels: Displacement and calcium dependence. The Journal of Neuroscience., 9(11), 3988-3997.

Hoffman, D., Zamir, N., Rubio, J., Altschuler, R., & Fex, J. (1985). Proenkephalin and prodynorphin related neuropeptides in the cochlea. Hearing Research, 17(1), 47-50.

Holley, M., & Ashmore, J. (1990). Spectrin, actin and the structure of the cortical lattice in mammalian cochlear outer hair cells. Journal of Cell Science. London, New York NY, 96(2), 283-291.

Holzinger A. Jasplakinolide: an actin-specific reagent that promotes actin polymerization. Methods Mol Biol. 2009;586:71-87.

Howard, J., & Hudspeth, A. (1987). Mechanical Relaxation of the Hair Bundle Mediates Adaptation in Mechanoelectrical Transduction by the Bullfrog's Saccular Hair Cell. Proceedings of the National Academy of Sciences of the United States of America, 84(9), 3064-3068.

Howard J, Hudspeth AJ. Compliance of the hair bundle associated with gating of mechanoelectrical transduction channels in the bullfrog's saccular hair cell. Neuron. 1988;1(3):189-199.

Hu, B., Henderson, D., & Nicotera, T. (2002). Involvement of apoptosis in progression of cochlear lesion following exposure to intense noise. Hearing Research, 166(1-2), 62-71.

Hudspeth AJ. The hair cells of the inner ear. They are exquisitely sensitive transducers that in human beings mediate the senses of hearing and balance. A tiny force applied to the top of the cell produces an electrical signal at the bottom. Sci Am. 1983;248(1):54-64.

Hudspeth, A. (1985). The cellular basis of hearing: The biophysics of hair cells. Science (New York, N.Y.), 230(4727), 745-752.

Hunter, D. R., Haworth, R. A., & Southard, J. H. (1976). Relationship between configuration, function, and permeability in calcium-treated mitochondria. The Journal of biological chemistry, 251(16), 5069–5077.

Indzhykulian, A., Stepanyan, R., Nelina, A., Spinelli, K., Ahmed, Z., Belyantseva, I., . . . Marcotti, W. (2013). Molecular Remodeling of Tip Links Underlies Mechanosensory Regeneration in Auditory Hair Cells (Molecular Remodeling of Tip Links). 11(6), E1001583.

Institute of Electrical Electronics Engineers, & IEEE Standards Coordinating Committee 14 on Quantities, Units, Letter Symbols. (1993). American national standard mathematical signs and symbols for use in physical sciences and technology. New York, NY: Institute of Electrical and Electronics Engineers.

International Electrotechnical Commission. (1994-07). IEV Ref 801-21-22. http://www.electropedia.org/iev/iev.nsf/display?openform&ievref=801-21-22

Itoh, M., & Nakashima, T. (1980). Structure of the hair rootlets on cochlear sensory cells by tannic acid fixation. Acta Oto-laryngologica., 90(5-6), 385-390.

Iwasa K. H. (1993). Effect of stress on the membrane capacitance of the auditory outer hair cell. Biophysical journal, 65(1), 492–498.

Ji, L., Lee, H., Wan, G., Wang, G., Zhang, L., Sajjakulnukit, P., . . . Corfas, G. (2019). Auditory metabolomics, an approach to identify acute molecular effects of noise trauma. Scientific Reports, 9(1), 9273.

Jia, S., Yang, S., Guo, W., & He, D. Z. (2009). Fate of mammalian cochlear hair cells and stereocilia after loss of the stereocilia. The Journal of neuroscience : the official journal of the Society for Neuroscience, 29(48), 15277–15285.

Johnsson, L. (1971). Reissner's Membrane in the Human Cochlea. Annals of Otology, Rhinology & Laryngology, 80(3), 425-438.

Kachar, B., Brownell, W., Altschuler, R. et al. Electrokinetic shape changes of cochlear outer hair cells. Nature 322**,** 365–368 (1986).

Kalinec F, Zhang M, Urrutia R, Kalinec G. Rho GTPases mediate the regulation of cochlear outer hair cell motility by acetylcholine. J Biol Chem. 2000;275(36):28000-28005.

Karavitaki, K. D., & Corey, D. P. (2010). Sliding adhesion confers coherent motion to hair cell stereocilia and parallel gating to transduction channels. The Journal of neuroscience : the official journal of the Society for Neuroscience, 30(27), 9051–9063.

Katsuno, T., Belyantseva, I., Cartagena-Rivera, A., Ohta, K., Crump, S., Petralia, R., . . . Kitajiri, S. (2019). TRIOBP-5 sculpts stereocilia rootlets and stiffens supporting cells enabling hearing. JCI Insight, 4(12), JCI insight, June 20, 2019, Vol.4(12).

Kawakami, M., Makimoto, K., Noi, O., & Takahashi, H. (1991). Relationship between cochlear blood flow and perilymphatic oxygen tension. European Archives of Oto-Rhino-Laryngology, 248(8), 465-470.

Kazmierczak, P., Sakaguchi, H., Tokita, J., Wilson-Kubalek, E., Milligan, R., Müller, U., & Kachar, B. (2007). Cadherin 23 and protocadherin 15 interact to form tip-link filaments in sensory hair cells. Nature, 449(7158), 87-91.

Kitajiri, S, Sakamoto, T, Belyantseva, I, Goodyear, R, Stepanyan, R, Fujiwara, I, Friedman, T. (2010). Actin-Bundling Protein TRIOBP Forms Resilient Rootlets of Hair Cell Stereocilia Essential for Hearing. Cell, 141(5), 786-798.

Krey, J., Krystofiak, E., Dumont, R., Vijayakumar, S., Choi, D., Rivero, F., Barr-Gillespie, P. (2016). Plastin 1 widens stereocilia by transforming actin filament packing from hexagonal to liquid. The Journal of Cell Biology, 215(4), 467-482.

Kujawa, S. G., & Liberman, M. C. (2006). Acceleration of age-related hearing loss by early noise exposure: evidence of a misspent youth. The Journal of neuroscience : the official journal of the Society for Neuroscience, 26(7), 2115–2123.

Kujawa, S. G., & Liberman, M. C. (2009). Adding insult to injury: cochlear nerve degeneration after "temporary" noise-induced hearing loss. The Journal of neuroscience : the official journal of the Society for Neuroscience, 29(45), 14077–14085.

Kujawa, S., Liberman, M. (2014). Hot Topics—Hidden hearing loss: Permanent cochlear-nerve degeneration after temporary noise-induced threshold shift. The Journal of the Acoustical Society of America, 135(4), 2311.

Lam, Y., Chen, X., & Pearson, O. (1999). Intertaxonomic Variability in Patterns of Bone Density and the Differential Representation of Bovid, Cervid, and Equid Elements in the Archaeological Record. American Antiquity, 64(2), 343-362. doi:10.2307/2694283

Lee, J., & Marcus, D. (2003). Endolymphatic sodium homeostasis by REISSNER's membrane. Neuroscience, 119(1), 3-8.

Liberman, M. C., & Beil, D. G. (1979). Hair cell condition and auditory nerve response in normal and noise-damaged cochleas. Acta oto-laryngologica, 88(3-4), 161–176.

Liberman, M. (1980). Morphological differences among radial afferent fibers in the cat cochlea: An electron-microscopic study of serial sections. Hearing Research, 3(1), 45-63.

Liberman, M. (1987). Chronic ultrastructural changes in acoustic trauma: Serial-section reconstruction of stereocilia and cuticular plates. Hearing Research, 26(1), 65-88.

Liberman, M., & Dodds, L. (1987). Acute ultrastructural changes in acoustic trauma: Serial-section reconstruction of stereocilia and cuticular plates. Hearing Research, 26(1), 45-64.

Liberman, M., Dodds, L., & Pierce, S. (1990). Afferent and efferent innervation of the cat cochlea: Quantitative analysis with light and electron microscopy. Journal of Comparative Neurology, 301(3), 443-460.

Liberman MC, Puria S, Guinan JJ Jr. The ipsilaterally evoked olivocochlear reflex causes rapid adaptation of the 2f1-f2 distortion product otoacoustic emission. J Acoust Soc Am. 1996;99(6):3572-3584.

Lin, J. (1996). Psychoacoustical Theory and Experiments on Human Auditory Organization of Complex Sounds and the Critical Bandwidth, ProQuest Dissertations and Theses.

Lioudyno, M., Hiel, H., Kong, J., Katz, E., Waldman, E., Parameshwaran-Iyer, S., Glowatzki, E., Fuchs, P. (2004) A synaptoplasmic cistern mediates rapid inhibition of cochlear hair cells. J Neurosci, 24(40), 11160-11164

Liu, Y., Qi, J., Chen, X., Tang, M., Chu, C., Zhu, W., . . . Zhong, G. (2019). Critical role of spectrin in hearing development and deafness. Science Advances, 5(4), Eaav7803.

Lumpkin, E. A., Marquis, R. E., & Hudspeth, A. J. (1997). The selectivity of the hair cell's mechanoelectrical-transduction channel promotes Ca^{2+} flux at low Ca^{2+} concentrations. Proceedings of the National Academy of Sciences of the United States of America, 94(20), 10997–11002.

Mancheño, M. R., Aristegui, M., & Sañudo, J. (2017). Round and Oval Window Anatomic Variability: Its Implication for the Vibroplasty Technique. Otology & Neurotology, 38(5), E50-E57.

Matsumoto N, Kitani R, Maricle A, Mueller M, Kalinec F. Pivotal role of actin depolymerization in the regulation of cochlear outer hair cell motility. Biophys J. 2010;99(7):2067-2076.

Misrahy, G., Shinabarger, E., & Arnold, J. (1958a). Changes in Cochlear Endolymphatic Oxygen Availability, Action Potential, and Microphonics during and following Asphyxia, Hypoxia, and Exposure to Loud Sounds. Journal of the Acoustical Society of America, 30(8), 701-704.

Misrahy, G., Arnold, J., Mundie, E., Shinabarger, V., & Garwood. (1958b). Genesis of Endolymphatic Hypoxia Following Acoustic Trauma. Journal of the Acoustical Society of America, 30(12), 1082-1088.

Nakagawa, Komune, Uemura, Akaike, & Nakagawa, T. (1991). Excitatory amino acid response in isolated spiral ganglion cells of guinea pig cochlea. Journal of Neurophysiology, 65(3), 715-723.

Nakashima, T., Suzuki, T., Morisaki, H., & Yanagita, N. (1991). Blood flow in the cochlea, vestibular apparatus and facial nerve. Acta oto-laryngologica, 111(4), 738–742.

Narayanan, P., Chatterton, P., Ikeda, A., Ikeda, S., Corey, D., Ervasti, J., & Perrin, B. (2015). Length regulation of mechanosensitive stereocilia depends on very slow actin dynamics and filament-severing proteins. Nature Communications, 6(1), 6855.

National Institution for Occupational Safety and Health. (1998). Occupational Noise Exposure Revised Criteria. https://www.cdc.gov/niosh/docs/98-126/pdfs/98-126.pdf?id=10.26616/NIOSHPUB98126

Nikaido, M. (1992). Normal structure of stereocilia and recovery from ciliary damage in the organ of Corti after acoustic overstimulation. Nihon Jibiinkoka Gakkai Kaiho, 95(2), 224-38.

Nouvian, R., Beutner, D., Parsons, T., & Moser, T. (2006). Structure and function of the hair cell ribbon synapse. Journal Of Membrane Biology, 209(2-3), 153-165.

Nouvian, R., Eybalin, M., & Puel, J. (2015). Cochlear efferents in developing adult and pathological conditions. Cell and Tissue Research, 361(1), 301-309.

Ohlemiller, K. K., Wright, J. S., & Dugan, L. L. (1999). Early elevation of cochlear reactive oxygen species following noise exposure. Audiology & neuro-otology, 4(5), 229–236.

Olson, E., & Mountain, D. (1991). In vivo measurement of basilar-membrane stiffness. Journal of The Acoustical Society Of America, 89(3), 1262-1275.

Osborne, M., Comis, P., & Pickles, S. (1984). Morphology and cross-linkage of stereocilia in the guinea-pig labyrinth examined without the use of osmium as a fixative. Cell and Tissue Research, 237(1), 43-48.

Ottersen, O., Takumi, Y., Matsubara, A., Landsend, A., Laake, J., & Usami, S. (1998). Molecular organization of a type of peripheral glutamate synapse: The afferent synapses of hair cells in the inner ear. Progress in Neurobiology, 54(2), 127-148.

Pacentine, I., Chatterjee, P., & Barr-Gillespie, P. (2020). Stereocilia Rootlets: Actin-Based Structures That Are Essential for Structural Stability of the Hair Bundle. International Journal of Molecular Sciences, 21(1), International journal of molecular sciences, January 3, 2020, Vol.21(1).

Pelliccia, Venail, Bonafé, Makeieff, Iannetti, Bartolomeo, & Mondain. (2014). Cochlea size variability and implications in clinical practice. Acta Otorhinolaryngologica Italica : Organo Ufficiale Della Societa Italiana Di Otorinolaringologia E Chirurgia Cervico-facciale, 34(1), 42-49.

Peng, B.G, Li, Q.X, Ren, T.Y, Ahmad, S, Chen, S.P, Chen, P, & Lin, X. (2004). Group i metabotropic glutamate receptors in spiral ganglion neurons contribute to excitatory neurotransmissions in the cochlea. Neuroscience, 123(1), 221-230.

Perrin, B., Sonnemann, K., Ervasti, J., & Tempel, B. (2010). β-Actin and γ-Actin Are Each Dispensable for Auditory Hair Cell Development but Required for Stereocilia Maintenance (Distinct Roles for β- and γ-Actin in Hair Cells). PLoS Genetics, 6(10), E1001158.

Pickles, J., Comis, S., & Osborne, M. (1984). Cross-links between stereocilia in the guinea pig organ of Corti, and their possible relation to sensory transduction. Hearing Research, 15(2), 103-112.

Pickles, J., Osborne, M., & Comis, S. (1987). Vulnerability of tip links between stereocilia to acoustic trauma in the guinea pig. Hearing Research, 25(2-3), 173-183.

Pickles, J., & Corey, D. (1992). Mechanoelectrical transduction by hair cells. Trends in Neurosciences, 15(7), 254-259.

Pickles JO. A model for the mechanics of the stereociliar bundle on acousticolateral hair cells. Hear Res. 1993;68(2):159-172.

Puel, J. (1995). Chemical synaptic transmission in the cochlea. Progress in Neurobiology, 47(6), 449,453-451,476.

Puel, J. L., Saffiedine, S., Gervais d'Aldin, C., Eybalin, M., & Pujol, R. (1995). Synaptic regeneration and functional recovery after excitotoxic injury in the guinea pig cochlea. Comptes rendus de l'Academie des sciences. Serie III, Sciences de la vie, 318(1), 67–75.

Ricci, A. J., & Fettiplace, R. (1998). Calcium permeation of the turtle hair cell mechanotransducer channel and its relation to the composition of endolymph. The Journal of physiology, 506 (Pt 1)(Pt 1), 159–173.

Roberto, M., Hamernik, R., & Turrentine, G. (1989). Damage of the Auditory System Associated with Acute Blast Trauma. Annals of Otology, Rhinology & Laryngology, 98(5_suppl), 23-34.

Robertson, D. (1983). Functional significance of dendritic swelling after loud sounds in the guinea pig cochlea. Hearing Research, 9(3), 263-278.

Roy, P., & Perrin, B. (2018). The stable actin core of mechanosensory stereocilia features continuous turnover of actin cross-linkers. Molecular Biology of the Cell, 29(15), 1856-1865.

Ruel, J., Chen, C., Pujol, R., Bobbin, R., & Puel, J. (1999). AMPA-preferring glutamate receptors in cochlear physiology of adult guinea-pig. Journal of Physiology-London, 518(3), 667-680.

Ruel, J., Wang, J., Rebillard, G., Eybalin, M., Lloyd, R., Pujol, R., & Puel, J. (2007). Physiology, pharmacology and plasticity at the inner hair cell synaptic complex. Hearing Research, 227(1-2), 19-27.

Russell, I., & Murugasu, E. (1997). Medial efferent inhibition suppresses basilar membrane responses to near characteristic frequency tones of moderate to high intensities. The Journal of the Acoustical Society of America, 102(3), 1734-1738.

Saunders, J., & Flock, A. (1986). Recovery of threshold shift in hair-cell stereocilia following exposure to intense stimulation. Hearing Research, 23(3), 233-243.

Saunders, J. C., Canlon, B., & Flock, A. (1986). Growth of threshold shift in hair-cell stereocilia following overstimulation. Hearing research, 23(3), 245–255.

Schaette, R., & McAlpine, D. (2011). Tinnitus with a normal audiogram: physiological evidence for hidden hearing loss and computational model. The Journal of neuroscience : the official journal of the Society for Neuroscience, 31(38), 13452–13457.

Schmoller, K., Semmrich, C., & Bausch, A. (2011). Slowdown of actin depolymerization by cross-linking molecules. Journal of Structural Biology, 173(2), 350-357.

Shen, B, Josephs, R.& Steck, T. (1986) Ultrastructure of the intact skeleton of the human erythrocyte membrane. The Journal of Cell Biology, 102(3), 997-1006.

Shin, J., Krey, J., Hassan, A., Metlagel, Z., Tauscher, A., Pagana, J.,. . . Barr-Gillespie, P. (2013). Molecular architecture of the chick vestibular hair bundle. Nature Neuroscience, 16(3), 365-374.

Shin, SA, Lyu, Ar, Jeong, Sh, Kim, Th, Park, Mj, & Park, Yh. (2019). Acoustic Trauma Modulates Cochlear Blood Flow and Vasoactive Factors in a Rodent Model of Noise-Induced Hearing Loss. International Journal of Molecular Sciences, 20(21), International Journal of Molecular Sciences, 2019 Nov, Vol.20(21).

Sliwinska-Kowalska, M., Parakkal, M., Schneider, M., & Fex, J. (1989). CGRP-like immunoreactivity in the guinea pig organ of Corti: A light and electron microscopy study. Hearing Research, 42(1), 83-95.

Smith DW, Keil A. The biological role of the medial olivocochlear efferents in hearing: separating evolved function from exaptation. Front Syst Neurosci. 2015;9:12. Published 2015 Feb 25.

Spoendlin H. (1971). Primary structural changes in the organ of Corti after acoustic overstimulation. Acta oto-laryngologica, 71(2), 166–176

Sridhara, S., Rivera, A., & Littlefield, P. (2013). Tympanoplasty for Blast-Induced Perforations: The Walter Reed Experience. Otolaryngology–Head and Neck Surgery, 148(1), 103-107.

Strelioff D, Flock A. Stiffness of sensory-cell hair bundles in the isolated guinea pig cochlea. Hear Res. 1984;15(1):19-28

Sziklai, M. (2001). Phosphorylation Mediates the Influence of Acetylcholine upon Outer Hair Cell Electromotility. Acta Oto-Laryngologica, 121(2), 153-156.

Szűcs, A., Szappanos, H., Batta, T., Tóth, J., Szigeti, A., Panyi, G., . . . Sziklai, G. (2006). Changes in Purinoceptor Distribution and Intracellular Calcium Levels following Noise Exposure in the Outer Hair Cells of the Guinea Pig. The Journal of Membrane Biology, 213(3), 135-141.

Szymko, Y. M., Nelson-Adesokan, P. M., & Saunders, J. C. (1995). Stiffness changes in chick hair bundles following in vitro overstimulation. Journal of comparative physiology. A, Sensory, neural, and behavioral physiology, 176(6), 727–735.

Tasaki, I., & Spyropoulos, C. (1959). Stria vascularis as source of endocochlear potential. Journal of Neurophysiology, 22(2), 149-155.

Tilney, L., DeRosier, D., & Mulroy, M. (1980). The organization of actin filaments in the stereocilia of cochlear hair cells. The Journal of Cell Biology, 86(1), 244-259.

Tilney, L., Saunders, J., Egelman, E., & DeRosier, D. (1982). Changes in the organization of actin filaments in the stereocilia of noise-damaged lizard cochleae. Hearing Research, 7(2), 181-197.

Tilney, L., Egelman, E., DeRosier, D., & Saunder, J. (1983). Actin filaments, stereocilia, and hair cells of the bird cochlea. II. Packing of actin filaments in the stereocilia and in the cuticular plate and what happens to the organization when the stereocilia are bent. The Journal of Cell Biology, 96(3), 822-834.

Tilney LG, Connelly P, Smith S, Guild GM. F-actin bundles in Drosophila bristles are assembled from modules composed of short filaments. J Cell Biol. 1996;135(5):1291-1308.

Van der Jeught, S., Dirckx, J., Aerts, J., Bradu, J., Podoleanu, R., & Buytaert, M. (2013). Full-Field Thickness Distribution of Human Tympanic Membrane Obtained with Optical Coherence Tomography. Journal of the Association for Research in Otolaryngology, 14(4), 483-494.

Vélez-Ortega AC, Freeman MJ, Indzhykulian AA, Grossheim JM, Frolenkov GI. Mechanotransduction current is essential for stability of the transducing stereocilia in mammalian auditory hair cells. eLife. 2017;10.7554/eLife.24661.

Wang, Y., Hirose, K., & Liberman, M. (2002). Dynamics of Noise-Induced Cellular Injury and Repair in the Mouse Cochlea. Journal of the Association for Research in Otolaryngology, 3(3), 248-268.

Wang, Hui, Yin, Shankai, Yu, Zhiping, Huang, Yanyan, & Wang, Jian. (2011). Dynamic changes in hair cell stereocilia and cochlear transduction after noise exposure. Biochemical and Biophysical Research Communications, 409(4), 616-621.

Wei–Ju, H., Xiao–Rui, S., & Nuttall, A. (2010). Noise exposure induced cochlear hair cell death pathways in guinea pig. Journal of Otology, 5(1), 51-56.

Weisz, C., Glowatzki, E., & Fuchs, P. (2009). The postsynaptic function of type II cochlear afferents. Nature, 461(7267), 1126-119.

Weyer, Praetorius, & Tisch. (2011). Update: Knall- und Explosionstraumata. HNO, 59(8), 811-818.

Wioland H, Guichard B, Senju Y, et al. ADF/Cofilin Accelerates Actin Dynamics by Severing Filaments and Promoting Their Depolymerization at Both Ends. Curr Biol. 2017;27(13):1956-1967.e7.

Yamane, Nakai, Takayama, Iguchi, Nakagawa, & Kojima. (1995). Appearance of free radicals in the guinea pig inner ear after noise-induced acoustic trauma. European Archives of Oto-Rhino-Laryngology, 252(8), 504-508.

Zhao, Y., Yamoah, E., & Gillespie, P. (1996). Regeneration of Broken Tip Links and Restoration of Mechanical Transduction in Hair Cells. Proceedings of the National Academy of Sciences of the United States of America, 93(26), 15469-15474.

Zhang M, Kalinec GM, Urrutia R, Billadeau DD, Kalinec F. ROCK-dependent and ROCK-independent control of cochlear outer hair cell electromotility. J Biol Chem. 2003;278(37):35644-35650.

Zhang, D., Piazza, V., Perrin, B., Rzadzinska, A., Poczatek, J.C., Wang, M., Lechene. C. (2012). Multi-isotope imaging mass spectrometry reveals slow protein turnover in hair-cell stereocilia. Nature, 481(7382), 520-524.

Zheng, J., Shen, W., He, D.Z., Long, K., Madison, L., & Dallos, P. (2000). Prestin is the motor protein of cochlear outer hair cells. Nature, 405(6783), 149-155.

VITA

Jonathan Michael Grossheim

EDUCATION

2005 – Bachelor of Science in Chemistry (Biochemistry tract),

Northern Kentucky University (NKU), Highland Heights, KY.

2009 – Bachelor of Science in Biology,

University of Texas at San Antonio (UTSA), San Antonio, TX.

2010 – Master of Science in Biology,

University of Texas at San Antonio (UTSA), San Antonio, TX.

PROFESSIONAL EXPERIENCE

2013-2019 Adjunct Professor. Bluegrass Community and Technical College

2011 Lecturer. University of Texas at San Antonio

2009-2010 Teaching Assistant. University of Texas at San Antonio.

HONORS & AWARDS

2014-2015 Outstanding Adjunct Faculty of the Year

Division of Natural Sciences at Bluegrass Community & Technical College

2008-2010 President's List

University of Texas at San Antonio

ABSTRACTS - Poster Presentations

Freeman MJ, Grossheim JM, Vélez-Ortega AC, Saatman KE, Gregory GI. Calpistatin Overexpression Ameliorates Permanent Noise-Induced Hearing Loss. ARO 41st Midwinter Meeting. San Diego, CA 2018. Abstract # PS-728.

Vélez-Ortega AC, Quiñones PM, Freeman MJ, Meenderink SW, Indzhykulian AA, Grossheim JM, Bozovic D, Frolenkov GI. Activity-dependent regulation of the hair cell stereocilia actin core in vertebrates. ARO 40th Midwinter Meeting. Baltimore, MD 2017. Abstract # PS-767.

Grossheim JM, Frolenkov GI. Damage and Recovery of the Stereocilia Actin Core After Mechanical Overstimulation. ARO 40th Midwinter Meeting. Baltimore, MD 2017. Abstract # PS-607.

Grossheim JM, Stepanyan R, Frolenkov GI. Actin Core Repair Underlies the Recovery of Overstimulation-Induced Stiffness Changes in Inner Hair Cell Stereocilia Bundles. ARO 39th Midwinter Meeting. San Diego, CA 2016. Abstract # PS-84.

Grossheim JM, Stepanyan R, Frolenkov GI. Mechanical Overstimulation Results in Decreased Stiffness of Inner Hair Cell Stereocilia Due to Actin Core Damage. Association for Research in Otolaryngology (ARO) 37th Midwinter Meeting. Baltimore, MD 2015. Abstract # PS-315.

ABSTRACTS - Podium Presentations

Frolenkov GI, Grossheim JM, Stepanyan R, Freeman MJ, Vélez-Ortega AC. Stereocilia Bundle Repair in Mechanically Damaged Mammalian Auditory Hair Cells. ARO 41st Midwinter Meeting. San Diego, CA 2018. Abstract # SYMP-79.

Vélez-Ortega AC, Quiñones PM, Galeano-Naranjo C, Meenderink SWF, Grossheim JM, Bozovic D, Frolenkov GI. Transduction-Depending Remodeling: a Unique Maintenance Mechanism of the Mammalian Auditory Stereocilia or a Common Hair Cell Trait? ARO 41st Midwinter Meeting. San Diego, CA 2018. Abstract # PD-18.

Frolenkov GI, Stepanyan R, Ricci AJ, Grossheim JM. Overstimulation-induced Damage to Stereocilia Tips Causes Loss of Resting Tension in the Mechanotransducer of the Mammalian Auditory Hair Cells. ARO 40th Midwinter Meeting. Baltimore, MD 2017. Abstract # PD-74.

PUBLISHED MANUSCRIPTS

Mahller YY, Williams JP, Baird WH, Mitton B, Grossheim JM, Saeki Y, Cancelas JA, Ratner N, Cripe TP. Neuroblastoma cell lines contain pluripotent tumor initiating cells that are susceptible to a targeted oncolytic virus. PLos One. 2009; 4(1):e4235.

Head E, Murphy HL, Dowling AL, McCarty KL, Bethel, SR, Nitz JA, Pleiss M, Vanrooyen J, Grossheim JM, Smiley JR, Murphy MP, Beckett TL, Pagani D, Bresch F, Hendrix C. A combination cocktail improves spatial attention in a canine model of human aging and Alzheimer's disease. J Alzheimers Dis. 2012; 32(4):1029-42.

Seco CZ, Giese Ap, Shafique S, Schraders M, Oonk AM, Grossheim JM, Oostrik J, Strom T, Hegde R, van Wilk E, Frolenkov GI, Azam M, Yntema HG, Free Rh, Riazuddin S, Verheij JB, Admiraal RJ, Qamar R, Ahmed Zm, Kremer H. Novel and recurrent CIB2 variants, associated with nonsyndromic deafness, do not affect calcium buffering and localization in hair cells. Eur J Hum Genet. 2016; 24(4):542-9.

Patel K, Giese AP, Grossheim JM, Hegde RS, Delio M, Samanich J, Riazuddin S, Frolenkov GI, Cai J, Ahmed ZM, Morrow BE. A novel C-terminal CIB2 (Calcium and Integrin Binding protein 2) mutation associated with non-syndromic hearing loss in a Hispanic family. PLoS One. 2015; 10(10)e0141259.

Vélez-Ortega AC, Freeman MJ, Indzhykulian AA, Grossheim JM, Frolenkov GI. Mechanotransduction current is essential for stability of the transducing stereocilia in mammalian auditory hair cells. eLife. 2017;10.7554/eLife.24661.

Jonathan **Michael** Grossheim